

## ABSTRACT

Title of Document: PERFORMANCE MEASUREMENT,  
SIMULATION, AND ANALYSIS OF THE  
COX TEE DEE 0.010, THE WORLD'S  
SMALLEST PRODUCTION INTERNAL  
COMBUSTION ENGINE

Troy Sookdeo, M.S., 2006

Directed By: Associate Professor Christopher Cadou,  
Department of Aerospace Engineering

The Cox Tee Dee 0.010 is a two-stroke 0.010 cubic inch model engine designed to power small propeller-based hobby aircraft. First manufactured in 1961, it remains the smallest working piston engine ever mass-produced, but no scientific measurements of its performance are available in the open literature. These measurements are important because they could facilitate the development of small unmanned air vehicles. This thesis reports measurements of power output and efficiency using a specialized dynamometer. An unsuccessful attempt is made to correlate the measurements with simulations based on Stanford University's Engine Simulation Program (ESP). Instead, the results are compared to the predictions of a simple zero-dimensional thermodynamic MATLAB simulation of an engine cycle developed at the University of Maryland. Differences and correlations are discussed and the engine performance is analyzed in the context of propulsion systems for small UAVs and for compact power generation.

PERFORMANCE MEASUREMENT, SIMULATION, AND ANALYSIS OF THE  
COX TEE DEE 0.010, THE WORLDS SMALLEST PRODUCTION IC ENGINE

By

Troy Sookdeo

Thesis submitted to the Faculty of the Graduate School of the  
University of Maryland, College Park, in partial fulfillment  
of the requirements for the degree of  
Master of Science  
2006

Advisory Committee:

Associate Professor Christopher Cadou, Chair

Associate Professor Kenneth Yu

Director of Gessow Rotorcraft Center, Gessow Professor Inderjit Chopra

© Copyright by  
Troy Sookdeo  
2006

# Dedication

To my parents: Kelvin and Shakila

## Acknowledgements

In completion of this work, much thanks goes to Professor Christopher Cadou for his overall guidance and access to the generous resources of the Micro-Reacting Flow Laboratory. Additionally, I must extend a great amount of gratitude to doctoral student Shyam Menon for his invaluable assistance throughout the entire process with both the laboratory and simulation work.

# Table of Contents

Dedication.....	ii
Acknowledgements.....	iii
Table of Contents.....	iv
List of Tables.....	vi
List of Figures.....	vii
1. Introduction.....	1
1.1 Advantage of IC Engines for Small-Scale Power Applications.....	2
1.2 Known Issues with Small-Scale Engines.....	4
1.2.1 Tolerances, Friction, Sealing.....	4
1.2.2 Combustion.....	6
1.2.3 Scavenging.....	8
1.3 Existing Work on Miniature Combustion Engines.....	8
1.3.1 Research Engines.....	8
1.3.2 Commercial Model Aircraft Scale Combustion Engines.....	18
1.4 Approach.....	20
1.4.1 Experiments.....	21
1.4.2 Simulation.....	22
2. Description of the Cox Tee Dee 0.010.....	23
2.1 History and Uses.....	23
2.1.1 Inception and Manufacturing.....	23
2.1.2 Aircraft Platforms.....	24
2.2 Engine Design and Specifications.....	26
2.2.1 Original Design.....	26
2.2.2 Micro-Flite Modified Design.....	30
2.3 Cycle Description.....	31
2.3.1 Power Stroke.....	31
2.3.2 Compression Stroke.....	33
2.3.3 Timing Diagram.....	35
2.4 Fuel.....	36
2.4.1 Background.....	36
2.4.2 Subject Blend.....	37
2.5 Performance.....	38
3. Performance Measurement.....	41
3.1 Dynamometer Apparatus.....	41
3.1.1 Previous Configuration (First Iteration).....	41
3.1.2 Modified Configuration (Final Iteration).....	43
3.2 Experimental Procedure.....	48
3.2.1 Before Starting Engine.....	48
3.2.2 During Engine Run.....	49
3.2.3 After Stopping Engine.....	50
3.3 Results and Analysis.....	51
3.3.1 Original Cox Tee Dee 0.010.....	51
3.3.2 Modified Micro-Flite Tee Dee 0.010 Engine A.....	58

3.3.3 Modified Micro-Flite Tee Dee 0.010 Engine B.....	63
3.4 Error Analysis .....	69
4. Simulation With MATLAB .....	72
4.1 Algorithm Description .....	72
4.2 Parameter Configuration.....	75
4.3 Results and Analysis.....	78
4.4 Error Analysis .....	83
5. Conclusion .....	85
5.1 Findings.....	85
5.2 Capability Assessment.....	86
5.3 Future Work .....	86
5.3.1 Measurement Tasks.....	86
5.3.2 Simulation Tasks.....	86
Appendix A: MATLAB Simulation Code.....	87
Appendix B: Simulation with the Stanford ESP.....	103
References.....	129

## List of Tables

- Table 1.1: Specifications of the Georgia Tech Free-Piston Engines  
Table 1.2: D-STAR Micro-Diesel Engine Generator Performance
- Table 2.1: Original Cox Tee Dee 0.010 Specifications  
Table 2.2: Micro-Flite Tee Dee 0.010 Fuel Properties  
Table 2.3: Published Tee Dee 0.010 Propeller Performance
- Table 3.1: Components of Original Dynamometer Design  
Table 3.2: Components of Modified Dynamometer Design  
Table 3.3: Original Cox Tee Dee 0.010 Measured Data  
Table 3.4: Original Cox Tee Dee 0.010 Calculated Performance  
Table 3.5: Modified Micro-Flite Cox Tee Dee 0.010 “Engine A” Measured Data  
Table 3.6: Modified Micro-Flite Cox TD 0.010 “Engine A” Calculated Performance  
Table 3.7: Modified Micro-Flite Cox Tee Dee 0.010 “Engine B” Measured Data  
Table 3.8: Modified Micro-Flite Cox TD 0.010 “Engine B” Calculated Performance  
Table 3.9: Original Cox Tee Dee 0.010 Measurement Uncertainty  
Table 3.10: Original Cox Tee Dee 0.010 Performance Uncertainty  
Table 3.11: Modified Micro-Flite Cox TD 0.010 “A” Measurement Uncertainty  
Table 3.12: Modified Micro-Flite Cox TD 0.010 “A” Performance Uncertainty  
Table 3.13: Modified Micro-Flite Cox TD 0.010 “B” Measurement Uncertainty  
Table 3.14: Modified Micro-Flite Cox TD 0.010 “Engine B” Performance Uncertainty
- Table 4.1: MATLAB Tee Dee 0.010 Results  
Table 4.2: MATLAB and Measured Power Comparison  
Table 4.3: MATLAB and Measured Airflow Comparison  
Table 4.4: MATLAB and Measured Volumetric Efficiency Comparison
- Table B.1: ESP Tee Dee 0.010 Inert Oil Performance Summary  
Table B.2: ESP Derived Inert Oil Performance Values  
Table B.3: ESP Tee Dee 0.010 Burned Oil Performance Summary  
Table B.4: ESP Derived Burned Oil Performance Values  
Table B.5: ESP and Measured Fuel Flow Comparison  
Table B.6: ESP and Measured Power Comparison  
Table B.7: ESP and Measured BSFC Comparison  
Table B.8: ESP and Measured Efficiency Comparison

## List of Figures

- Figure 1.1: Specific Energy Comparison for Various Energy Sources  
Figure 1.2: 72-Hour Mission Capability for Various Energy Sources  
Figure 1.3: MAV Endurance as a Function of Conversion and Storage Efficiency  
Figure 1.4: Surface Area-to-Volume Ratio for a Range of Hobby Engines  
Figure 1.5: Effect of Piston Blow-By as Engine Size Decreases  
Figure 1.6: Effect of Quenching as Engine Size Decreases  
Figure 1.7: MEMS-Fabricated Components of the Berkeley Rotary Engine  
Figure 1.8: Meso-Scale Version of the Berkeley Rotary Engine  
Figure 1.9: Dynamometer Results for the Berkeley Meso-Scale Rotary Engine  
Figure 1.10: MEMS-Fabricated Rotor for the MIT Microturbine Engine  
Figure 1.11: Cross Section of the Integrated MIT Microturbine Engine  
Figure 1.12: Schematic of the Georgia Tech Free-Piston Engine  
Figure 1.13: Schematic of the Honeywell ‘Knock’ Engine Experiment  
Figure 1.14: Photo of the Honeywell ‘Knock’ Engine Components  
Figure 1.15: Cross Section of the Aerodyne Meso-Scale Free-Piston Engine  
Figure 1.16: Schematic and Photo of the University of Michigan Swing Engine  
Figure 1.17: Summary of the Packaged Swing Engine Power Generation System  
Figure 1.18: D-STAR Micro-Diesel Engine with Propeller and Generator  
Figure 1.19: Ron Valentine’s 0.05cc Diesel Rova Blitz  
Figure 1.20: University of Maryland’s Specialized Small Engine Dynamometer  
Figure 1.21: Measured and Reported Hobby Engine Power Output  
Figure 1.22: The Cox Tee Dee 0.010 Relative to a U.S. Nickel
- Figure 2.1: William Atwood, 1/A Engine Designer  
Figure 2.2: The Original Cox Tee Dee and The Modern Micro-Flite Version  
Figure 2.3: The Control-Line Thimble Drome TD-1 and TD-3 Aircraft  
Figure 2.4: Small Radio-Controlled Aircraft Powered by the Tee Dee 0.010  
Figure 2.5: Flying Kite Design Powered by the Tee Dee 0.010  
Figure 2.6: Model Bomber Design Powered by Six Tee Dee 0.010s  
Figure 2.7: Original Cox Tee Dee 0.010 3-View  
Figure 2.8: Tee Dee 0.010 Piston and Cylinder  
Figure 2.9: Tee Dee 0.010 Crankcase and Intake housing  
Figure 2.10: Tee Dee 0.010 Assembled Crankcase and Cylinder  
Figure 2.11: Exploded View of the Original Cox Tee Dee 0.010  
Figure 2.12: The Micro-Flite Modified Tee Dee 0.010  
Figure 2.13: Exploded View of Micro-Flite Throttle Mechanism  
Figure 2.14: Beginning of the Tee Dee 0.010 Power Stroke  
Figure 2.15: Cox Tee Dee 0.010 Power Stroke  
Figure 2.16: Scavenging and the Beginning of the Tee Dee 0.010 Compression Stroke  
Figure 2.17: Cox Tee Dee 0.010 Compression Stroke  
Figure 2.18: Cox Tee Dee 0.010 Timing Diagram  
Figure 2.19: Micro-Flite Customized Tee Dee 0.010 Fuel  
Figure 2.20: Published Cox Tee Dee Power Output

Figure 3.1: Diagram of Original Dynamometer Design  
 Figure 3.2: Diagram of Modified Dynamometer Starter Configuration  
 Figure 3.3: Diagram of Modified Dynamometer Load-Control Configuration  
 Figure 3.4: Reflective Tape and Remote Speed Sensor Beam Positioning  
 Figure 3.5: Complete Modified Dynamometer Configuration  
 Figure 3.6: Three-Piece “Spider” Shaft Coupling  
 Figure 3.7: Three-Piece Plastic and Brass Coupling  
 Figure 3.8: One-Piece Rubber and Brass Coupling  
 Figure 3.9: Fuel Line, Air Line, and Thermocouple Attachment  
 Figure 3.10: Original Cox TD 0.010 Speed Data  
 Figure 3.11: Original Cox TD 0.010 Temperature Data  
 Figure 3.12: Original Cox TD 0.010 Massflow Data  
 Figure 3.13: Original Cox TD 0.010 Volumetric Efficiency Data  
 Figure 3.14: Original Cox TD 0.010 Efficiency Data  
 Figure 3.15: Original Cox Tee Dee Stacked Performance Plots  
 Figure 3.16: Micro-Flite TD 0.010 “Engine A” Speed Data  
 Figure 3.17: Micro-Flite TD 0.010 “Engine A” Temperature Data  
 Figure 3.18: Micro-Flite TD 0.010 “Engine A” Massflow Data  
 Figure 3.19: Micro-Flite TD 0.010 “Engine A” Volumetric Efficiency Data  
 Figure 3.20: Micro-Flite TD 0.010 “Engine A” Efficiency Data  
 Figure 3.21: Micro-Flite Tee Dee “Engine A” Stacked Performance Plots  
 Figure 3.22: Micro-Flite TD 0.010 “Engine B” Speed Data  
 Figure 3.23: Micro-Flite TD 0.010 “Engine B” Massflow Data  
 Figure 3.24: Micro-Flite TD 0.010 “Engine B” Volumetric Efficiency Data  
 Figure 3.25: Micro-Flite TD 0.010 “Engine B” Efficiency Data  
 Figure 3.26: Micro-Flite Tee Dee “Engine B” Stacked Performance Plots  
 Figure 3.27: Cox Tee Dee 0.010 Stacked Performance Plots

Figure 4.1: MATLAB Engine Model  
 Figure 4.2: Matrix of differential equations solved by MATLAB  
 Figure 4.3: Original Cox Tee Dee Measured Equivalence Ratios  
 Figure 4.4: MATLAB Tee Dee 0.010 Temperatures  
 Figure 4.5: MATLAB Tee Dee 0.010 Masses  
 Figure 4.6: MATLAB Tee Dee 0.010 Pressures  
 Figure 4.7: MATLAB Tee Dee 0.010 P-V Diagrams  
 Figure 4.8: MATLAB Tee Dee 0.010 Volumetric Efficiency  
 Figure 4.9: Cox Tee Dee 0.010 Power Curves

Figure B.1: ESPJAN Reactant Selection Window  
 Figure B.2: ESPJAN Reactant Selection Window  
 Figure B.3: ESPJAN Reactant Moles Specification Window  
 Figure B.4: ESPJAN Product Selection Window  
 Figure B.5: ESPJAN Pressure Specification Window  
 Figure B.6: ESPCAM Program Setup Window  
 Figure B.7: ESPCAM Valve Lift Specification Window  
 Figure B.8: Tee Dee 0.010 Transfer Port Opening Curve

Figure B.9: Tee Dee 0.010 Exhaust Port Opening Curve  
Figure B.10: ESP Main Setup Window  
Figure B.11: ESP Tee Dee 0.010 Inert Oil P-V Diagram  
Figure B.12: ESP Tee Dee 0.010 Inert Oil Cycle Temperatures  
Figure B.13: ESP Tee Dee 0.010 Inert Oil Cycle Temperatures (Zoomed)  
Figure B.14: ESP Tee Dee 0.010 Inert Oil Cycle Masses  
Figure B.15: ESP Tee Dee 0.010 Inert Oil Cycle Masses (Zoomed)  
Figure B.16: ESP Tee Dee 0.010 Inert Oil Cycle Mass Flows  
Figure B.17: ESP Tee Dee 0.010 Inert Oil Cycle Mass Flows (Zoomed)  
Figure B.18: ESP Tee Dee 0.010 Inert Oil Cycle Pressures  
Figure B.19: ESP Tee Dee 0.010 Inert Oil Cycle Energy Rates  
Figure B.20: ESP Tee Dee 0.010 Inert Oil Cycle Flow Velocities  
Figure B.21: ESP Tee Dee 0.010 Burned Oil P-V Diagram  
Figure B.22: ESP Tee Dee 0.010 Burned Oil Cycle Temperatures  
Figure B.23: ESP Tee Dee 0.010 Burned Oil Cycle Temperatures (Zoomed)  
Figure B.24: ESP Tee Dee 0.010 Burned Oil Cycle Masses  
Figure B.25: ESP Tee Dee 0.010 Burned Oil Cycle Masses (Zoomed)  
Figure B.26: ESP Tee Dee 0.010 Burned Oil Cycle Mass Flows  
Figure B.27: ESP Tee Dee 0.010 Burned Oil Cycle Mass Flows (Zoomed)  
Figure B.28: ESP Tee Dee 0.010 Burned Oil Cycle Pressures  
Figure B.29: ESP Tee Dee 0.010 Burned Oil Cycle Energy Rates  
Figure B.30: ESP Tee Dee 0.010 Burned Oil Cycle Flow Velocities  
Figure B.31: ESP Power Curve (Inert Oil)  
Figure B.32: Average ESP Performance Difference from Measured (Inert Oil)

# 1. Introduction

Recent years have seen a sharp increase in interest in miniature power devices. As portable machines are becoming smaller while requiring yet even more power and longevity, researchers have been looking for power sources that can keep up with the demands of the emerging applications. The most pressing demands include power for portable electronic devices like laptops or portable battery chargers and propulsion devices for micro air vehicles (MAV).

Until very recently, most of these portable applications have been utilizing conventional chemical batteries to store energy. Unfortunately, the energy densities of such electric systems are so low that they are limiting the performance capabilities or utility of the miniature systems they are designed to power. The Defense Advanced Research Projects Agency (DARPA), for instance, wants to build a micro air vehicle weighing less than 50 g capable of performing missions at least 30 minutes long. Even with the most advanced technology, the batteries required for such range would be too heavy to implement into any workable flying vehicle [9]. Hydrocarbon fuels have acceptable energy density for such demanding applications and a strategy for releasing this energy is the internal combustion (IC) engine.

Research data and analysis of miniature power devices utilizing the combustion of hydrocarbon fuels, has until recently, been somewhat limited. Several teams have been working on exotic micro-scale devices such as micro-rotary [27] and microturbine [25] engines that show potential, but have yet to produce any useable systems. Other teams have focused attention the meso-scale range of miniature engines [16, 23] which sacrifice the size advantage, but offer an immediate level of functionality and reliability that micro-engines have failed to match. In contrast, commercial IC hobby engines have been successfully implemented for decades as propulsion devices for miniature hobby vehicles. As a result, it may be possible to use them in immediate or very near future specialized power applications.

Even with decades of development by the model aircraft industry, there is little information on the performance of these engines in the scientific literature. If researchers can gain a scientific understanding of how power and efficiency scale with engine size, some of the shortcomings of these working engines could be overcome. These lessons could also be applied to micro-scale devices in order to bring them closer to functioning reality. Additionally, some working meso-scale engines are currently small enough to fulfill the power and size requirements of emerging advanced applications such as small unmanned aerial vehicles (UAV) and portable power generators. If the performance of these engines can be further optimized, the advantage gap between the size of the micro-scale engines and the functionality of smaller meso-scale engines can be narrowed.

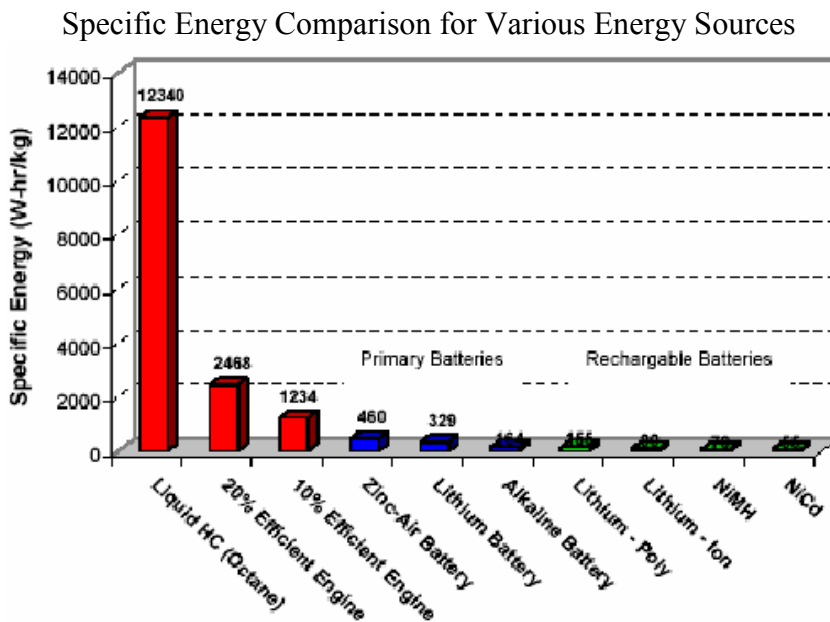
This thesis focuses on the performance of an engine at the very bottom end of the hobby engine size scale: the Cox Tee Dee 0.010. This is a 0.010 cubic inch two-

stroke single piston engine first manufactured in the early 1960's. It remains today the smallest mass-produced engine in the world. The engine is tested with a custom-built dynamometer. An unsuccessful attempt is made to simulate the engine using Stanford's Engine Simulation Program. Instead, the measured performance is compared to the output of a simple MATLAB-based thermodynamics model. These results are used to draw conclusions on the engine performance and its ability to be used as a power device for emerging applications such as MAV.

1.1 Advantage of IC Engines for Small-Scale Power Applications

Traditionally, power-hungry miniature devices have been limited in performance by the energy storage capabilities of chemical batteries and fuel cells [46]. In order to meet the desired performance of emerging high-power applications such as micro air vehicles and portable soldier power [17] however, higher energy densities along with more efficient energy conversion must be achieved than is currently available.

DARPA has provided funding for several engine research projects under the Palm Power initiative which seeks to find devices capable of producing at least 20 W of power with 1000 W-hr/kg for a three-hour mission, 2000 W-hr/kg for a three-day mission, and 3000 W-hr/kg for a ten-day mission [17]. As shown in Figure 1.1 [50], an engine capable of extracting only 10% of the energy stored in liquid hydrocarbon fuel (plotted as the three left-most columns in red) will still meet DARPA's goals and surpass the capabilities of the most advanced battery technologies.



(Source: Pello, 2002 [50])

Figure 1.1

A review of state-of-the-art power systems done by the National Research Council (NRC) [46] shows that internal combustion engines running on hydrocarbon fuel

outperform even the most advanced fuel cells particularly with regards to long mission requirements. Figure 1.2 is a plot of the capabilities of the NRC-reviewed systems for a 20 W output 72-hour mission requirement. The IC engine datum point is the D-STAR 50 W micro diesel and the Stirling engine datum point is a Sunpower Stirling engine.

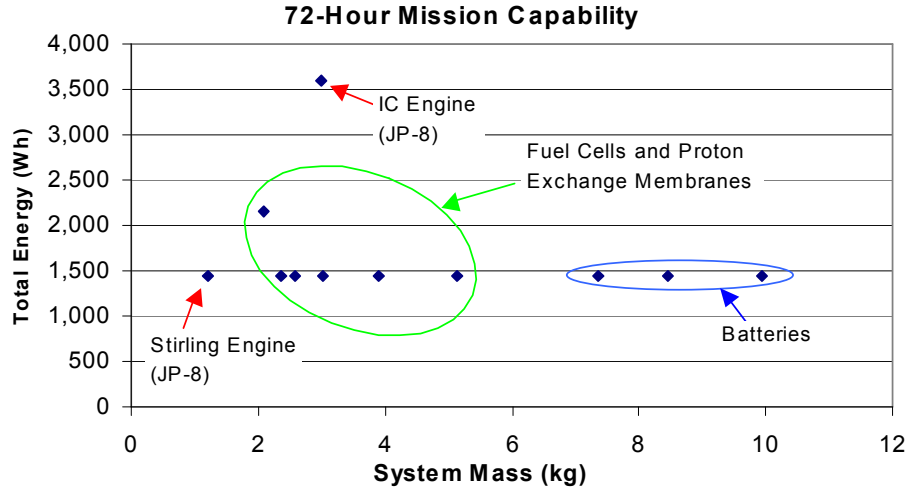


Figure 1.2

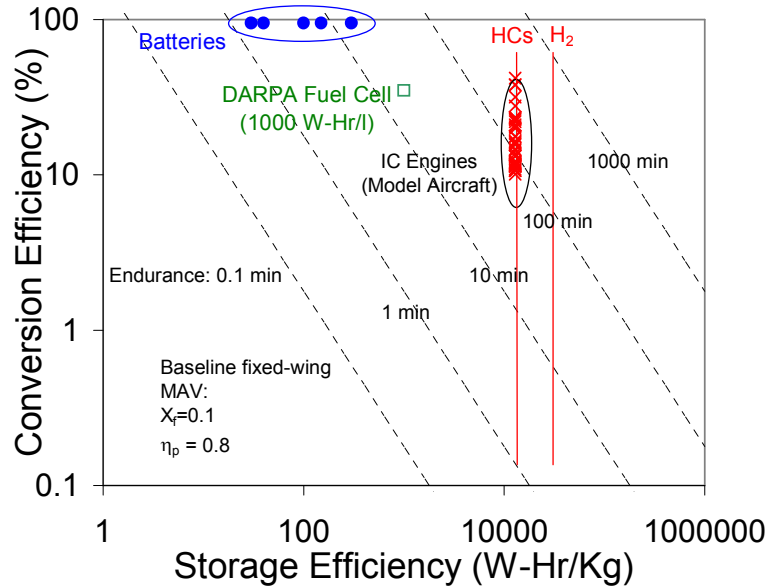
A further understanding of the advantage of IC engines specifically for micro air vehicles can be gained by examining an adaptation of Brequet's range formula [32: pg. 152] shown in Equation 1.1. This equation determines aircraft endurance time,  $\tau$ , in terms of energy conversion efficiency,  $\eta_{pwr}$ , fuel specific energy,  $Q_R$ , acceleration due to gravity,  $g$ , propulsion efficiency  $\eta_{prop}$ , mass of fuel,  $m_f$ , mass of vehicle,  $m_v$ , lift to drag ratio ( $L/D$ ), and vehicle cruise speed  $v$  [9]:

$$\tau = \left( \eta_{pwr} \frac{Q_R}{g} \right) \left( \frac{\eta_{prop} L}{v D} \right) \ln \left( 1 + \frac{m_f}{m_v} \right) \quad (\text{Eq. 1.1})$$

From the terms relevant to the power system in the first set of parentheses, it is clear that while improving the efficiency of IC engines ( $\eta_{pwr}$ ) is important, it is the orders of magnitude difference in the energy density ( $Q_R$ ) of hydrocarbon fuels that give it the large advantage over batteries for vehicle performance. Furthermore, keeping the engine as small as possible reduces the relative vehicle mass ( $m_v$ ) which also increases endurance.

Figure 1.3 shows the relative performance of many model aircraft IC engines based on manufacturers published data using Equation 1.1 while assuming typical MAV values including a fuel to vehicle mass fraction of 0.1 and a propulsion efficiency of 0.8 [9]. Later work has shown the power of these hobby engines to be well below manufacturer claims [8, 9], but even modest performance from these engines can yield significant advantages over conventional batteries. In fact, as seen in Figure 1.3,

hydrocarbon engines need only to achieve an efficiency of ~5% or greater to gain an advantage over batteries. The large scatter amongst the model aircraft engines shown in the figure is most likely a result of inconsistent testing conditions from which manufacturers have reported engine performance.



(Source: Cadou, 2002 [9])

MAV Endurance as a Function of Conversion and Storage Efficiency  
Figure 1.3

The work presented in this thesis aims to identify the capability of the smallest of these hobby engines and contribute to the overall understanding of power and efficiency loss mechanisms encountered when IC engines are scaled down. Understanding these losses will allow researchers to develop miniaturized power systems that are appropriate for use in MAVs and for powering a wide range of miniature devices.

## 1.2 Known Issues with Small-Scale Engines

### 1.2.1 Tolerances, Friction, Sealing

As overall engine size decreases, so must the components that serve as the working parts of the engine. Smaller parts mean tighter tolerances that require very precise machining. Furthermore, inherent geometric relations dictate that reducing engine size increases the surface area to volume ratio. This trend is clearly demonstrated with a plot of cylinder surface area/volume as a function of engine mass for a range of hobby engines as shown in Figure 1.4. Since frictional and thermal losses scale with surface area to volume ratio, they are expected to become more important as the size of the device is reduced.

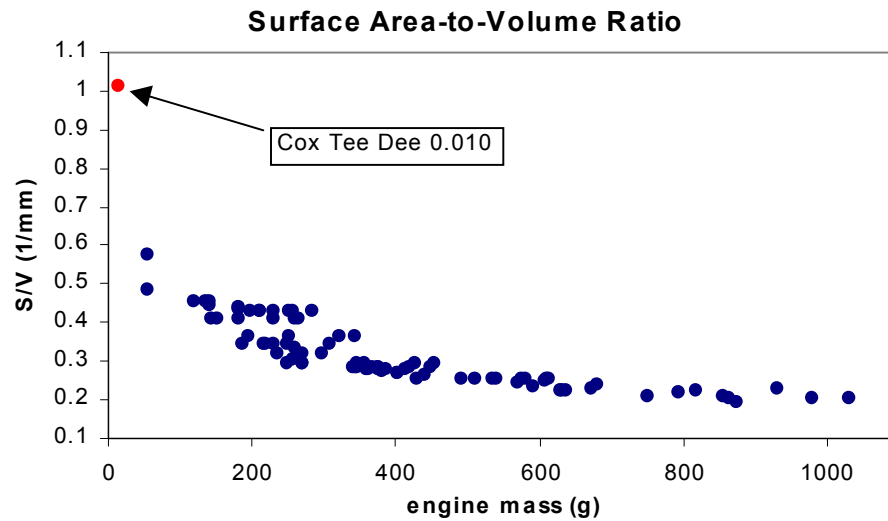
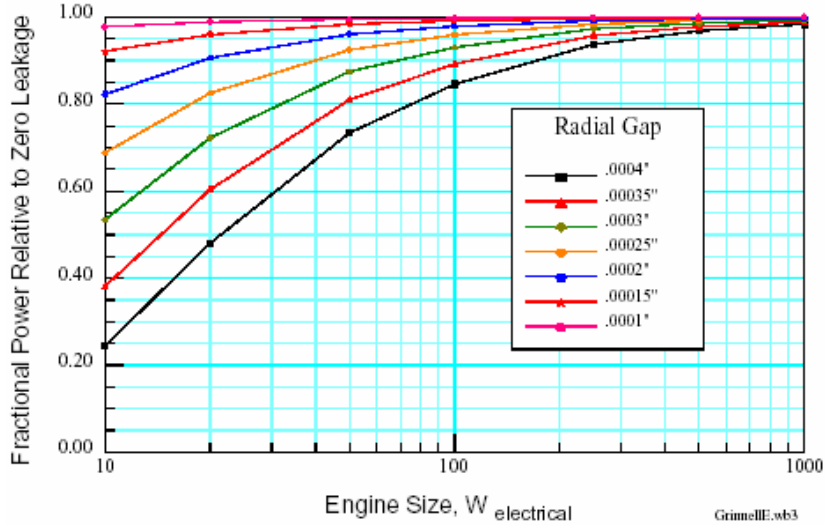


Figure 1.4

Even with recent advances in Micro Electro-Mechanical System (MEMS) fabrication techniques, teams working on engines in the micro-scale regime have found great challenges to manufacture engine parts to correct precision while maintaining engine sealing and low-friction bearings [10, 22, 39, 40, 67, 68].

These scaling issues are illustrated by Figure 1.5 from a model developed by Aerodyne to simulate the effect of piston blow-by on the performance of piston engines as their size is reduced [6]. Size is reported in terms of electrical power output and efficiency loss is reported as the ratio of the combustion power to the combustion power in the absence of leakage. The results demonstrate a need for tighter gap tolerances as engine size decreases.



(Source: Annen, 2003 [6])  
 Effect of Piston Blow-By as Engine Size Decreases  
 Figure 1.5

### 1.2.2 Combustion

As the size of the combustion chamber and overall engine decrease, so does the output torque. Therefore, small engines must operate at very high speeds to produce adequate power. Some small hobby engines, for instance, reach peak power output well in excess of 20,000 revolutions per minute (RPM) and the Massachusetts Institute of Technology (MIT) microturbine design is intended to operate in the millions of RPM range [25].

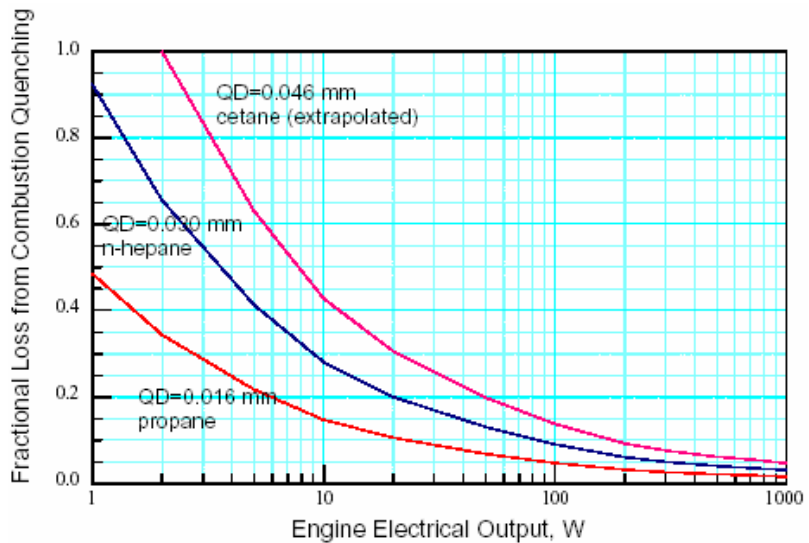
In piston engines, these very high operating speeds present a serious challenge with respect to the residence time a volume of charge spends in the combustion chamber during each cycle. As the speed increases, the residence time decreases and the charge has less time to completely burn. If the charge is not allowed to fully combust, unburned fuel exits the chamber taking with it wasted energy and thus decreasing engine efficiency.

Contributing to the combustion inefficiency in the small scale are losses from poor fuel-air mixing. In very small engines, the high speed allows only a short amount of time and distance for fuel to be mixed with incoming air before entering the combustion chamber [62: pg. 409]. Furthermore, mixing in this regime is limited by flow behavior that can be examined via the Reynolds number defined by Equation 1.2 [32: pg. 100].

$$Re = \frac{\rho UL}{\mu} \quad (\text{Eq. 1.2})$$

Given flow density,  $\rho$ , flow viscosity,  $\mu$ , characteristic flow velocity,  $U$ , and characteristic subject length,  $L$ , the Reynolds number is a dimensionless value that describes the ratio of inertia forces to viscous forces in a flow and can be used to predict the point at which flow transfers from laminar to turbulent behavior [5, et al]. Even as small engines operate at higher cycle rates that increase the  $U$  term, assuming density and viscosity remain equal, the orders of magnitude reductions in  $L$  cause Reynolds numbers of micro and meso-scale engines to become very small. Preliminary Reynolds number estimation of the Cox Tee Dee 0.010 [54] yields a value of 2400; barely large enough to accommodate turbulence for enhancing mixing. Therefore, the issue of laminar flow poses a serious obstacle to combustion at engine sizes smaller than the Tee Dee 0.010 [50, 62, et al].

Another consequence of a small combustion chamber is greater heat loss that can contribute to flame quenching [2, 6, 50, et al]. Flame quenching occurs when factors such as heat loss and poor fuel mixing cause a combustion flame to extinguish before fully burning. As shown in Figure 1.6, Aerodyne’s small engine combustion model predicts heavy quenching due to cylinder-wall heat losses as engine size decreases [6].



(Source: Annen, 2003 [6])

Effect of Quenching as Engine Size Decreases

Figure 1.6

To mitigate these drawbacks of combustion in small engines, engineers have investigated ways to improve combustion efficiency using catalysts to speed reaction time [56], insulation to reduce heat loss [6], and, in the case of hobby engines, nitromethane to increase available oxygen (described in Section 1.3.2).

### 1.2.3 Scavenging

Scavenging is the process by which exhaust gases are expelled from the combustion chamber and fresh charge is introduced. Unlike in four-stroke engines, in two-stroke engines, this exchange occurs almost simultaneously during the single expansion/power stroke. Most hobby-sized engines, including the Cox Tee Dee, are loop-scavenged, which means that only the piston is used to control the opening and closing of the inlet and exhaust ports near the bottom of the cylinder wall [53]. (This process is described in more detail for the Cox Tee Dee 0.010 in Section 2.3 and depicted in Figure 2.16.)

With smaller engines, the intake and exhaust valves must be less complex and closer together. As a result, scavenging is less efficient, so the exhaust gases are not fully expelled, and thus linger in the combustion chamber to obstruct the combustion of incoming fresh charge. Losses due to combustion inefficiencies described in Section 1.2.2 exacerbate this phenomenon by lowering the temperature rise and hence the discharge pressures of exhaust gases.

Because scavenging is better controlled with complex valves and spark ignition [53], small hobby engines are at a further disadvantage for efficient scavenging because they are glow-ignited and have very simple valve systems. Research on improving scavenging in small two-stroke engines has been conducted [22], but it still remains an area of finesse and a significant challenge for overall engine efficiency [28].

## 1.3 Existing Work on Miniature Combustion Engines

While there is no solid rule for distinguishing ‘micro-scale’ from ‘meso-scale’ devices, in this work, micro-scale refers to devices with components on the millimeter scale or smaller (typically these components are constructed using MEMS fabrication techniques). Meso-scale on the other hand refers to devices on the centimeter scale. While a significant amount of research has been conducted in both size regimes, no working true micro-scale internal combustion engine has been produced to date. Meso-scale versions of micro-scale designs along with other meso-scale designs have, however, yielded some notable functionality. The difficulty of achieving a working micro engine reflects the lack of strong understanding and a lack of solutions to performance loss phenomena as engine size is scaled down. The following is a review of some of the smallest micro-scale engines that researchers are trying to develop.

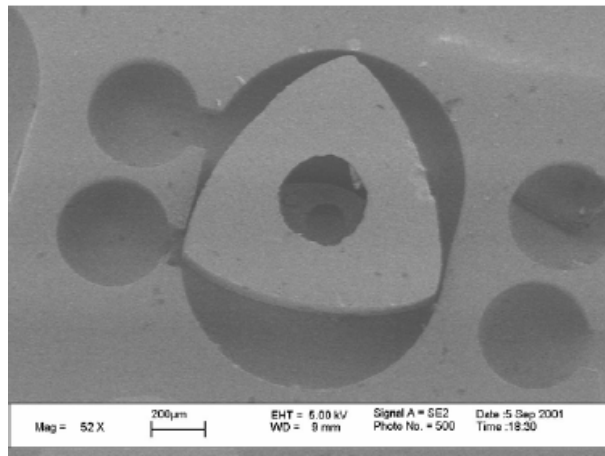
### 1.3.1 Research Engines

The engine designs listed below are either pure research projects or designs that are, for the most part, still in the developmental stage. None are yet considered as production items.

## Rotary Design

The University of California, Berkeley has conducted research funded by DARPA that seeks to develop a micro-scale rotary engine. The engine parts, including a design using a 1 mm rotor, are manufactured using MEMS fabrication techniques commonly used for microchip manufacturing. The engine uses a triangular-shaped (Reuleaux triangle) rotor to create a four-stroke combustion cycle for every revolution within an oval-shaped (epitrochoid) chamber. The advantages of the rotary “Wankel” design include high specific power, mechanical simplicity, and the planar nature of the components which facilitates manufacturing with MEMS wafer techniques [27].

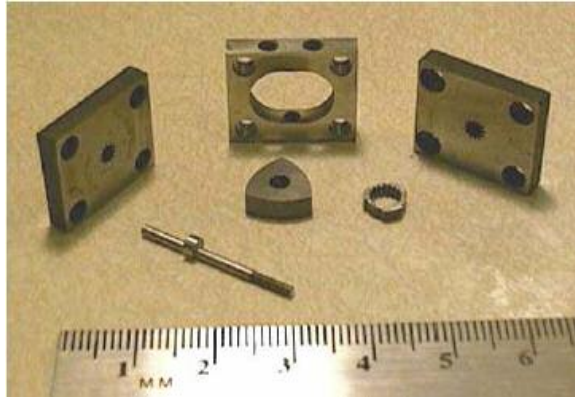
Berkeley’s MEMS Rotary Combustion Lab lists the specifications of this assembled engine as  $0.077 \text{ mm}^3$  in displacement with an estimated power output of 30 mW at 40,000 RPM and an energy density of 2,300 W-hr/kg [27, 65], however to date, no working micro-scale engine has been produced. Major obstacles to achieving a working system with this design include manufacturing, sealing, integration, and power conversion [10, 65]. The team has designed parts for two sizes of micro-scale engines. Figure 1.7 shows a photograph of the MEMS components fabricated for the larger of the two micro engines.



(Source: Fu, 2002 [27])

MEMS-Fabricated Components of the Berkeley Rotary Engine  
Figure 1.7

The Berkeley lab has also produced a meso-scale version of the rotary engine design. Unlike the micro-scale engine, this engine has been assembled, operated, and tested on a dynamometer. Major considerations for this project include assembly, sealing, fuel delivery, combustion, and thermal management [27, 65]. Figure 1.8 shows a photograph of the engine components with visible dimensions and a table of engine specifications [27].

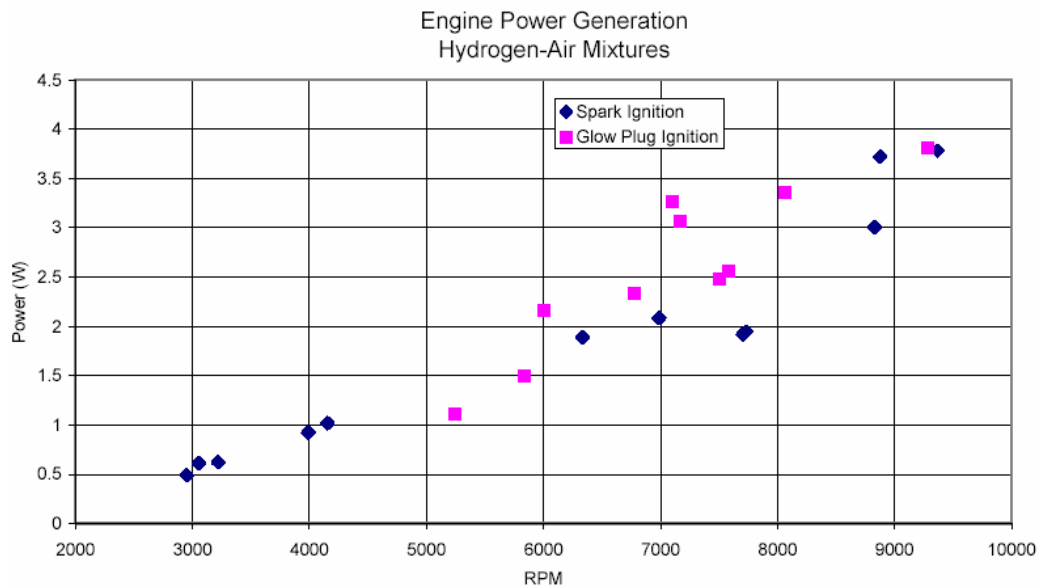


Rotor Diameter:	13 mm
Depth:	9 mm
Displacement:	348 mm <sup>3</sup>
Fuel Consumption:	62 mL/hr
CO <sub>2</sub> Output:	2086 mL/min
Heat Output:	486 W

(Source: Fu, 2002[27])

Meso-Scale Version of the Berkeley Rotary Engine  
Figure 1.8

Dynamometer testing of this engine with hydrogen has resulted in a max power output of 3.7 W at 9,300 RPM as shown in Figure 1.9, however the team projects that an output of 15 W is achievable at 30,000 RPM [27].



(Source: Fu, 2002 [27])

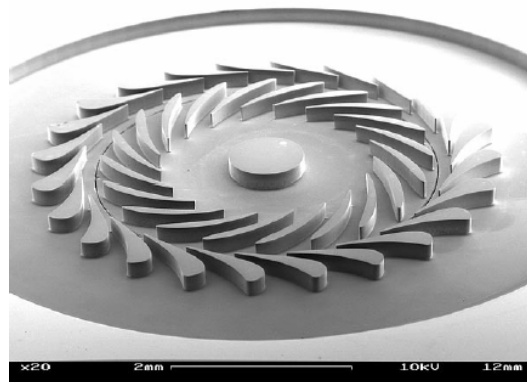
Figure 1.9

Most recently, the engine project has evolved as an application for a refrigeration compressor and work at Berkeley is continuing into the development of the rotary design for mini compression [51].

### *Turbine Design*

Several research teams have examined the design, manufacturing, and operation of miniature turbines for power generation [15, 33, 34, 68]. The leading effort is the Massachusetts Institute of Technology Gas Turbine Lab's ongoing development work

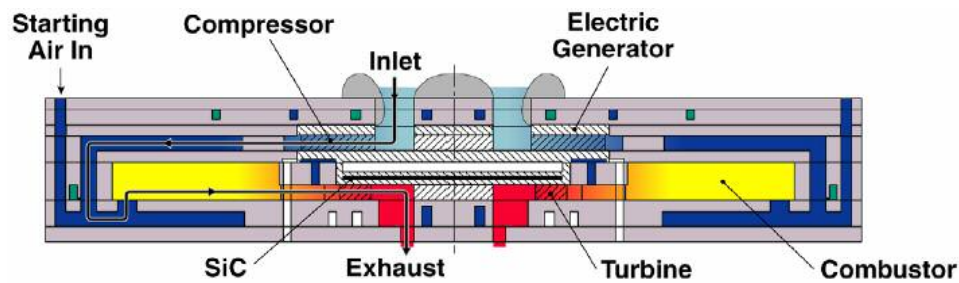
on a micro-scale gas turbine engine system. Like the Berkeley rotary engine, the parts for this device, such as the rotor shown in Figure 1.10, are manufactured using MEMS fabrication techniques with very tight tolerances [24, 25]. Accordingly, much of the research work so far has focused on manufacturing the components to correct precision while addressing sealing, friction, and rotor dynamics [29, 39, 40, 57, 68]. Other research includes improving the micro-scale combustion efficiency with catalytic processes [56] and converting the mechanical output to electric power with micro-generators [18, 59]. Notably, the team has been able to demonstrate turbocharger operation at 480,000 RPM with compressed gas, and electrical power generation of 108  $\mu\text{W}$  at 245,000 RPM with a micro-scale electroquasistatic induction generator and 1.1W at 120,000 RPM with a micro-scale permanent magnet generator [34].



(Source: Epstein , 2003 [24])

MEMS-Fabricated Rotor for the MIT Microturbine Engine  
Figure 1.10

While only individual subcomponents of the system have been tested so far, an integrated self-sustaining engine is expected to be assembled by the end of 2006 [35]. The current design involves a 4 mm rotor with an engine mass of 3.5 g and complete system mass of 10 g. Projected performance of the system is 5% efficiency at 0.95 - 1.2 million RPM with net power of 10 W and energy density of 13,000 W-hr/kg using a hydrocarbon fuel [35]. A cross-sectional diagram of the microturbine system is shown in Figure 1.11.



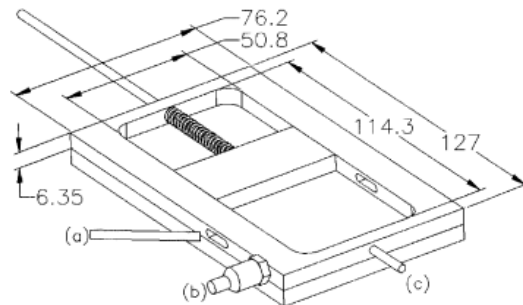
(Source: Jacobson, 2004 [34])

Cross Section of the Integrated MIT Microturbine Engine  
Figure 1.11

### Free-Piston Design

Several research teams have examined the concept of small free-piston engines [1, 6, 15, 22, 38]. Free-piston designs are attractive for engineers of miniature engines because of the simplicity of components and the lack of moving parts.

A team from the Georgia Institute of Technology (Georgia Tech) built and produced power from a slim planar free-piston design fueled by propane. The rectangular ‘flat’ geometry of the engine posed several challenges to the system including losses from inefficient scavenging and sealing, however, the thin, layered nature of the design lent itself well to fabrication by MEMS techniques traditionally used for microchip manufacturing. Figure 1.12 shows a schematic of the engine (with dimensions in mm) and Table 1.1 shows the specifications and measured performance of three different configurations [22]. Mechanical power was measured by integrating the work resulting from the volume (determined by piston position) and pressure readings from the chamber. Additionally, electrical power measurements were made by connecting the piston to a voice coil. It is worth noting that while the thickness dimension of the smallest engine is in the micro-scale regime, the length and width dimensions are rather large and perhaps better labeled as meso-scale.



(Source: Disseau, 2003 [22])

Schematic of the Georgia Tech Free-Piston Engine  
Figure 1.12

Thickness (mm)	3.175	6.35	6.35
Sealing Technique*	I	I	II
Power <sub>mechanical</sub> (W)	11.6	21.5	29.7
Power <sub>electrical</sub> (W)	1	15	N.A.
Frequency (Hz)	36	31	41
Stroke (mm)	27.2	42.4	42.4
Piston Weight (g)	54	91	91

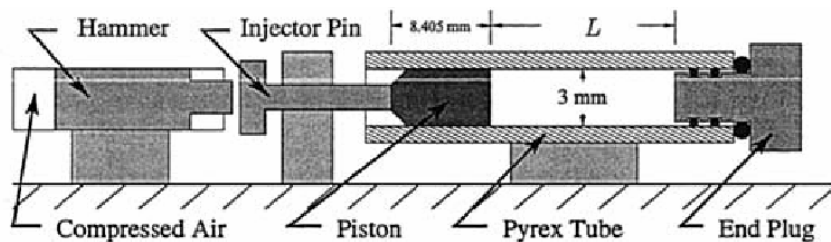
Seal technique I - frontal Teflon seal

Seal technique II - Seal Technique I + split piston design

(Source: Disseau, 2003 [22])

Specifications of the Georgia Tech Free-Piston Engines  
Table 1.1

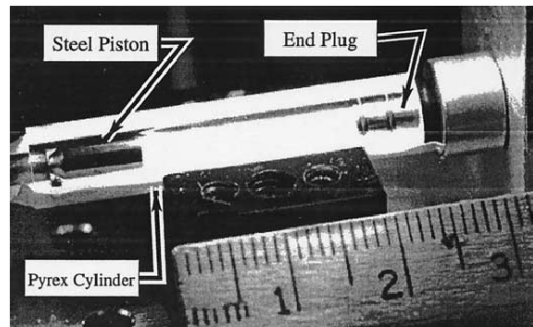
Honeywell in conjunction with the University of Minnesota has conducted research on a micro-scale free-piston ‘knock’ engine. This research investigated the micro-scale application of homogeneous charge compression ignition (HCCI); a phenomenon where the fuel-air mixture spontaneously ignites during the compression stroke. Advantages to this approach include the flexibility to ignite very lean mixtures and the characteristic that ignition occurs in multiple locations of the combustion chamber so the fuel is burned quickly [1]. This work has since concluded [3], but the team was able to demonstrate HCCI with a micro-scale free piston in single-shot experiments, develop models for the combustion and piston physics, and define design parameters that can be applied to future work in this area [1]. A diagram of the experiment is shown in Figure 1.13 and a photo of the single shot combustion experiment alongside dimensions is shown in Figure 1.14.



(Source: Aichlmayr, 2003 [1])

Schematic of the Honeywell ‘Knock’ Engine Experiment

Figure 1.13



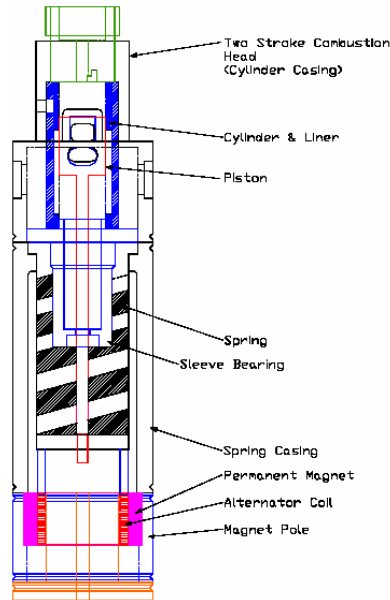
(Source: Aichlmayr, 2003 [1])

Photo of the Honeywell ‘Knock’ Engine Components

Figure 1.14

Aerodyne Research, Inc. has developed a cylindrical meso-scale free-piston engine which, like the Georgia Tech engine, uses a linearly oscillating piston anchored by a spring. The engine runs on either hydrogen or propane and uses a glow-ignited two-stroke combustion cycle to extract electrical power via an attached alternator. Notably, the researchers were able to demonstrate pure linear motion inside the cylinder with a precise double helix spring. The exact alignment minimizes wall friction and allows the engine to operate oil-free using only a solid film lining for lubrication. Based on laboratory tests, the team has estimated power output at about 3 W and conversion efficiency as high as 7.5% yielding an energy density of 640 W

hr/kg. Projections for future improved designs include a 25 g overall system mass, the capability to achieve 20 W of output power, a fuel consumption rate between 7 g/hr and 11.7 g/hr, and an energy density between 1,200 W hr/kg and 1,800 W hr/kg. The test engine shown in Figure 1.15 was developed as a 10 W design, has a mass of 15 g, and dimensions of 15 mm in diameter and 45 mm in length.

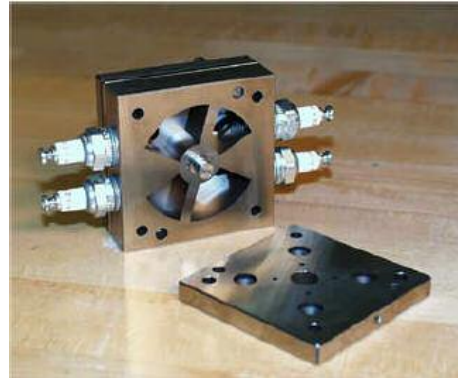
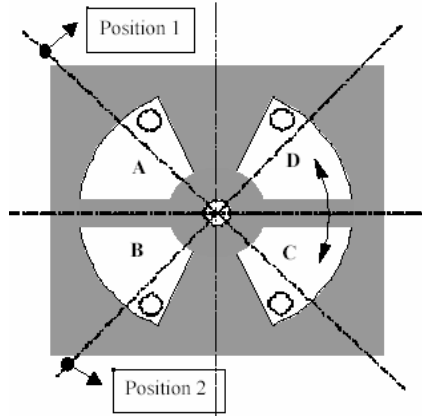


(Source: Annen, 2003 [6])

Cross Section of the Aerodyne Meso-Scale Free-Piston Engine  
Figure 1.15

### *Swing Design*

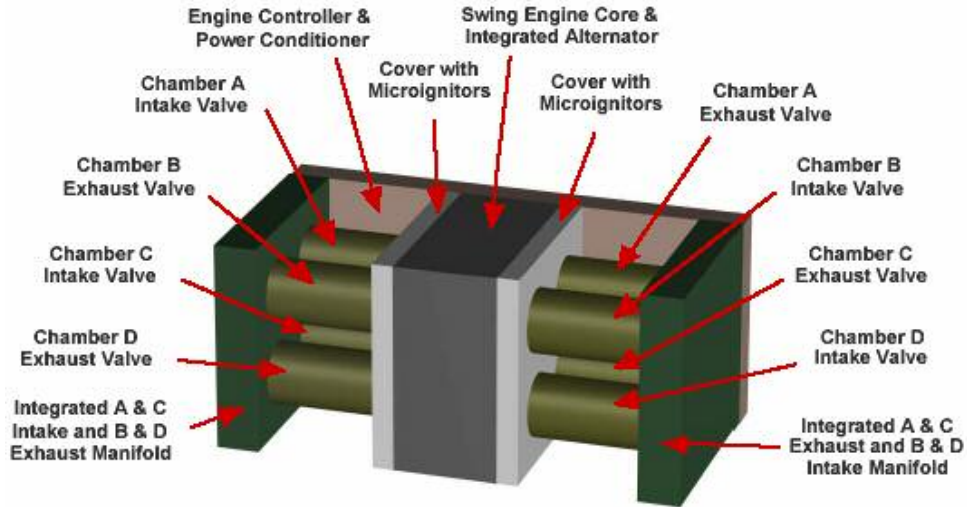
The University of Michigan has developed and packaged a meso-scale swing engine for portable power generation. This engine uses a single oscillating arm to separate two semi-circular chambers into four combustion chambers. As fuel is combusted within two diametrically opposed chambers, the arm ‘swings’ to compress the intake mixture of the other two chambers for combustion. When the other two chambers expand from combustion, the arm swings back to expel the exhaust gases and compress new intake mixture to repeat the cycle. In this method, the engine ignites all four chambers for each cycle as the swing arm oscillates back and forth in a ‘see-saw’ manner. The oscillating characteristic of the power shaft in this design presents a challenge for propeller-based propulsion, but lends itself well to electric power generation by induction. A diagram and photo of the swing engine is shown in Figure 1.16.



(Source: Dahm, 2002 [16])

Schematic and Photo of the University of Michigan Swing Engine  
Figure 1.16

This project has achieved a significant progress towards the DARPA goals relative to other small-scale power generation efforts. The team has recently been able to package the device in a compact (16.7 cc, 54 g) energy conversion system and demonstrate a net 21.1 W of electric power generation. A drawing of the integrated power generation system (without the fuel tank) is shown in Figure 1.17 along with a summary of the system specifications [16].



(Source: Dahm, 2002 [16])

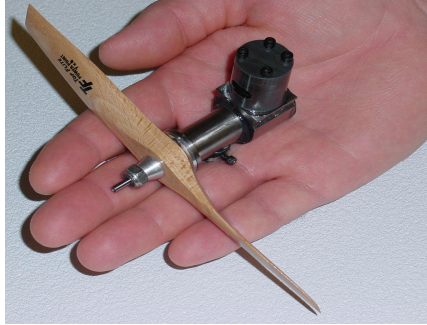
Fuel	Butane vapor, 300 K, 1atm	Swing engine mass	30.6 g
Consumption rate	1.81 (10 <sup>-5</sup> ) g/stroke	Cycle speed	102.8 Hz
Consumption per hour	13.33 g	Net work/cycle	0.152 J
Oxidizer	Air, 300 K, 1 atm	Specific fuel consump.	358.4 g/kWh
Consumption rate	5.87 (10 <sup>-4</sup> ) g/stroke	Thermal efficiency	21.90%
Consumption per hour	434.5 g	Mechanical power	37.20 W
Air-fuel mass ratio	32.6 : 1	Inductive efficiency	65%
Stoichiometric A/F ratio	15.4 : 1	Parasitic losses	3.1 W
Flame speed	87 cm/s	Net electrical power	21.1 W
Combustion duration	4 ms		

Summary of the Packaged Swing Engine Power Generation System  
Figure 1.17

### *Conventional Piston Design*

D-STAR Inc. has developed a set of diesel-fueled miniature piston engines to address small-scale power demands of unmanned aerial vehicles and portable soldier power for the military. These engines are sized similar to traditional model aircraft engines, however they do not rely on glow ignition for combustion. Instead, the engines use JP-8 diesel fuel that is readily available in mass quantities as a logistical fuel in military field operations. They have further been able to boost the power density and efficiency of these engines beyond the published performance numbers of similarly sized hobby engines [23].

The smallest design is the D-STAR 0.050 Micro-Diesel Engine shown on the left in Figure 1.18 equipped with a propeller and on the right attached to an electric generator. The 0.050 cubic inch, 2-ounce two-stroke engine produces 0.12 hp and operates at 18,000 RPM on JP-8 with 0.3% oil [20, 23].



(Source: Dev, 2004 [20])



(Source: Dev, 2004 [21])

D-STAR Micro-Diesel Engine with Propeller and Generator  
Figure 1.18

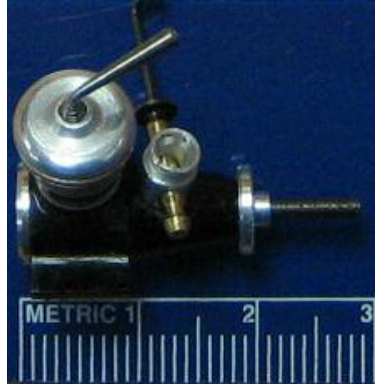
When coupled to the generator while operating on diesel fuel of lower heating value (LHV) 42.8 MJ/kg, the D-STAR system produces a net power output of 50 W with performance specifications as listed in Table 1.2 [19]. However, even with the increased performance, the overall efficiency is still relatively low.

D-STAR MGS-50 : Diesel Fueled Micro Generator Set Performance				
	Peak		Continuous	
	Current	Projected	Current	Projected
Specific Fuel Consumption (lb/HP/hr)	1.5	1.2	1.5	1.0
Fuel flow (g/min)	1.2	0.87	1.2	0.66
Engine mech output energy (MJ/kg)	3.95	4.93	3.95	5.92
Efficiency : fuel LHV to engine (%)	9	12	9	14
Overall efficiency - Fuel to DC Output (%)	5	8	5	10

(Derived from Dev, 2005 [19])

Table 1.2

The Rova Blitz is a 0.05 cubic centimeter two-stroke diesel engine with variable compression ratio built by hobby modeler Ronald Valentine for use with model aircraft. The engine is notable here because it is actually smaller than Cox Tee Dee 0.010 (0.164 cubic centimeters), but it has not been widely produced or used as a working engine within the industry and no published data exists on its performance. The Micro-Reacting Flow Lab at the University of Maryland has obtained and attempted to operate this engine (shown next to dimensions in Figure 1.19 with numbered increments in cm), but has not been able to run it successfully. Other non-production or unavailable engines of similar or smaller size over the years include the British Davies-Charlton 0.0094 cubic inch diesel Bambi, the Dragonfly, and a number of early engines by Ray Arden with displacements as small as 0.0015 cubic inches [11].



Ron Valentine's 0.05cc Diesel Rova Blitz  
Figure 1.19

### 1.3.2 Commercial Model Aircraft Scale Combustion Engines

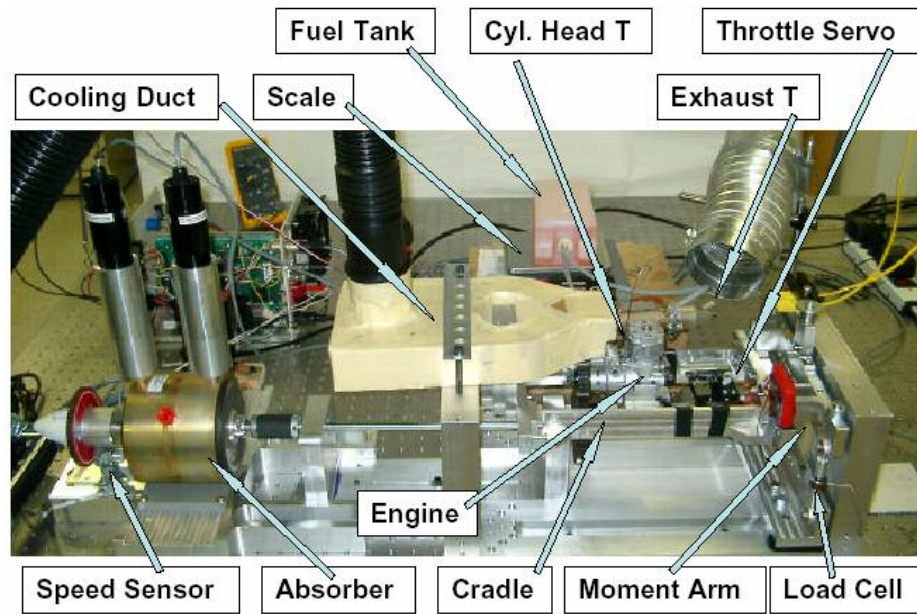
Recognizing the theoretical difficulties of the more exotic true micro-scale combustion engines, the Micro-Reacting Flow lab at the University of Maryland has focused research on the proven technologies in meso-scaled model aircraft engines. These engines are relatively inexpensive and have been tested and proven as working propulsion devices. While their excessive noise and vibration and low efficiencies present a challenge for implementation in military applications or portable power [49], by examining the loss mechanisms, performance characteristics, and scaling laws of these larger engines, researchers can gain insight into the critical design considerations of micro-scale engines. Additionally, if researchers can find ways to quiet these engines and optimize them by increasing efficiency and power output, they can be implemented immediately as power generation or propulsion for advanced miniature devices in the meso-scale regime [23].

Within the hobby industry, miniature piston engines over a wide size range have been developed, manufactured, and optimized to propel model aircraft, cars, and boats for decades [28]. Unfortunately, because these efforts are mainly undertaken in the support of recreation, scholarly and scientific research on this topic has been at a minimum. Outside of the work recently performed at the University of Maryland [7, 8, 9, 45] and a few academic publications [21, 49, 62], most hobby engine analysis has been performed for model airplane and radio-controlled magazine reviews. C. David Gierke, who has written many such articles, has published perhaps the only comprehensive book on this topic entitled *2-Stroke Glow Engines For R/C Aircraft* [28]. The book includes detailed descriptions of the physics, operation, and maintenance of model aircraft engines and was a valuable reference for the work presented in this paper.

The vast majority of hobby-class piston engines are single-cylinder, two-stroke 'glow' engines. They employ a hot glowing filament at the center of the cylinder head to ignite a specialized 'glow' fuel composed of methanol ( $\text{CH}_3\text{OH}$ ), nitromethane ( $\text{CH}_3\text{NO}_2$ ), and castor oil ( $\text{C}_{18}\text{H}_{34}\text{O}_3$ ) [45]. Methanol is the main fuel for combustion

while nitromethane is included as a boosting oxidizer. Even though the addition of nitromethane effectively lowers the energy density of the overall fuel composition, the oxygen that it provides to the reaction allows for a larger amount of fuel to be reacted per charge volume entering the engine [8]. In general, higher nitromethane content produces higher power output at the cost of higher operating temperatures and lower energy density. Castor oil is included in the fuel mixture because these engines are too small for complex lubrication delivery mechanisms. The oil lubricates the engine as it travels with the fuel, is assumed to go unburned, and largely gets expelled with the exhaust.

Early investigations into trends among engine performance found possible power scaling laws but weak conclusions on efficiency based solely on manufacturers' published data [9]. A custom dynamometer system, shown in Figure 1.20, was built to address such issues by testing the engines to obtain reliable data for comparison to the published data and to produce verifiable power and efficiency measurements [8, 45].

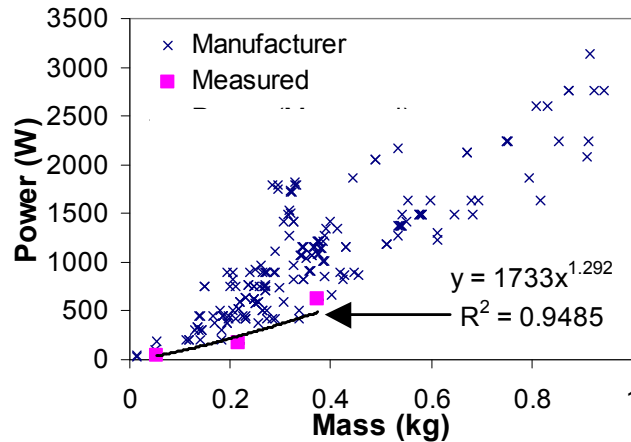


(Source: Cadou, 2003 [8])

University of Maryland's Specialized Small Engine Dynamometer  
Figure 1.20

Dynamometer data has shown strong confirmation of a power scaling law with size, but power measurements have consistently been lower than values reported by the manufacturer [7, 8, 45]. Figure 1.21 shows a comparison of measured data for three engines with previously collected data from manufacturers of over 200 engines [7]. The crosses represent the engines peak power as reported by the manufacturer while the solid squares represent power as measured in the lab on the dynamometer shown in Figure 1.20.

## Measured and Reported Hobby Engine Power Output



(Source: Cadou, 2004 [7])

Figure 1.21

There are several possible reasons for the discrepancy between reported and measured performance. One reason could be that manufacturers quote power output using high nitromethane content fuels. Another reason could be that the reported performance was recorded with different fuel delivery and mixture settings.

The measured data also confirmed the low efficiency of these engines, but has not yet been able to decipher any clear trends on sizing [7]. As with power readings, factors such as engine speed, fuel composition, and mixture settings can have significant effects on efficiency measurements. Other research into the loss mechanisms of these engines has concluded that poor mixing leading to incomplete combustion is the primary cause of energy losses [49].

To clarify these issues of performance trends and loss mechanisms, more data from a wider range of engines are needed. Of particular interest to micro-engine and miniature device engineers are the characteristics of the smallest of these engines that have demonstrated reliable power output.

### 1.4 Approach

The Cox Tee Dee 0.010 is the smallest mass-produced hobby engine and, aside from unverifiable projects such as those described in Section 1.3.1, is the smallest working piston engine known to exist. Unfortunately, no significant set of scientific data on the performance characteristics of this engine has been published. Because of its lack of formal data, proven functionality, proximity to the micro-scale regime, and convenient utility as a compact power source, the Tee Dee 0.010 (shown in Figure 1.22 next to a U.S. nickel) was chosen for examination in this work.



(Source: Cox, 2006 [14])

The Cox Tee Dee 0.010 Relative to a U.S. Nickel  
Figure 1.22

#### 1.4.1 Experiments

To assess the true operating characteristics and overall performance of the Cox Tee Dee 0.010, it will be mounted on a small custom-built dynamometer in the Micro-Reacting Flow Laboratory at the University of Maryland, College Park. The dynamometer system, described in previous work [7, 8, 45], measures engine torque, speed, fuel and air flow rates as well as a variety of temperatures. As it was initially constructed to test larger hobby engines, it will need to be modified to test the delicate Tee Dee 0.010 and accurately measure the relatively low torque output.

Since the original Tee Dee 0.010 was not designed to be throttled, a Micro-Flite modified Tee Dee will also be tested. This is simply an original Tee Dee 0.010 that has been fitted with a throttle sleeve mechanism on the cylinder.

The following data will be collected:

- torque
- speed
- fuel flow
- air flow
- cylinder/exhaust port temperature

From these, performance values including fuel/air ratio, power output, volumetric efficiency and overall thermodynamic efficiency will be determined.

#### 1.4.2 Simulation

An attempt was first made to model the Tee Dee 0.010 with Stanford University's Engine Simulation Program (ESP). This non-commercial software program was developed by the late W. C. Reynolds and calculates thermodynamic properties for the compression, combustion, expansion, and gas exchange stages of the engine cycle. As ESP was intended to simulate larger four-stroke engines, it was found to be incapable of accurately modeling the Tee Dee 0.010 (as shown in Appendix B).

As an alternative, a work-in-progress MATLAB model currently under development at the University of Maryland will be examined. While not as complex as ESP, since the MATLAB model was designed to simulate small two-stroke engines such as the Tee Dee 0.010, it has the potential for far greater accuracy. Once tailored to model the Tee Dee 0.010, the MATLAB simulation will be run and the “first cut” output will be briefly analyzed against expected engine behavior and laboratory-measured results.

## 2. Description of the Cox Tee Dee 0.010

### 2.1 History and Uses

#### 2.1.1 Inception and Manufacturing

Model aircraft engines began major development in the 1930's based much off the designs of existing two-stroke motorcycle engines. Early designs utilized spark ignition, but by 1947 the glow plug was introduced and soon became the standard. At that time, engine size group designations were: Class A for displacements smaller than 0.20 cubic inches, Class B for displacements from 0.20 cubic inches to 0.30 cubic inches and Class C for displacements from 0.30 cubic inches to 1.25 cubic inches. Later, as smaller engines were manufactured, a group referred to as 1/2A emerged for engines with displacements less than 0.097 cubic inches. [28: pg. 69].

In 1960, a respected 1/2A engine designer William Atwood (shown in Figure 2.1) joined the L. M. Cox Manufacturing Company headed by Leroy Cox. At the time, all Cox engines utilized reed valve induction, but Cox wanted engines that could produce better performance for flying competitions. As a result, Atwood designed the "TD" line of front-rotary valve induction engines named after the early Thimble Drome model cars and planes by Leroy Cox [43]. A front-rotary valve is constructed by cutting a hole of specific width into the hollow crankshaft as to allow intake gases to enter the crankshaft and crankcase at a specified crank angle. This valve design offered a dramatic improvement for hobby-sized engines because of its simplicity and reliability.



(Source: Mackey, 2001 [43])

William Atwood, 1/A Engine Designer

Figure 2.1

The "Tee-Dee" series was first released in February of 1961 and consisted of four displacement sizes: 0.010, 0.020, 0.049, and 0.15 cubic inches [63]. At the time, the Davies-Charlton company had stopped producing their 0.0094 cubic inch Bambi [11], so aside from custom projects such as those described in Section 1.3.1, the Cox Tee Dee 0.010 was then and remains today the smallest production engine in existence. Over time, this engine size and corresponding model aircraft regime has come be

known as “1/8A” class [26] (even as the Tee Dee 0.010 is technically smaller than 1/16 of the Class A limitation).

Aside from the theoretical scaling issues outlined in Section 1.2, limits on manufacturing capabilities may have been the dominant reason why Cox and others have not mass-produced a working engine smaller than the Tee Dee 0.010. The engine design required manufacturing tolerances down to 25-millionths of an inch [43], and Leroy Cox is quoted as saying, “We could reduce its size only slightly. If we get it much smaller, it becomes a jewelers job, requiring a great deal of special equipment that would run the cost way out of line.” [26]

The engine has been in production principally under the original design since 1961. In 1996, Cox was purchased by the Estes/Centuri Corporation [31], but still offers hobby products under the Cox name. In 2004, Cox granted Micro-Flite full rights to manufacture and sell the Tee Dee 0.010 with a custom fitted exhaust sleeve throttle and some minor component improvements [26]. When released in 1961, Cox sold the original engine for \$7.98 (USD) [11]. As of writing, the new engine with throttle upgrade can be purchased from Micro-Flite for \$79.99 (USD) [4]. Figure 2.2 shows a Tee Dee 0.010 in vintage 1960’s packaging (on the left) and the new Micro-Flite/Cox version in modern packaging (on the right).



(Source: Hepperle, 2005 [31])

The Original Cox Tee Dee (1960’s) and The Modern Micro-Flite Version  
Figure 2.2

### 2.1.2 Aircraft Platforms

Cox first designed the Tee Dee 0.010 for use with control line type model aircraft such as the 24.4” wingspan Thimble Drome TD-1 from 1959 (on left) and the 17.1” wingspan Thimble Drome TD-3 (on right) from 1960 pictured in Figure 2.3. When the engine was first released, there was discussion in the industry of using it for tiny

indoor flying aircraft, but the high noise and power of the engine never allowed for such realization [11].



(Source: Hepperle, 2005 [31])



(Source: Hepperle, 2005 [31])

The Control-Line Thimble Drome TD-1 and TD-3 Aircraft

Figure 2.3

However, with the advent of micro servos and radio receivers, hobbyists have adapted the small engine design to sub-sized radio control aircraft models such as the flying-wing type models shown in Figure 2.4. With the advantage of a throttle-equipped Tee Dee 0.010, modelers have also created unique implementations such as the flying kite design shown in Figure 2.5 and the six-engine 39.25" wingspan bomber design in Figure 2.6. The Micro-Flite Tee Dee has also been implemented in MAV projects at the Worcester Polytechnic Institute, the Rochester Institute of Technology, and the Milwaukee School of Engineering [26].



(Source: Jumper, 2003 [37])



(Source: Jumper, 2003 [37])

Small Radio-Controlled Aircraft Powered by the Tee Dee 0.010

Figure 2.4



(Source: Alder, 2005 [4])

Flying Kite Design Powered by the Tee Dee 0.010  
Figure 2.5



(Source: Alder, 2005 [4])

Model Bomber Design Powered by Six Tee Dee 0.010s  
Figure 2.6

Ultimately, many factors determine the kind and size of aircraft the Tee Dee 0.010 can power. Payload, fuel type, and fabrication materials all drastically affect the capabilities of an aircraft equipped with an engine of this size. The work presented here provides an attempt to examine the performance characteristics of the engine so that engineers can gain a fundamental understanding of small engine behavior and better adapt potential applications for the Tee Dee 0.010 or other engines in this size regime.

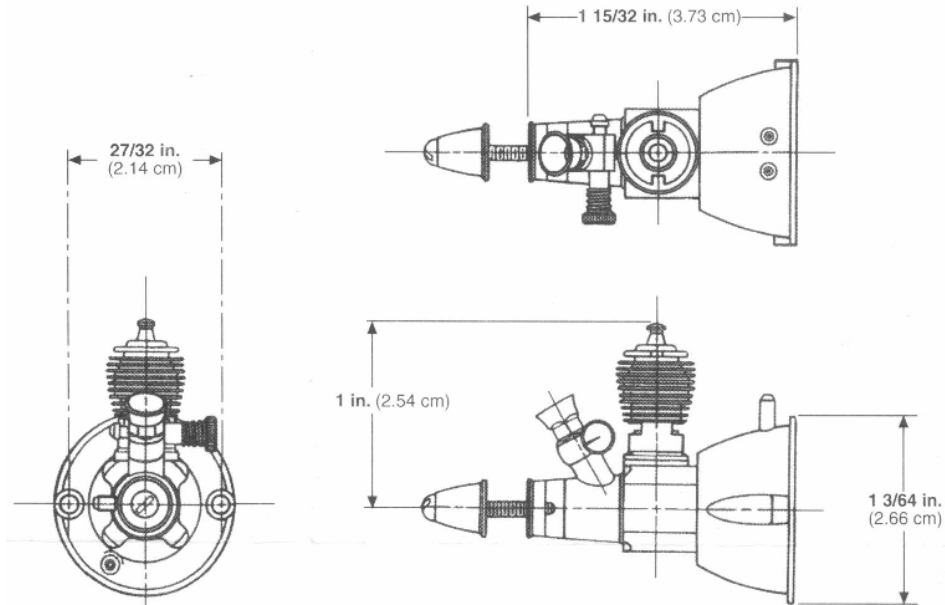
## 2.2 Engine Design and Specifications

### 2.2.1 Original Design

The Tee Dee 0.010 is a single-piston two-stroke design including a crankcase charged induction system [28: pg. 49] with a crankshaft rotary valve (a concept that originated

with model engines [28: pg. 50]) and reverse-flow or opposed porting for scavenging [28: pg. 67] (as depicted in Section 2.3). It uses a finned integral steel cylinder (without a sleeve) and a lapped (non-ringed) steel piston [28: pg. 81].

The engine has a radial mount from the back of the crankcase using a plastic cap that doubles as a crankcase seal. The engine can also be obtained with a small plastic fuel tank that doubles as the crankcase back seal and engine-mounting platform. A three-view of the engine (plus fuel tank) is shown in Figure 2.7 along with overall dimensions. Table 2.3 shows a list of specifications in SI and English units [12].



(Source: Cox, 2000 [13])

Original Cox Tee Dee 0.010 3-View

Figure 2.7

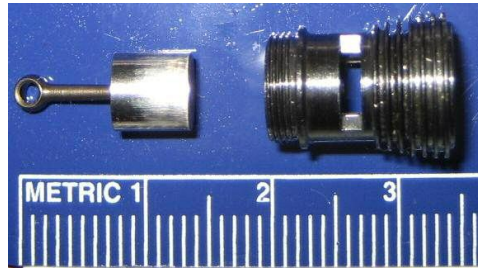
	SI	English
<b>Bore</b>	6.02 mm	0.237 in
<b>Stroke</b>	5.74 mm	.226 in
<b>Displacement</b>	0.1634 cc	0.00997 cu in
<b>Mass without tank</b>	13 g	0.46 oz
<b>Mass with tank</b>	15.3 g	0.54 oz

Original Cox Tee Dee 0.010 Specifications

Table 2.3

The connecting rod is approximately 1 cm long, the piston skirt is approximately 0.5 cm long, and the assembled connecting rod plus piston is approximately 1.3 cm long. With a stroke-to-bore ratio of 0.95, it has a slightly “over square” configuration which helps to reduce friction losses, but may leave it more susceptible to leakage losses around the large piston circumference [28: pg. 39].

The following figures show sub-components of the engine alongside measurement units (with numbered increments in cm): the disassembled piston and cylinder in Figure 2.8, the crankcase with intake housing in Figure 2.9, and the assembled cylinder with crankcase in Figure 2.10.



Tee Dee 0.010 Piston and Cylinder  
Figure 2.8



Tee Dee 0.010 Crankcase and Intake housing  
Figure 2.9



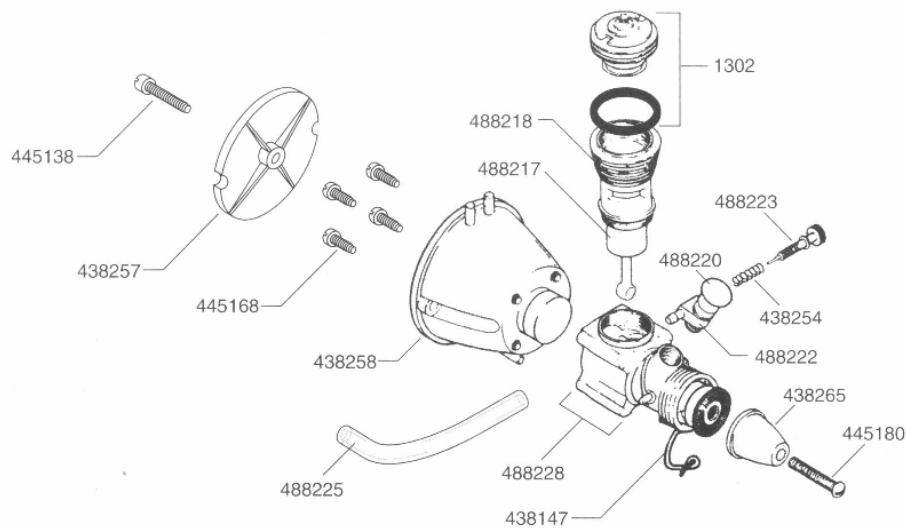
Tee Dee 0.010 Assembled Crankcase and Cylinder  
Figure 2.10

The design of the Tee Dee 0.010 is very similar to the larger Tee Dee 0.20, 0.049, 0.051, and 0.09 models. The crankcase, constructed from extruded aluminum, is attached to a nose section made of plastic. The aluminum venturi carburetor screws into the nose section and feeds the fuel-air mixture into the crankcase via a hollow

crankshaft cut with a rotary valve. A steel needle-valve assembly chokes the carburetor and is kept tight with a spring wrapped around the needle [12].

The steel cylinder is finned for enhanced cooling and is screwed directly into the crankcase. It has two opposing rectangular exhaust ports and two opposing flute transfer ports that provide the channels for charge to flow into the cylinder. The steel piston is coupled to the hardened steel connecting rod with a ball and socket joint. The cylinder head screws onto the cylinder and has a conical internal geometry with the “glow”-plug filament at the top center [12].

Figure 2.11 shows an exploded view of the engine (plus fuel tank) with individual components labeled according to their manufacturer-issued part number [13].



COX ITEM #	DESCRIPTION
CO1302	Glow Head with Gasket
438147	Starter Spring
438254	Needle Valve Spring
438257	Tank Back with Gasket
438258	Fuel Tank
438265	Propeller Spinner
445138	Screw #2-56 x 1/2"
445168	Screw #2-56 x 1/4"
445180	Screw #2-56 x 5/8"
488217	Piston/Rod Assembly
488218	Cylinder
488220	Venturi with Gasket
488222	Needle Valve Body
488223	Needle Valve
488225	Fuel Line 1 3/8"
488228	Crank Case/Carb Body/Ret

(Source: Cox, 2000 [13])

Exploded View of the Original Cox Tee Dee 0.010  
Figure 2.11

### 2.2.2 Micro-Flite Modified Design

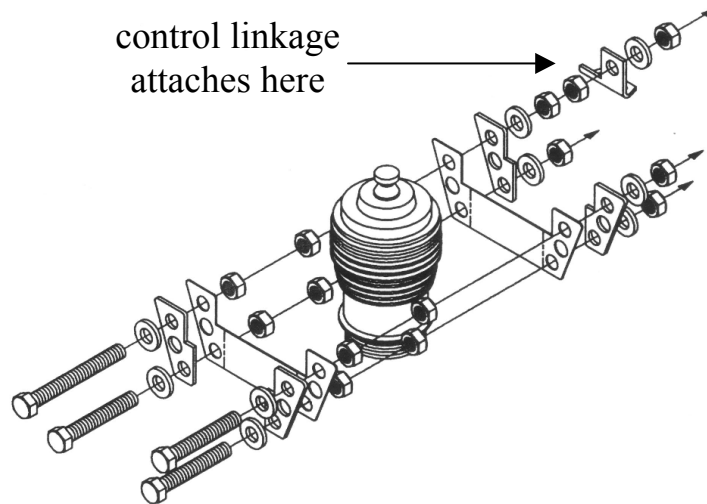
The Micro-Flite version of the Cox Tee Dee 0.010 (shown in Figure 2.12) maintains the fundamental components and operation of the original engine design. Minor component upgrades include an improved crankcase gasket to reduce pressure losses between the engine mount and the crankcase, a silicone needle valve seal to reduce leaks through the needle valve and damp vibrations, and a socket head cap to allow for needle valve adjustments from a safe distance with a ball driver wrench [26].



(Source: Alder, 2005 [4])

The Micro-Flite Modified Tee Dee 0.010  
Figure 2.12

The most significant feature in the Micro-Flite engine design is the copper sleeve attachment around the exhaust ports of the cylinder which serves as an exhaust-baffle-based throttle system. The original Tee Dee 0.010 was designed for control line aircraft and therefore lacked a throttle mechanism. The Micro-Flite upgrade adds this significant capability to the engine so that it may be used with full four-channel (three control surfaces and one throttle) radio controlled aircraft systems. An exploded diagram demonstrating the sleeve attachment to the Tee Dee 0.010 cylinder is shown in Figure 2.13.



(Source: Freiheit, 2005 [26])

Exploded View of Micro-Flite Throttle Mechanism

Figure 2.13

The sleeve fits snugly when the engine is cold but undergoes thermal expansion as the cylinder becomes hot in order to maintain the proper baffle capability. When a servo arm is attached to provide external control, the sleeve is designed to slide around the exhaust port section of the cylinder so that the servo varies the effective exhaust port opening. By limiting the exhaust flow, the sleeve limits the charge flow rate through the engine and hence limits the speed and power output. With this throttle system, Micro-Flite has claimed to achieve an idle as low as 4,400 RPM and a wide-open throttle speed over 29,000 RPM [26]. An extensive explanation of the construction, operation, and performance characteristics of this custom throttle device is included in Micro-Flite's *"1/8A" ENGINE MANUAL & HANDBOOK* [26], therefore further description will be withheld here.

### 2.3 Cycle Description

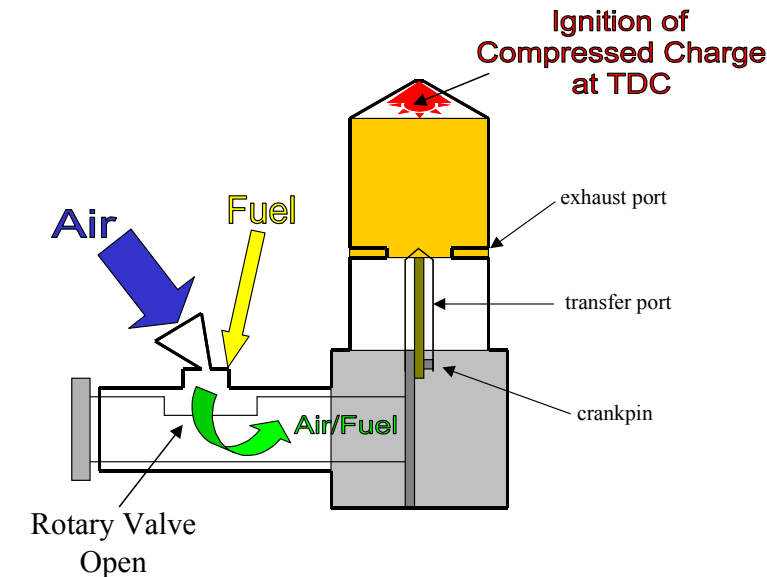
For the purposes of this paper, the two-strokes that comprise one complete cycle of the Tee Dee 0.010 will be referred to as the power stroke and the compression stroke. The power stroke will refer to the first half of one crankshaft revolution when the piston travels from top dead center (TDC) to bottom dead center (BDC), or when the crankpin travels from  $0^\circ$  to  $180^\circ$ . The compression stroke will refer to the second half of one crankshaft revolution when the piston travels from BDC to TDC, or when the crankpin travels from  $180^\circ$  to  $360^\circ$ .

#### 2.3.1 Power Stroke

At the beginning of the power stroke, the piston is at TDC and the charge is fully compressed within the cylinder. The hot glow plug ignites the charge and initiates the expansion of hot combustion gases that begins to push the piston downward as shown

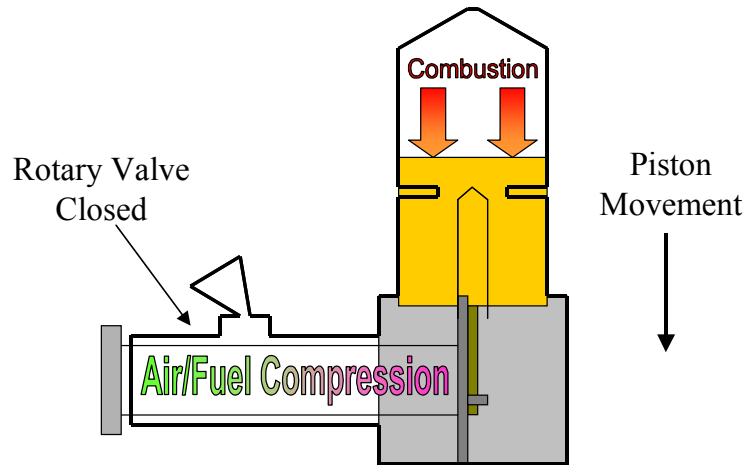
in Figure 2.14 (not to scale). (In reality, the exact time of ignition can vary, but for the purposes of this cycle summary, ignition is assumed to occur at TDC.)

Also during this time, the front rotary inlet valve (which is simply a 0.18 inch x 0.09 inch rectangular hole [66] cut into the hollow crankshaft) is open and fresh air is pulled through the conical venturi of the intake assembly. As the air is pulled in, fuel is atomized from the needle valve through pinholes located at the bottom of the venturi. The combined fuel and air mixture is pulled into the hollowed-out crankshaft and crankcase by a pressure differential created during the previous compression stroke. That pressure differential is created because the vertical motion of the piston increases the volume of the crankcase thereby lowering the pressure in the crankcase.



Ignition and Beginning of the Tee Dee 0.010 Power Stroke  
Figure 2.14

As the piston travels downward and the crankshaft rotates, the inlet valve closes at approximately  $30^\circ$  from TDC. After it is closed, the fresh fuel-air mixture is sealed within the crankshaft and crankcase. As the piston descends, it reduces the volume of the crankcase and therefore compresses the air-fuel mixture as shown in Figure 2.15.

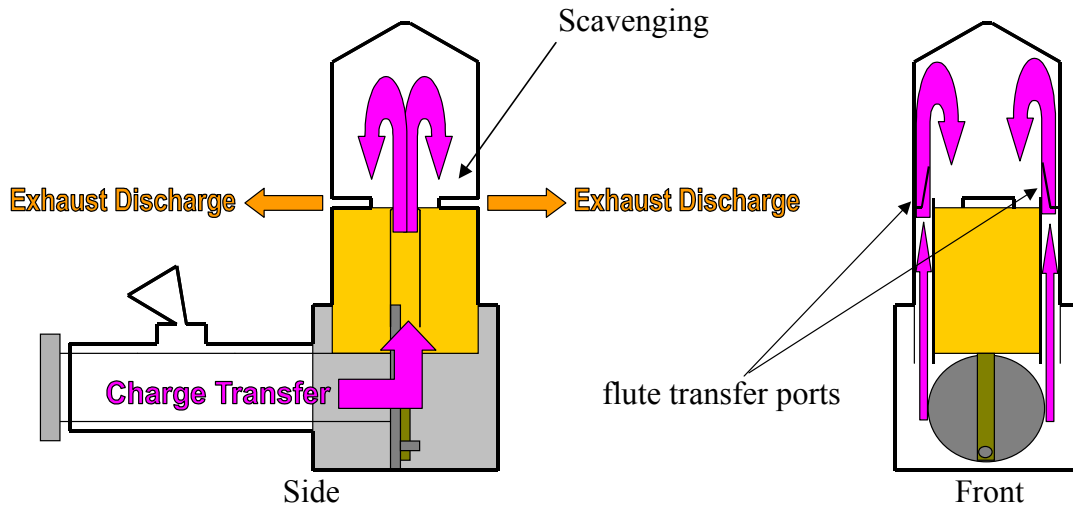


Cox Tee Dee 0.010 Power Stroke  
Figure 2.15

Continuing along the power stroke, at approximately  $120^\circ$  from TDC, the piston's top surface will begin to pass the exhaust ports cut into the sides of the cylinder. As this happens, hot high-pressure combustion gases start to discharge through the ports into the atmosphere. Shortly after, at approximately  $140^\circ$  from TDC, the piston will begin to uncover the transfer ports that connect the crankcase to the cylinder via flute notches in the cylinder wall. The opening of the transfer ports initiates the transfer of the compressed air/fuel charge from the crankcase into the cylinder.

### 2.3.2 Compression Stroke

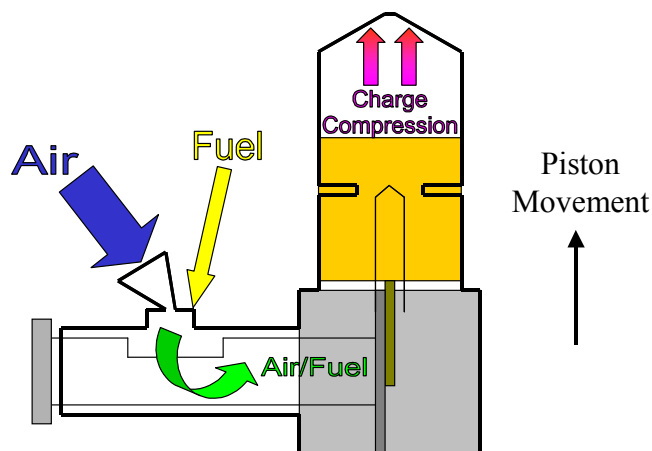
When the piston reaches BDC, the power stroke has ended, the exhaust ports and transfer ports are fully open, and the compression stroke begins. At this point, as shown in Figure 2.16, the critical act of scavenging occurs with the exchange of old and new charge from the cylinder. This is when the pressurized charge from the crankcase floods the cylinder through the transfer ports and helps to push out the exhaust gases that are already discharging due to the pressure differential with the external atmosphere. Ideally, all of the combusted gases will escape from the cylinder and only the fresh charge will remain. In reality, scavenging is imperfect, so some exhaust gases remain and some fresh charge gets expelled to the atmosphere. This lack of scavenging efficiency is a major cause of performance losses in small two-stroke engines as described in Section 1.2.3. At very high RPM, another major loss mechanism is the drop in volumetric efficiency that occurs as the naturally aspirated engine becomes less capable of pulling in air fast enough from the ambient atmosphere.



Scavenging and the Beginning of the Tee Dee 0.010 Compression Stroke  
Figure 2.16

As the piston ascends upwards from BDC, the piston surface begins to close the transfer and exhaust ports. At approximately  $220^\circ$  from TDC, the transfer ports fully close and the exhaust ports fully close soon after at approximately  $240^\circ$  from TDC. With the exhaust and transfer ports closed, the new charge is sealed in the cylinder and is compressed as the piston moves toward TDC.

The inlet valve begins to open at approximately  $250^\circ$  from TDC, becomes fully open at approximately  $310^\circ$ , and then begins to close at  $330^\circ$ . When the piston ascends upward, it increases the volume of the crankcase region and therefore creates a negative pressure differential with the external atmosphere. The resulting suction pulls in fresh air and fuel from the intake assembly when the inlet valve opens as shown in Figure 2.17.

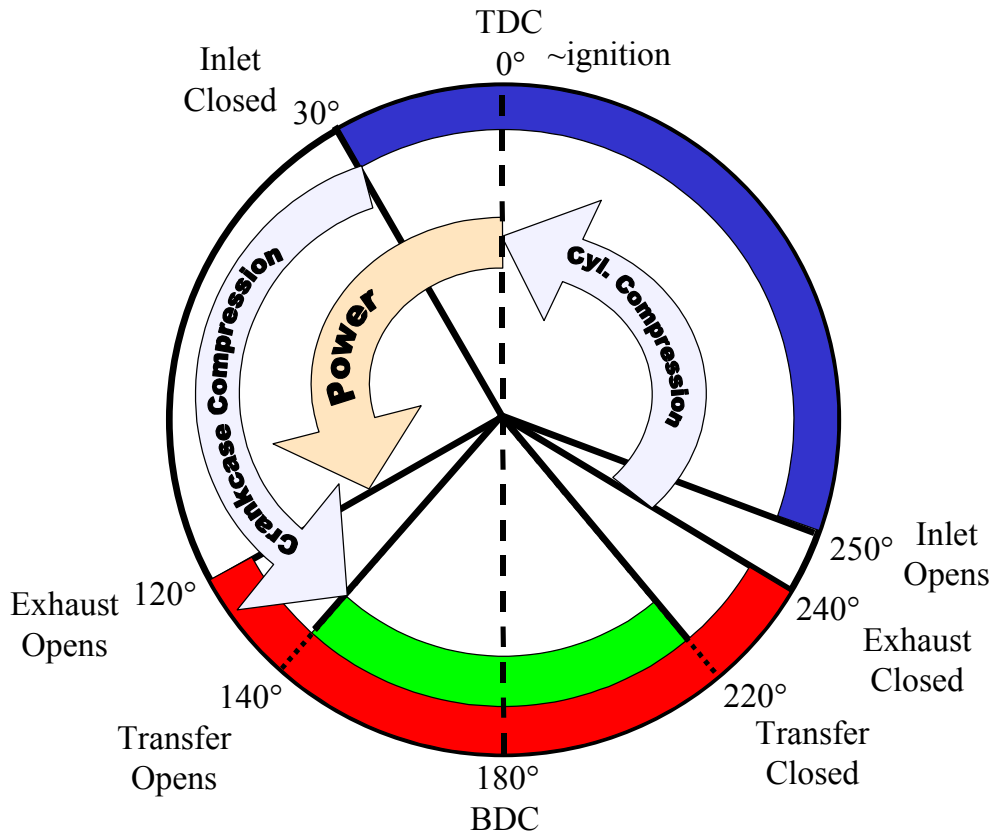


Cox Tee Dee 0.010 Compression Stroke  
Figure 2.17

Once the piston has reached TDC, the compression stroke ends, the charge ignites to begin the power stroke, and the entire cycle then repeats itself (from Section 2.3.1).

### 2.3.3 Timing Diagram

Figure 2.18 is a timing diagram summarizing the major events during the two-strokes including valve and port timing with corresponding crankpin locations based on approximate measurements. The solid blue region (from 250° to 30°) identifies when the air-fuel inlet valve is open, the solid red region (from 120° to 240°) identifies when the exhaust ports are open, and the solid green region (from 140° to 220°) identifies when the charge transfer ports are open. The striped orange region identifies the power-producing portion of the cycle and the striped blue regions identify charge compression portions of the cycle.



Cox Tee Dee 0.010 Timing Diagram  
Figure 2.18

## 2.4 Fuel

### 2.4.1 Background

Two-stroke model engines such as the Tee Dee 0.010 run on a specialized fuel mixture referred to as “glow” fuel (named after the glow plug used for ignition). As mentioned in Sec 1.3.2, this fuel is actually a combination of fuel, lubricant, and often oxidizing booster.

The main fuel agent, methanol (CH<sub>3</sub>OH), is the first oxidation product of methane and is usually the most abundant substance in glow fuel mixtures [60]. The combustion of pure methanol produces an almost invisible flame in air and is described in Equation 2.1. Methanol is also hydrophilic; so if left in an open container, it will quickly absorb water vapor from the air and degrade the effectiveness of the fuel mixture [60].



Lubricant is included in glow fuel because model engines are often too small to utilize complex lubricant delivery systems. Traditionally, pure castor oil (C<sub>18</sub>H<sub>34</sub>O<sub>3</sub> [47]) has been used for lubrication, however varying amounts of synthetic oil are also used in some blends. Castor oil has a spontaneous ignition temperature below that of methanol [49], but as a lubricant, is intended to go unburned as it travels through the engine. In reality, some of the oil probably burns (with combustion as described in Equation 2.2) and may significantly affect the performance characteristics of the engine [45].



Depending on the engine and operational application, glow fuels can contain widely varying amounts of an oxygen-rich booster in the form of nitromethane (CH<sub>3</sub>NO<sub>2</sub>). As shown by the combustion reaction in Equation 2.3, twice the mols of nitromethane will react with the same 3 mols of oxygen relative to methanol. Translating to a mass basis, this means that methanol requires four times the airflow required by nitromethane to fully react [28: pg. 18].



Therefore, even as nitromethane has a lower energy content [49] and burn speed [28: pg. 18] than methanol, the extra oxygen it carries allows it to react four times the fuel mass per given charge of air in the combustion chamber. For this reason, at the expense of higher temperatures and excessive wear on the engine, nitromethane is extensively used in small engines where air induction is less efficient relative to larger engines.

## 2.4.2 Subject Blend

Model engine fuels typically have an oil content of 10%-20%, a nitromethane content of 0-50%, and the remaining percentage of methanol by volume [49]. Magazine reviews suggest a minimum of 10% nitromethane is required to run the Tee Dee 0.010 [66], however, most fuel mixtures marketed for 1/2A size engines contain at least 25% and competition fuel blends may contain up to 50%. The fuel (shown in Figure 2.19) used for the experimental work presented in this paper is a customized blend developed by Micro-Flite for optimal performance of the Micro-Flite Tee Dee 0.010 containing 35% nitromethane, 45% methanol, and 20% pure castor oil.

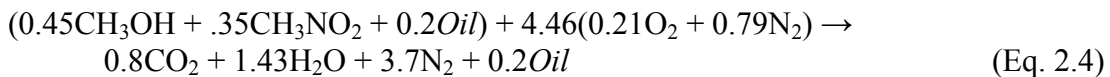


(Source: Alder, 2005 [4])

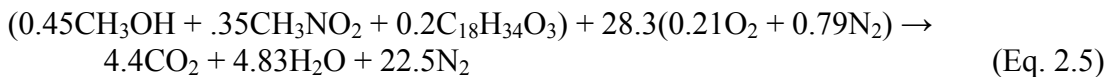
Micro-Flite Customized Tee Dee 0.010 Fuel

Figure 2.19

Using the known ingredient percentages in the Micro-Flite mixture and the percentage of oxygen and nitrogen in air, a theoretical combustion reaction can be balanced as shown in Equation 2.4 assuming the oil does not react. The stoichiometric fuel/air ratio is 0.224 by moles and 0.742 by mass. The stoichiometric fuel/mixture (i.e. fuel/(fuel+air)) ratio by mass is 0.426. If the presence of oil is ignored completely, the isolated combustion reaction has a stoichiometric fuel/air ratio of 0.278 by mass and the stoichiometric fuel/mixture ratio is 0.218 by mass.



If we assume the oil is completely burned, the reaction is described in Equation 2.5. The fuel/air ratio is 0.0353 by mols and 0.117 by mass. The fuel/mixture ratio by mass is 0.105.



Using Equations 2.4 and 2.5, the overall fuel mixture density and energy content can be calculated with Equations 2.6 and 2.7 [45] as shown in Table 2.4 where  $\chi$  is mols,  $\rho$  is density, and  $Q_r$  is lower heating value (energy content) of the reaction. The subscripts *mix*, *m*, *nm*, and *o* denote mixture, methanol, nitromethane and oil respectively. The mixture energy content assuming inert oil is calculated using Equations 2.4 and 2.5 with the oil terms neglected.

$$\rho_{mix} = \rho_m \chi_m + \rho_{nm} \chi_{nm} + \rho_o \chi_o \quad (\text{Eq. 2.6})$$

$$Q_{r,mix} = \frac{Q_{r,m} \rho_m \chi_m + Q_{r,nm} \rho_{nm} \chi_{nm} + Q_{r,o} \rho_o \chi_o}{\rho_{mix}} \quad (\text{Eq. 2.7})$$

Component	$\chi$	$\rho$ (g/cm <sup>3</sup> )	$Q_r$ (kJ/g)
Methanol (CH <sub>3</sub> OH)	0.45	0.79	22.60
Nitromethane (CH <sub>3</sub> NO <sub>2</sub> )	0.35	1.11	11.60
Castor Oil (C <sub>18</sub> H <sub>34</sub> O <sub>3</sub> )	0.20	0.96	44.00
Mixture	1.00	0.94	<b>22.33</b>
Mixture (Oil Inert)	1.00	0.94	<b>16.86</b>

Micro-Flite Tee Dee 0.010 Fuel Properties  
Table 2.4

These values can then be used along with performance measurements to determine metrics such as thermodynamic efficiency as demonstrated in Section 5.

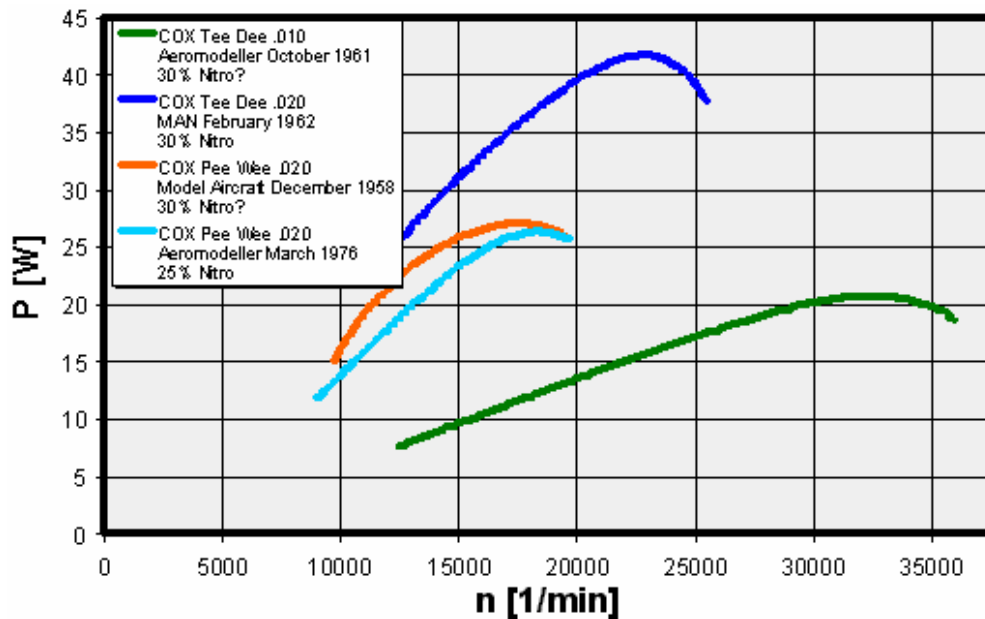
### 2.5 Performance

To date, almost all reports of the Tee Dee 0.010 performance exist in model aircraft periodicals where authors and readers are primarily concerned only with maximum achievable speed using various propellers. Table 2.5 lists some Tee Dee 0.010 speed data published in various periodical reviews with corresponding propeller sizes [11, 12, 66] (where diameter is the length of the entire propeller and pitch is the distance the propeller would travel after one revolution in a perfect fluid [36]).

Propeller Diameter (inches)	Propeller Pitch (inches)	% Nitro	RPM
5.5	4.00	>=10	5,500
6	3.00	>=10	5,800
5.25	3.00	>=10	6,000
5	4.00	>=10	6,000
5	3.00	>=10	7,000
5.25	3.50	>=10	7,800
4.5	2.50	?	9,600
4.5	3.00	30?	10,800
3	1.25	30	27,400
2.875	1.25	?	27,500
2.75	1.25	?	28,600
2.625	1.25	?	29,800
2.5	1.25	50	32,400

Published Tee Dee 0.010 Propeller Performance  
Table 2.5

Very few sources have suggested an actual power rating for the Tee Dee 0.010. Paul Ronney lists the output power as 3 W in a University of Southern California lecture on microcombustion [54], but provides no source or method for arriving at that value. Figure 2.20 shows other data compiled from several periodical reviews of the Tee Dee series including the 0.010 (shown as the bottom curve in green). According to the plot, the engine is capable of power output ranging from approximately 7.5 W to 21 W and speeds over 35,000 RPM using perhaps a 30% nitromethane mix. The relatively flat nature of the curve suggests the Tee Dee 0.010's performance may not be as closely tied to RPM as larger engines.



(Source: Hepperle, 2005 [31])

Published Cox Tee Dee Power Output  
Figure 2.20

While the existing performance data may provide a rough baseline, they lack detailed experimental documentation and were not obtained under repeatable conditions. Fuel composition and air-fuel mixture settings, for instance, are known to dramatically affect the performance capabilities of these engines [45]. To address this issue, the work presented in this paper is an attempt to provide a reliable set of performance data acquired under well-documented and repeatable conditions.

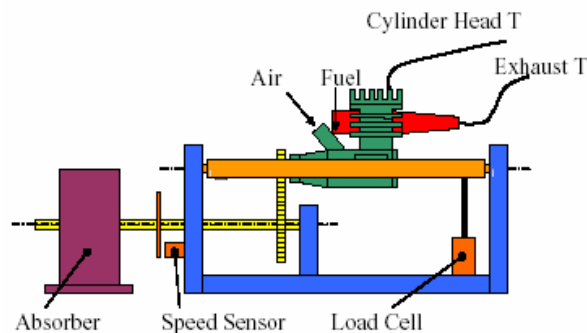
## 3. Performance Measurement

### 3.1 Dynamometer Apparatus

#### 3.1.1 Previous Configuration (First Iteration)

A specialized dynamometer was used to measure the performance of the two Tee Dee engine versions. As a starting point, an attempt was first made to use the exact dynamometer configuration used in previous model aircraft engine testing at the University of Maryland as described in Section 1.3.2 and pictured in Figure 1.20.

In that configuration (diagramed in Figure 3.1), the engine is mounted in a freely rotating cradle and attached to a hysteresis brake that serves as the external load via a geared shaft. Unlike other dynamometers for small engines [49] that measure the torque produced at the drive shaft of the engine while the engine is mounted rigidly, this configuration measures the reaction torque produced at the cradle support when a load is applied to the drive shaft. The advantage of this method is that no corrections for losses in gear train (transmission) are required. This is important because these losses are unknown and can be quite large relative to the power produced by the engine.



(Source: Cadou, 2003 [8])

Diagram of Original Dynamometer Design

Figure 3.1

A load cell is used to measure the downward force exerted on it by a rigid linkage as the engine reaction torque rotates the cradle. Because the connection distance of the linkage from the center of rotation (the moment arm) is known, the torque created by the engine can be simply calculated using Equation 3.1 where  $r$  is the moment arm length,  $F$  is the force registered by the load cell, and  $\Gamma$  is the calculated engine torque.

$$\Gamma = F \cdot r \quad (\text{Eq. 3.1})$$

Other measurements include airflow, fuel flow, cylinder temperature, and shaft rotational speed. It was found that a plenum was required between the intake and

airflow meter in order to damp cycle oscillations for an accurate steady-state airflow reading.

A computer collects the data with a Lab View based data acquisition interface in a burst capture mode. The burst mode is manually activated at the desired time and captures a fixed set of points at regular time intervals (as described in Section 3.2). During post-processing, the captured datum points for each burst collection are then averaged to obtain one value for each collection event. Sources of error for this configuration are the uncertainty in the load cell, speed sensor, airflow sensor, and fuel flow sensor.

Table 3.1 lists the instruments used in the system along with the purpose, data type, and systematic uncertainty for each. Previous work contains detailed discussion, theoretical background, and verification for each component of this dynamometer configuration [8, 45], so further explanation will be withheld here.

Component	Purpose	Data Type	Uncertainty
Sensotek 31 5-lb load cell	engine torque	voltage	0.0079 V
Omega steel-sheathed K type thermocouple	cylinder temperature	degrees C	--
TSI 4021 airflow sensor	massflow of air	voltage	2% V
DEA Engineering FMTD4 microflowmeter	massflow of fuel	frequency	0.5% freq
ElectroSensors magnetic speed sensor	engine speed	voltage	0.1% V
Magtrol HB-880 double hysteresis brake	load control	torque	--
Lab View data acquisition system	data logging	voltage	0.005 V

Components of Original Dynamometer Design  
Table 3.1

To start the engine with this setup, a starter motor is manually applied to the end of the brake shaft while terminals attached to a separate battery heat the glow plug. Once the engine is started, the starter motor is removed and the fuel mixture setting is leaned until maximum RPM is achieved.

Unfortunately, when the engine was tried in this configuration, it was found to be incapable of sustained operation. With the starter motor engaged, the engine “turned over” as combustion firing was heard, but when the starter was removed, the engine quickly wound down to a stop. When the hysteresis brake was removed in an attempt to lower the dynamic friction of the shaft, the engine started, but could only turn at a RPM well below its normal speed.

Problem: Resistance of hysteresis brake/transmission system was too large.

Solution: Replace brake/transmission with a lower friction DC motor/generator attached directly to the engine. Varying the load resistance across the generator varies the load applied to the engine enabling power curves to be measured.

### 3.1.2 Modified Configuration (Final Iteration)

After noting that the engine had difficulty overcoming the dynamic friction of the gear and hysteresis brake in the original dynamometer configuration, an attempt was made to redesign the load control device.

To avoid the gear interface, the modified load design involves coupling a small electric direct current (DC) motor directly to the drive shaft of the engine. The chosen brushed motor runs on 9V-12V, is rated to 27,000 RPM, and is mounted on an assembly of aluminum rods composing a stiff lattice that is fixed to the cradle base.

To start the engine in this design, the DC motor is connected to an external 12 V battery to apply the starting torque to the drive shaft as shown in the diagram of Figure 3.2. Once the engine is started, the DC motor terminals are disconnected from the battery and reconnected to a 1 K-ohm variable resistor (or rheostat). At this point, the engine and DC motor assembly acts as an electric power generator and engine load is dynamically controlled simply by varying the resistance of the circuit via the variable resistor as shown in the diagram of Figure 3.3.

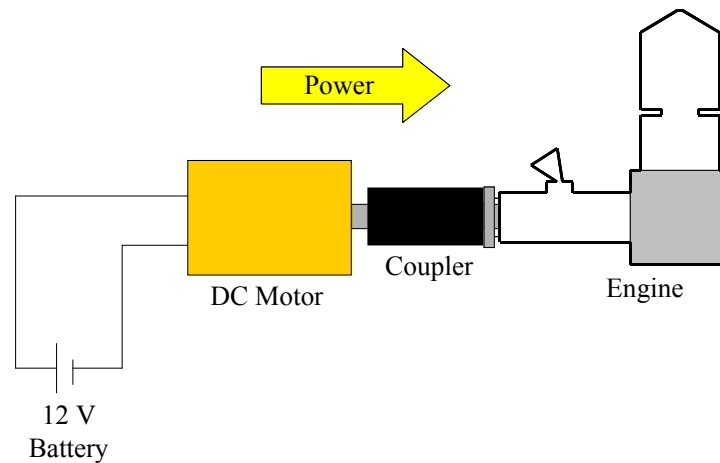


Diagram of Modified Dynamometer Starter Configuration  
Figure 3.2

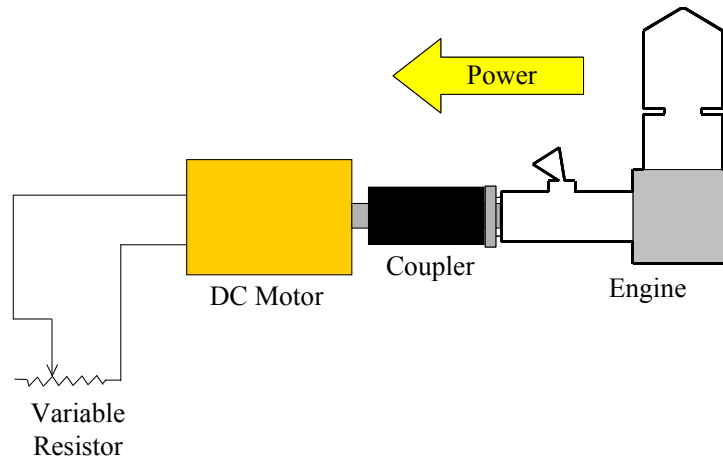
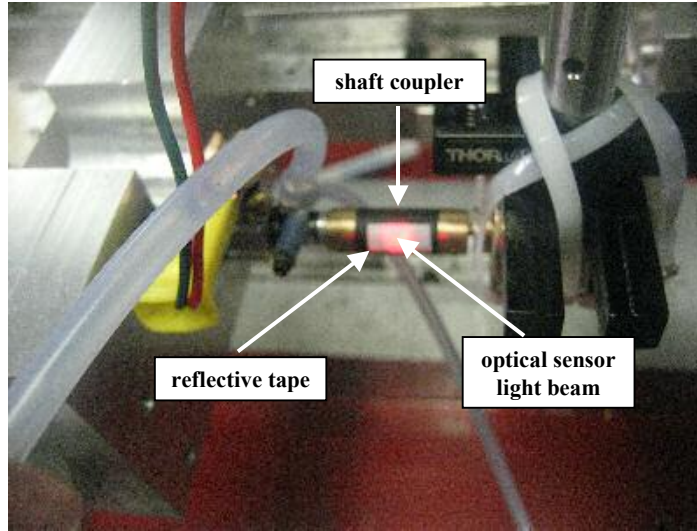


Diagram of Modified Dynamometer Load-Control Configuration  
Figure 3.3

After reducing the moment arm to a length of 1 inch, most of the new design remains the same as the original. Due to the lower airflow rates, however, a smaller rectangular air plenum (approximately 7 x 3 x 2 inches) was used in order to minimize losses. Additionally, the relatively low fuel flow was determined by measuring the change in mass of the fuel tank on an electric scale over a measured period of time.

Since the speed sensor of the original configuration was attached to the brake shaft, a new device had to be implemented to measure shaft speed. For this modified configuration, the shaft speed was collected with the use of a remote optical sensor and a piece of reflective tape on the shaft coupler as shown in Figure 3.4. The advantage of using this method is that no additional attachments were needed on the shaft which might add inertia and increase the dynamic friction. Each revolution of the shaft causes one pass of the tape that reflects light back to the active sensor that then produces a square voltage pulse counted by an attached oscilloscope. The oscilloscope output is then logged to an Excel spreadsheet via a data acquisition (DAQ) interface.

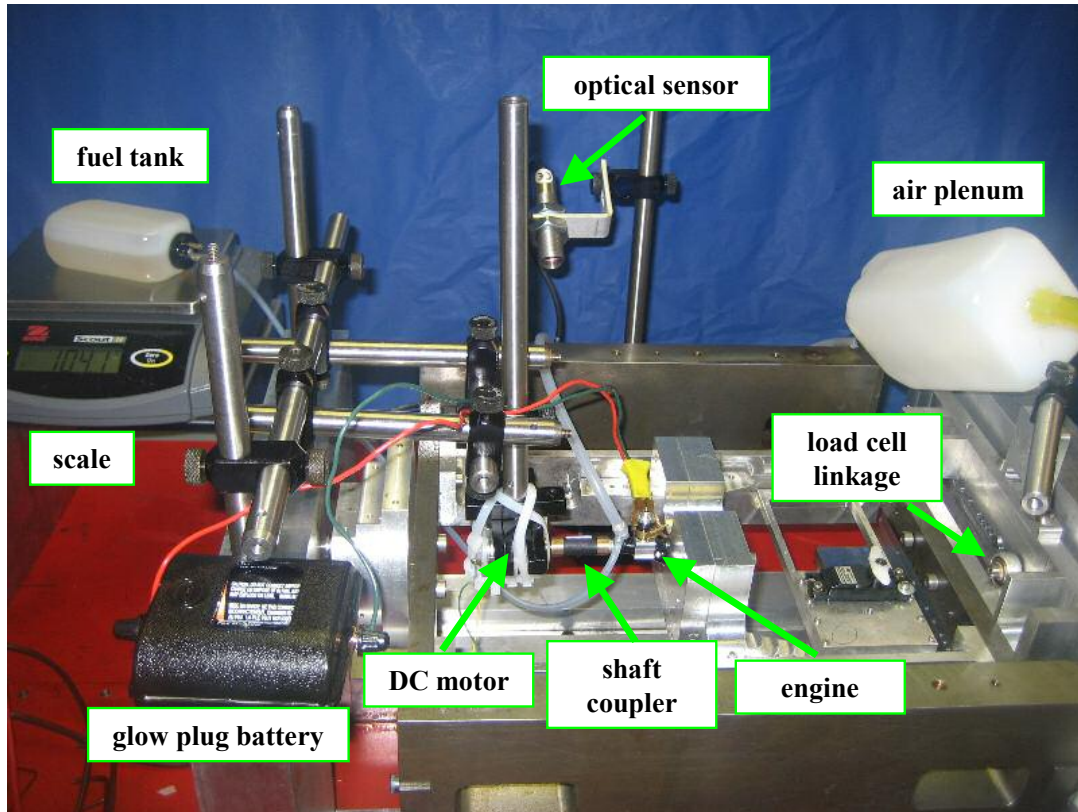


Reflective Tape and Remote Speed Sensor Beam Positioning  
Figure 3.4

Table 3.2 lists the instruments used in the experiment along with the purpose, data type, and systematic uncertainty for each device. Figure 3.5 shows the complete setup with labeled components.

Component	Purpose	Data Type	Uncertainty
Sensotek 31 5-lb load cell	engine torque	voltage	0.0079 V
steel-sheathed K type thermocouple	cylinder temperature	degrees C	--
TSI 4021 airflow sensor	massflow of air	voltage	2% V
Ohaus Scout portable electric scale	massflow of fuel	grams	0.1 g
Monarch Instrument ROS-W optical sensor	engine speed	frequency	--
Clarostat 73JA 1K Variable Resistor	load control	ohms	5% ohms
Lab View data acquisition system	data logging	voltage	0.005 V

Components of Modified Dynamometer Design  
Table 3.2

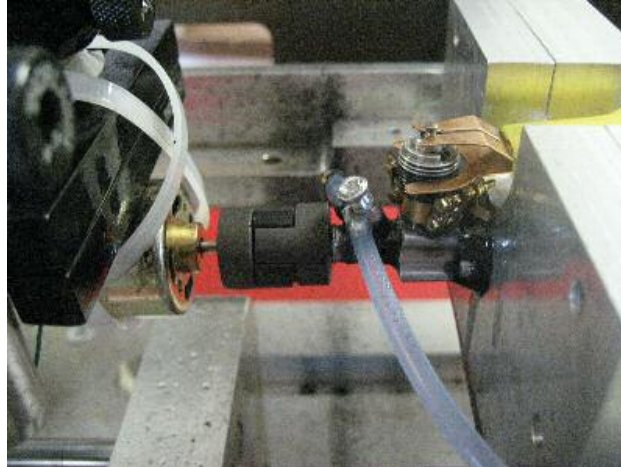


Complete Modified Dynamometer Configuration  
Figure 3.5

*Shaft Coupling Issues:*

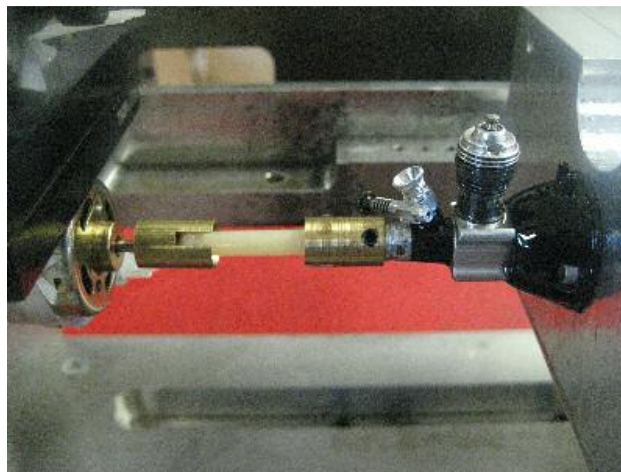
When this design was first configured, difficulty was once again encountered with starting the engine. Suspecting that the issue may have involved the direct drive shaft coupling, several coupling designs were used in order to achieve the smoothest and most secure rotation possible.

Figure 3.6 shows the first coupling that was tried: a three-piece “spider” coupling from McMaster-Carr. The rubber “spider” insert of this coupling provides compensation for axial compression and lateral misalignment of the shaft. Because the three pieces are not attached to each other, this coupling provides no axial tension. After repeated attempts, the engine was able to successfully “turn-over”, but was unable to run sustained.



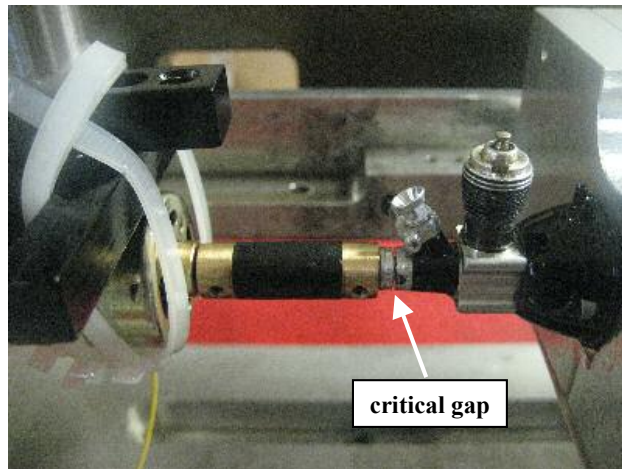
Three-Piece “Spider” Shaft Coupling  
Figure 3.6

Figure 3.7 shows the second coupling attempted: a three-piece plastic and brass coupling. This coupling has a plastic bar connected to brass ends with a ball-and-socket type interface that allows it to swivel for large lateral misalignment. Because the plastic rod is rigid, this coupling does not provide compensation for axial compression. The ball end of the rod is not anchored to the socket joints, however, thus allowing for free axial movement when pulled apart. As a result, this coupling provides no axial tension. Unfortunately, like the spider coupling, the engine “turned-over” with this attachment, but could not run sustained.



Three-Piece Plastic and Brass Coupling  
Figure 3.7

Figure 3.8 shows the third coupling that was tried: a one-piece rubber tube with attached brass ends. Because of the unitary nature of this coupler, it is the only one of the three couplings to provide axial tension compensation as well as compensation for axial compression and lateral misalignment. The engine was finally able to successfully start and run sustained while attached to the DC motor using this coupler.



One-Piece Rubber and Brass Coupling  
Figure 3.8

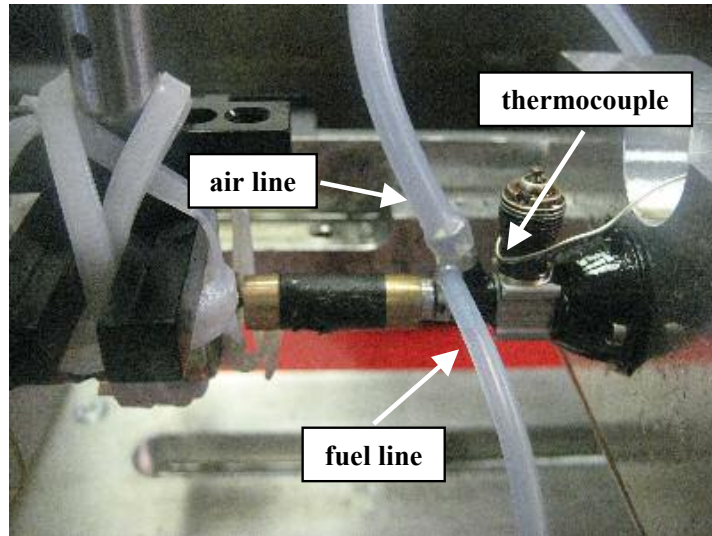
It was found that the tension (caused by the stretching of the rubber) of this one-piece coupler is essential to having the engine start successfully. In addition to the requirement that the DC motor be carefully aligned and securely fixed on the cradle base, the Tee Dee also requires the drive plate be in slight tension to the engine body. This tension provides an essential gap clearance (depicted in Figure 3.8) between the drive plate and the engine body retainer nut. Without this gap, even slight contact of the drive plate to the retainer nut causes sufficient friction to stop the engine. In standard operation on a model aircraft, the aerodynamic propulsive force of the propeller provides the tension to maintain this gap.

### 3.2 Experimental Procedure

Three different engines were tested: one original Cox Tee Dee 0.010 and two modified Micro-Flite Tee Dee 0.010s (“Engine A” and “Engine B”). The following procedure describes the steps used to operate and measure the performance of each engine with the dynamometer.

#### 3.2.1 Before Starting Engine

If the engine to be tested had been run for prolonged periods of time with a castor oil based fuel (such as the Micro-Flite fuel), it was cleaned with a devarnishing solution sold by Micro-Flite to assure optimal performance [26]. Once it was clean, the Micro-Flite fuel (described in Section 2.4.2) was transferred to the external plastic fuel tank via an electric fuel pump. (The Tee Dee’s integrated fuel tank was disconnected and was not used for this testing.) The fuel line was then connected to the nipple on the needle valve assembly and the plenum tubing was fitted over the venturi opening to measure intake flow as shown in Figure 3.9. A blower duct was also positioned on the cradle base and directed over the engine for cooling.



Fuel Line, Air Line, and Thermocouple Attachment  
Figure 3.9

The fuel tank was placed on a scale to measure fuel flow rate and a thermocouple was placed in contact with the cylinder near the exhaust port as shown in Figure 3.9. The speed sensor beam was also checked to verify that it was centered on the reflective tape on the shaft coupler. If the load cell had been disconnected to avoid damage during preparation, it was reattached to the cradle such that the moment arm length was 1 inch long. The DAQ equipment was then powered on and the software reset in order to accept a new data set.

To start the engine, the glow plug heater clip was applied to the cylinder head and the DC motor leads were connected to a 12 V battery. As the DC motor spun the engine drive shaft and induced ignition firing, the fuel mixture setting was adjusted via the needle valve until the engine started and ran sustained.

### 3.2.2 During Engine Run

Once the engine was started, the DC motor leads were disconnected from the battery and the glow plug heater clip was removed from the cylinder head. The fuel mixture setting was then adjusted until a maximum and sustained RPM (perceived from sound) was achieved. (This usually meant leaning the mixture as much as possible.)

#### *The Original Cox Tee Dee and Micro-Flite Tee Dee “Engine A” (full throttle)*

For this engine, the 10-turn variable resistor was first turned to the lowest resistance before connecting the DC motor leads. Once the leads were connected and the engine RPM stabilized, a data set (comprised of two datum bursts) was acquired. For the load cell, airflow, and temperature measurements, a data set was acquired by collecting two bursts of data in 15-second durations at 80 Hz. This equates to 1,200 datum points for each burst or 2,400 datum points for each data set. The speed

measurements were acquired by a separate oscilloscope counter that collected two sets of data each comprised of 15 points at 1 Hz. The fuel flow rate was determined by measuring the time required for the scale to drop 1 g in mass with a hand stopwatch. (In rare cases, the engine stopped before the mass could drop exactly 1g. When that happened, the mass change up to that point was noted and divided by the measured time.)

The load was then adjusted by turning the variable resistor slowly to increase resistance. For each resistance setting, a data set was recorded and the fuel flow measured when the engine RPM stabilized. The resistance was increased after every data set until the engine stopped and was not able to restart at that load level. For the original Cox Tee Dee, measurements were taken at 0 turns, 5 turns, 6 turns, 7 turns, and 8 turns. For the Micro-Flite Tee Dee “Engine A”, measurements were taken with full throttle at 0 turns, 5 turns, 6 turns, 7 turns, 8 turns, 8.5 turns, and 8.75 turns (where 10-turns equates to the maximum resistance of the resistor).

#### *The Micro-Flite Tee Dee Engine B*

For this engine, the variable resistor was not attached to the circuit (therefore maintaining constant load), but measurements were instead taken at different throttle settings. A data set was first acquired at full throttle by turning the exhaust baffle until maximum sustained RPM (perceived by sound) was achieved. Because it was difficult to see how much of the exhaust port was covered with each throttle position, the baffle was adjusted until the perceived RPM dropped for three consecutive data set acquisitions until the engine was on the verge of stopping. Finally, the engine was returned to the full throttle setting and another measurement was recorded.

#### 3.2.3 After Stopping Engine

##### *Calibration*

To calibrate the load cell, after each engine stopped and while all instrument (fuel, air, temperature) lines were still attached, a data set was acquired. Then a 50 g weight was placed on one side of the cradle at a moment arm length of 5.75 inches and another data set was acquired. This was repeated for weight masses of 100 g and 200 g. The same weights were then placed on the opposite side of the cradle at the same moment arm length and data sets were once again recorded for each mass. Finally, another data set was taken with no weights attached to the cradle.

##### *Data Processing*

For each acquisition burst of the load cell, airflow, and temperature measurements, the 1,200 points comprising the 15 seconds of steady-state data were averaged. The two bursts of each data set were then averaged to get a single value for each measurement. The two 15-point bursts of speed data were also averaged to produce a single value for each data set measurement.

The calibrated load cell data were used to compute a torque versus voltage line for the load cell. The slope of this line was then used as a scaling factor to calculate the resultant torque from the registered voltage of the cell for each engine measurement.

Airflow measurements were scaled by the known instrument factor of 75 liters per minute per volt and fuel flow was calculated by dividing the mass change by the measured stopwatch time. These values were then applied to the governing equations and plotted for analysis as described in Section 3.3.

### 3.3 Results and Analysis

#### 3.3.1 Original Cox Tee Dee 0.010

The averaged measurements for the original Cox Tee Dee engine are shown in Table 3.3.

Original Cox Tee Dee 0.010 Measured Data					
Resistor Load (turns out of 10)	Speed (RPM)	Torque (N-m)	Temperature (C)	Airflow (kg/s)	Fuel Flow (kg/s)
0	15935	5.819E-03	133.64	3.151E-05	1.124E-05
5 (500 ohms)	15470	5.419E-03	136.22	3.037E-05	1.220E-05
6 (600 ohms)	16567	5.403E-03	132.29	3.386E-05	1.316E-05
7 (700 ohms)	16417	5.517E-03	140.99	3.368E-05	1.124E-05
8 (800 ohms)	15839	4.401E-03	152.78	3.145E-05	7.143E-06

Table 3.3

From the standard definition [45], power,  $P$ , (in watts) was calculated using Equation 3.2 where  $\Gamma$  is torque in N-m and  $\omega$  is shaft rotation in rad/s.

$$P = \Gamma \omega \quad (\text{Eq. 3.2})$$

The power measurements were adjusted by standard procedure [45, 55] to correct for atmospheric variation. Equation 3.3 shows how the corrected power,  $P_r$ , was calculated where  $P$  is the power computed using Equation 3.2 and  $\alpha_c$  is the correction factor.

$$P_r = \alpha_c P \quad (\text{Eq. 3.3})$$

The correction factor,  $\alpha_c$ , is calculated via Equation 3.4 where  $f_a$  is the atmospheric factor and  $f_m$  is the engine factor.

$$\alpha_c = (f_a)^{f_m} \quad (\text{Eq. 3.4})$$

The atmospheric factor,  $f_a$ , is calculated via Equation 3.5 where  $p_r$  is the laboratory atmospheric pressure,  $\phi_r$  is the laboratory relative humidity,  $p_{sr}$  is the laboratory saturated vapor pressure,  $T_r$  is the laboratory temperature,  $p$  is the standard pressure

(defined as 100 kPa),  $\phi$  is the standard relative humidity (defined as 0.3),  $p_s$  is the standard saturated water vapor pressure [52] (defined as 0.0531 kPa), and  $T$  is the standard temperature (defined as 298 K).

$$f_a = \left( \frac{p_r - \phi_r p_{sr}}{p - \phi p_s} \right) \left( \frac{T}{T_r} \right)^{0.7} \quad (\text{Eq. 3.5})$$

The engine factor,  $f_m$ , for a two-stroke engine is calculated via Equation 3.6 where  $q$  is the volumetric fuel/air ratio and  $r_r$  is the intake charge to atmospheric pressure ratio (defined as 1 for loop-scavenged engines such as the Tee Dee 0.010).

$$f_m = 0.036 \left( \frac{q}{r_r} \right) - 1.14 \quad (\text{Eq. 3.6})$$

For the original Cox Tee Dee engine testing, the laboratory had a relative humidity of 0.58, atmospheric pressure of 101.2 kPa [61], temperature of 27.01 °C, and saturated water vapor pressure of 0.0656 kPa [52].

The volumetric efficiency,  $\eta_V$ , of the engine was approximated for each measurement using Equation 3.7 where  $Q_{air}$  is the measured air intake volume rate,  $\omega$  is the measured engine speed, and  $V_{cyl}$  is the cylinder volume. The numerator is the actual airflow into the cylinder per cycle based on measurement and the denominator is the theoretical airflow needed to completely fill the cylinder with fresh charge every cycle. (The volume of the cylinder head and the volume of atomized fuel were ignored for this estimation.) The ratio of these two values represents the engine's capability to inhale enough air to fully combust the incoming charge for each cycle.

$$\eta_V = \frac{Q_{air}}{\omega V_{cyl}} \quad (\text{Eq. 3.7})$$

Other useful performance values [45] can be calculated for the cycle as follows:

*Power Density*, as described in Equation 3.8, where  $P$  is the corrected power and  $m$  is the total engine mass (without fuel tank):

$$\text{Power Density} = \frac{P}{m} \quad (\text{Eq. 3.8})$$

*Overall efficiency*, as described in Equation 3.9, where  $P$  is corrected power,  $\dot{m}_f$  is fuel mass flow and  $Q_r$  is lower heating value of the fuel:

$$\eta_o = \frac{P}{\dot{m}_f Q_r} \quad (\text{Eq. 3.9})$$

*Brake specific fuel consumption (BSFC)*, as described by Equation 3.10, where  $\dot{m}_f$  is fuel mass flow and  $P$  is corrected power:

$$BSFC = \frac{\dot{m}_f}{P} \quad (\text{Eq. 3.10})$$

The resulting performance values for this particular engine are listed in Table 3.4 where Efficiency (IO) and Efficiency (BO) are the overall thermodynamic efficiencies assuming inert oil and burned oil respectively.

Original Cox Tee Dee 0.010 Calculated Performance							
Speed (RPM)	Fuel/Air Mixture	Vol. Efficiency	Power (W)	Efficiency (IO)	Efficiency (BO)	BSFC (kg/W-hr)	Power Density (W/kg)
15935	0.357	0.6029	10.24	0.0541	0.0408	3.95E-03	788
15470	0.402	0.5985	9.26	0.0450	0.0340	4.74E-03	712
16567	0.389	0.6231	9.89	0.0446	0.0336	4.79E-03	760
16417	0.334	0.6255	10.00	0.0528	0.0399	4.04E-03	769
15839	0.227	0.6053	7.70	0.0639	0.0483	3.34E-03	592

Table 3.4

Figure 3.10 shows the speed data for this engine plotted against the approximate resistor load (where 0 turns is minimal load and 10 turns is the maximum resistance of 1000 ohms). Immediately after each load change during the experiment, there was an audible fluctuation in the engine speed before eventually stabilizing. However, as shown in the figure, the speed did not show the expected decreasing trend with increasing load until the last three measurements. Note that the error bars for resistor load in Figure 3.10 are based on the 5% error rated by the resistor manufacturer. The error bars for all the remaining plots of this engine are derived from calculations described in Section 3.4.

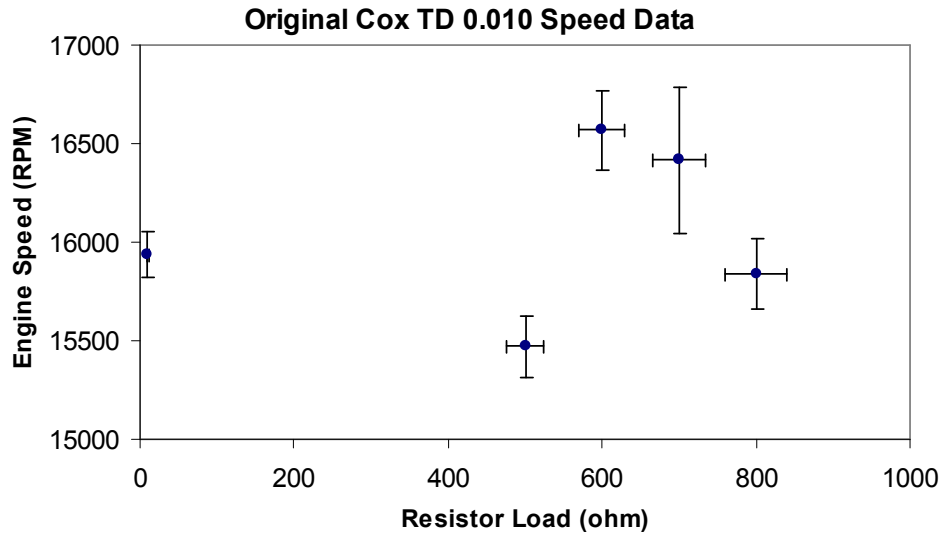


Figure 3.10

Figure 3.11 shows cylinder temperature as measured from the thermocouple versus engine speed. Once again, the curve is relatively flat suggesting very little correlation of cylinder temperature to engine speed over the operating test range. Note that the temperature error bars are relatively small because only random error was included in the error analysis while assuming the systematic error of the thermocouple to be 0.

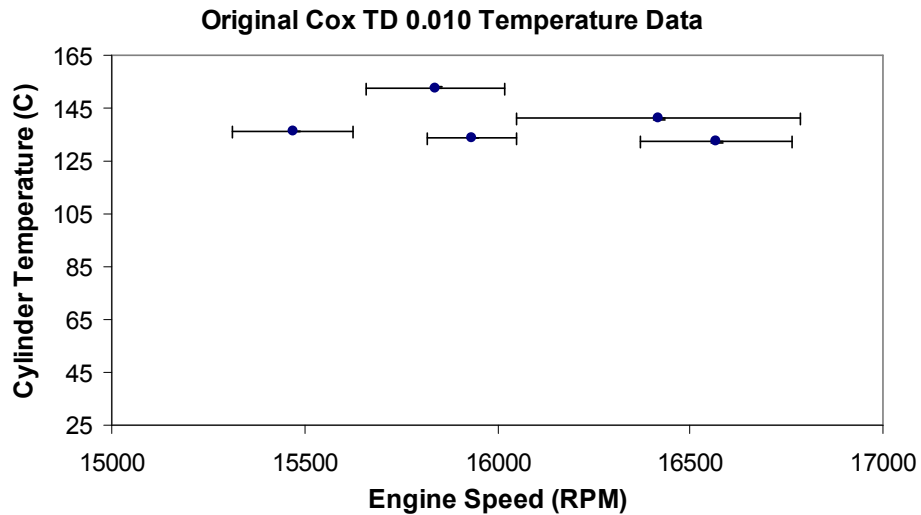


Figure 3.11

Figure 3.12 shows the mass flow rates versus engine speed. Over the speed range of this test, the both rates appear to be relatively consistent. The large fuel flow error bar shown for the 15,839 RPM point is a result of a very small time sampling for the flow rate measurement because the engine cut off before reaching the desired time interval.

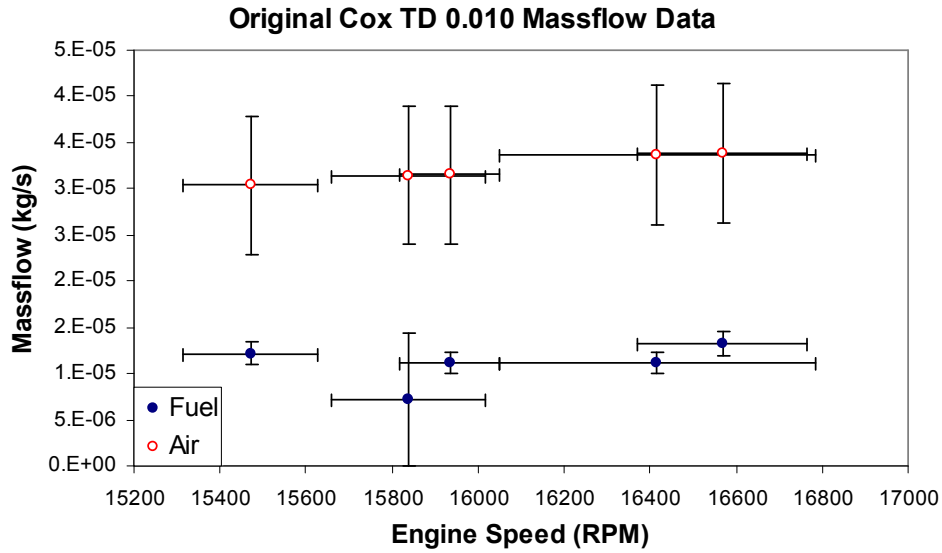


Figure 3.12

Figure 3.13 shows the volumetric efficiency trend of this engine over the four measurements obtained. While the values demonstrate a clear lack of ability for the engine to inhale enough air for ideal combustion (thus confirming the importance of extra oxygen in the nitromethane additive), the flat nature of the trend once again suggests the engine performance does not change appreciably over the operating range tested.

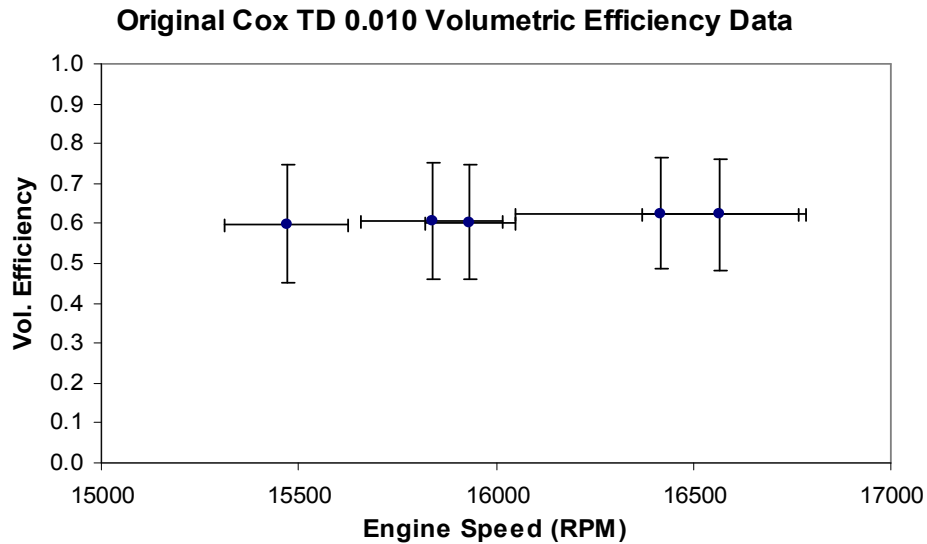


Figure 3.13

The lack of performance correlation to speed for this engine can also be seen in a plot of efficiency values (assuming inert oil) in Figure 3.14. Once again, the large error at the 15,839 point is a derivative of a low quality fuel flow rate measurement.

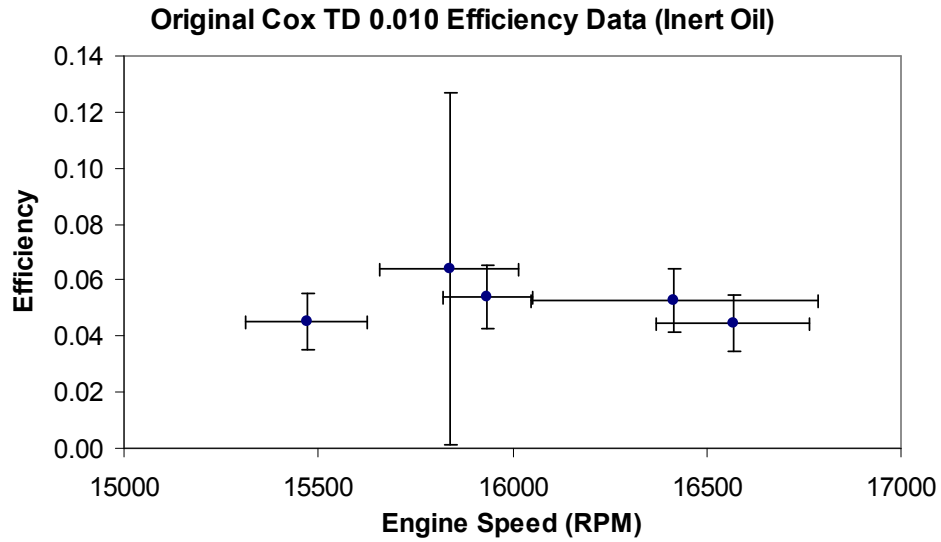
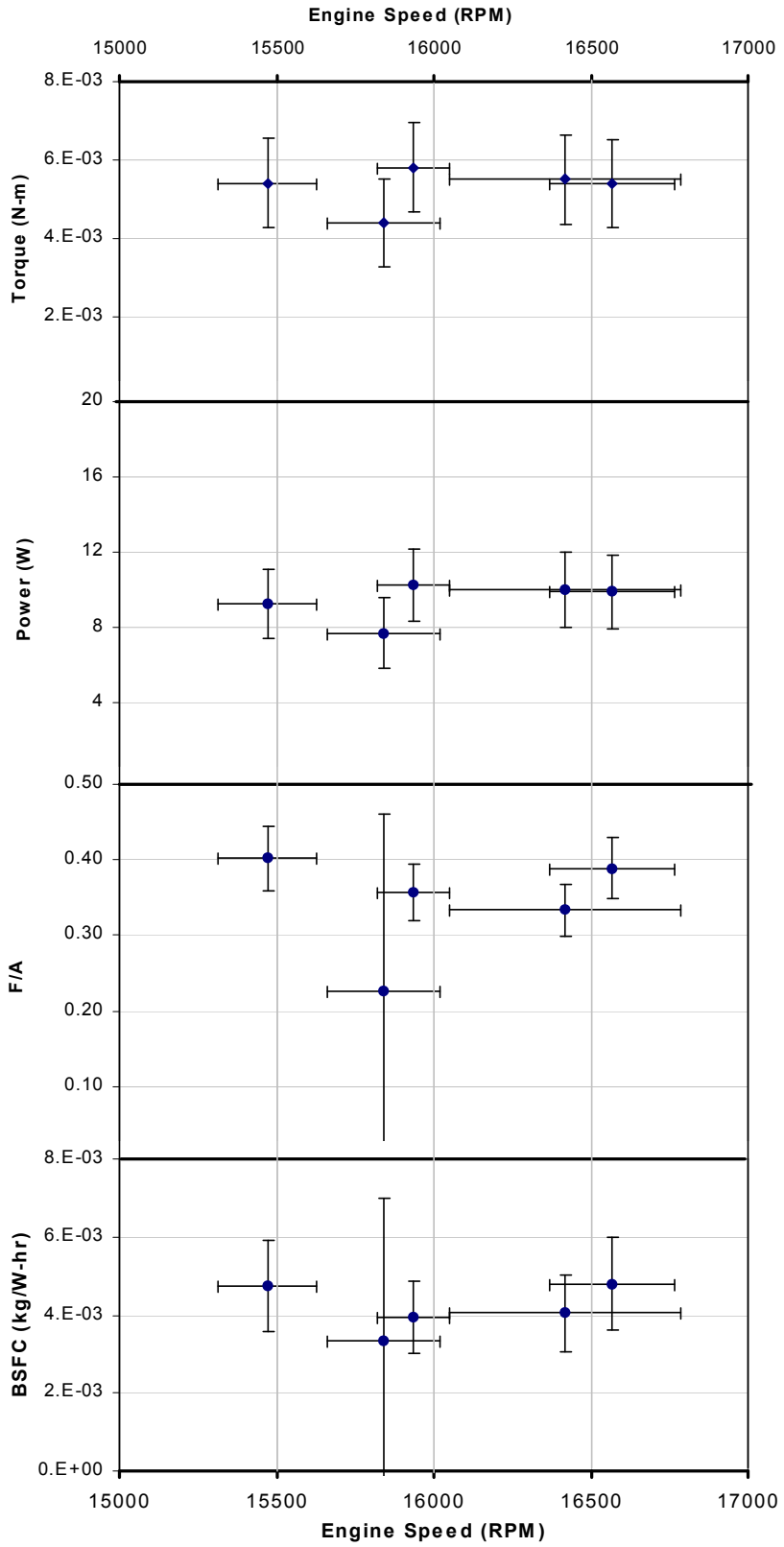


Figure 3.14

Figure 3.15 additionally demonstrates a lack of performance trend via a set of stacked plots depicting torque, power, fuel/air ratio, and BSFC for the original Cox Tee Dee 0.010. It can also be noted that the engine maintains a rich fuel-air mixture ratio (based on the stoichiometric value of 0.278) throughout most of the measurements.



Original Cox Tee Dee Stacked Performance Plots  
Figure 3.15

### 3.3.2 Modified Micro-Flite Tee Dee 0.010 Engine A

The averaged measurements for the Micro-Flite Tee Dee “Engine A” at full throttle are shown in Table 3.5. After noting the inconsistently large torque values of the first three measurements (0, 5, and 6 resistor turns), an erroneous bias (perhaps from fuel or air tubing tension) in the cradle assembly was suspected. Consequently, those data were not considered into the experimental results. Additionally, no temperature data were recorded during the 8-turn resistor load measurement because the thermocouple slipped off the cylinder surface.

Modified Micro-Flite Tee Dee 0.010 "Engine A" Measured Data					
Resistor Load (turns out of 10)	Speed (RPM)	Torque (N-m)	Temperature (C)	Airflow (kg/s)	Fuel Flow (kg/s)
0	18719	1.506E-02	151.84	3.891E-05	1.587E-05
5 (500 ohms)	18483	1.535E-02	155.79	3.901E-05	1.639E-05
6 (600 ohms)	18406	1.559E-02	151.78	3.947E-05	1.613E-05
7 (700 ohms)	18648	3.093E-03	144.35	3.997E-05	1.695E-05
8 (800 ohms)	17558	5.055E-03	–	3.893E-05	1.316E-05
8.5 (850 ohms)	17034	3.991E-03	149.39	3.854E-05	1.395E-05
8.75 (875 ohms)	17163	4.429E-03	142.45	3.946E-05	1.111E-05

Table 3.5

For the Micro-Flite “Engine A” testing, the power was corrected for atmosphere as described in Section 3.3.1 using a relative humidity of 0.76, atmospheric pressure of 100.8 kPa [61], temperature of 27.01 °C, and saturated water vapor pressure of 0.0692 kPa [52]. Equations 3.3, 3.7, 3.8, 3.9, and 3.10 were then applied to find the corresponding computed performance values as shown in Table 3.6.

Micro-Flite Tee Dee 0.010 "Engine A" Calculated Performance							
Speed (RPM)	Fuel/Air Mixture	Vol. Efficiency	Power (W)	Efficiency (IO)	Efficiency (BO)	BSFC (kg/W-hr)	Power Density (W/kg)
18648	0.424	0.653	6.40	0.0224	0.0169	9.53E-03	492
17558	0.338	0.676	9.85	0.0444	0.0335	4.81E-03	757
17034	0.362	0.690	7.54	0.0321	0.0242	6.66E-03	580
17163	0.282	0.701	8.43	0.0450	0.0340	4.74E-03	649

Table 3.6

Figure 3.16 shows the speed data for this engine plotted against the approximate resistor load. Predictably, the engine speed is seen dropping as the applied load to the engine shaft increases. Note that the error bars for resistor load in Figure 3.16 are based on the 5% error rated by the resistor manufacturer. The error bars for all the remaining plots of this engine are derived from calculations described in Section 3.4.

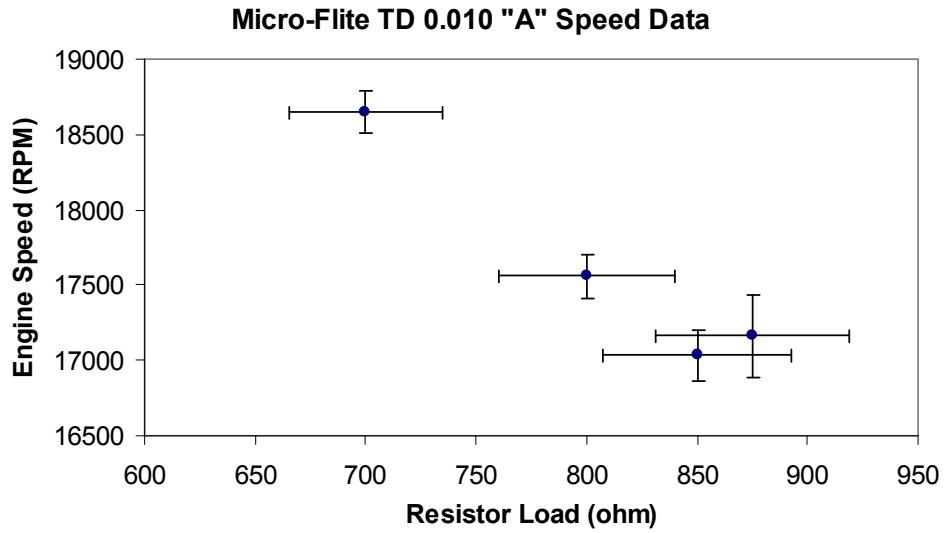


Figure 3.16

Figure 3.17 shows cylinder temperature as measured from the thermocouple versus engine speed. As with the original Cox engine, the curve is relatively flat suggesting very little temperature variation as engine speed is varied over the operating test range. Note again that the temperature error bars are relatively small because only random error was included in the error analysis.

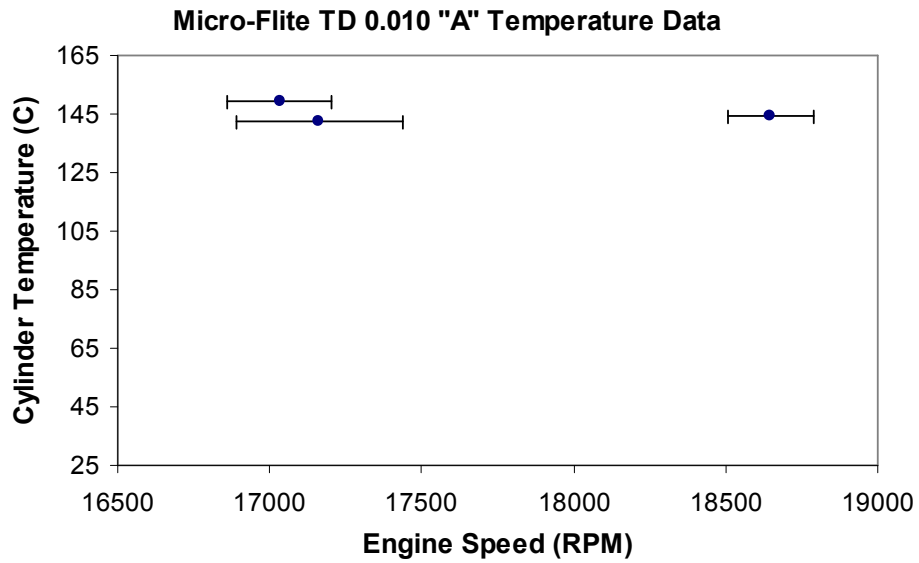


Figure 3.17

Figure 3.18 shows the mass flow rates versus engine speed. Over the speed range of this test, the both rates appear to be relatively consistent.

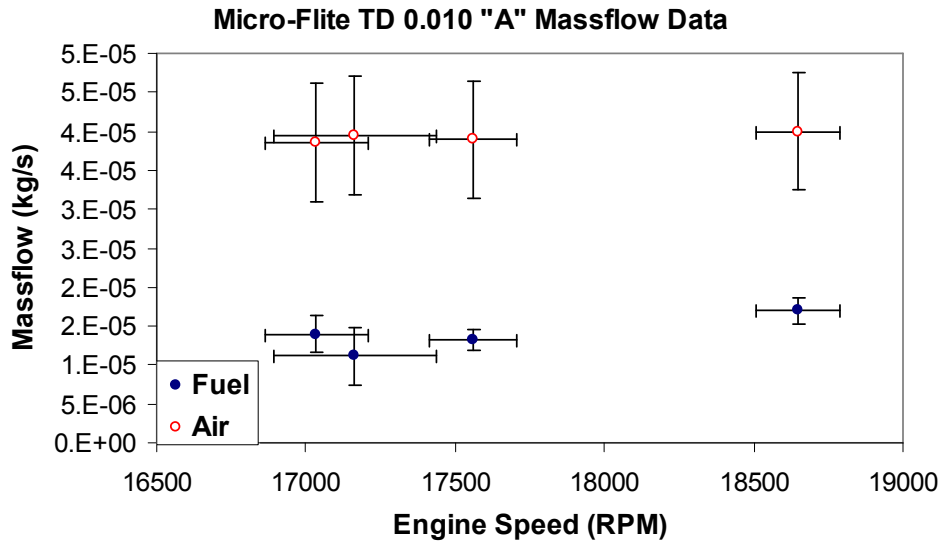


Figure 3.18

The volumetric efficiency values for this engine, shown in Figure 3.19, are slightly higher than those of the Original Cox engine, however reflect a similar flat trend.

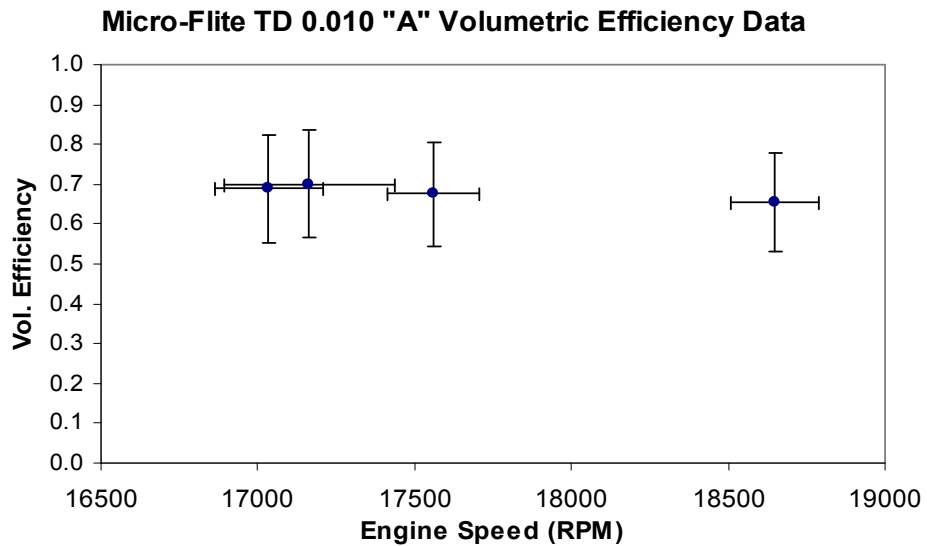


Figure 3.19

The efficiency data for this engine as shown in Figure 3.20 does not indicate a clear overall trend, however, the relatively low efficiency of the last point may represent a predictable drop in efficiency as the engine reaches very high RPM.

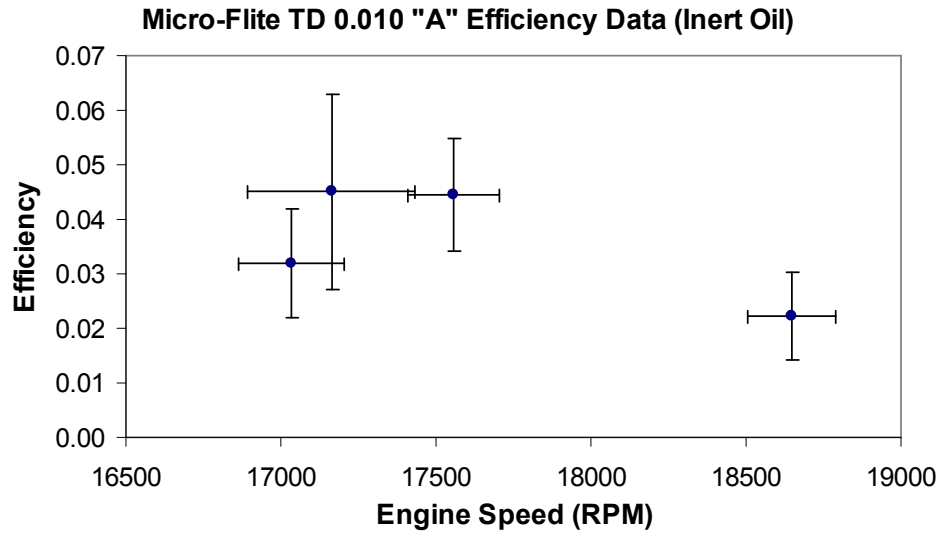
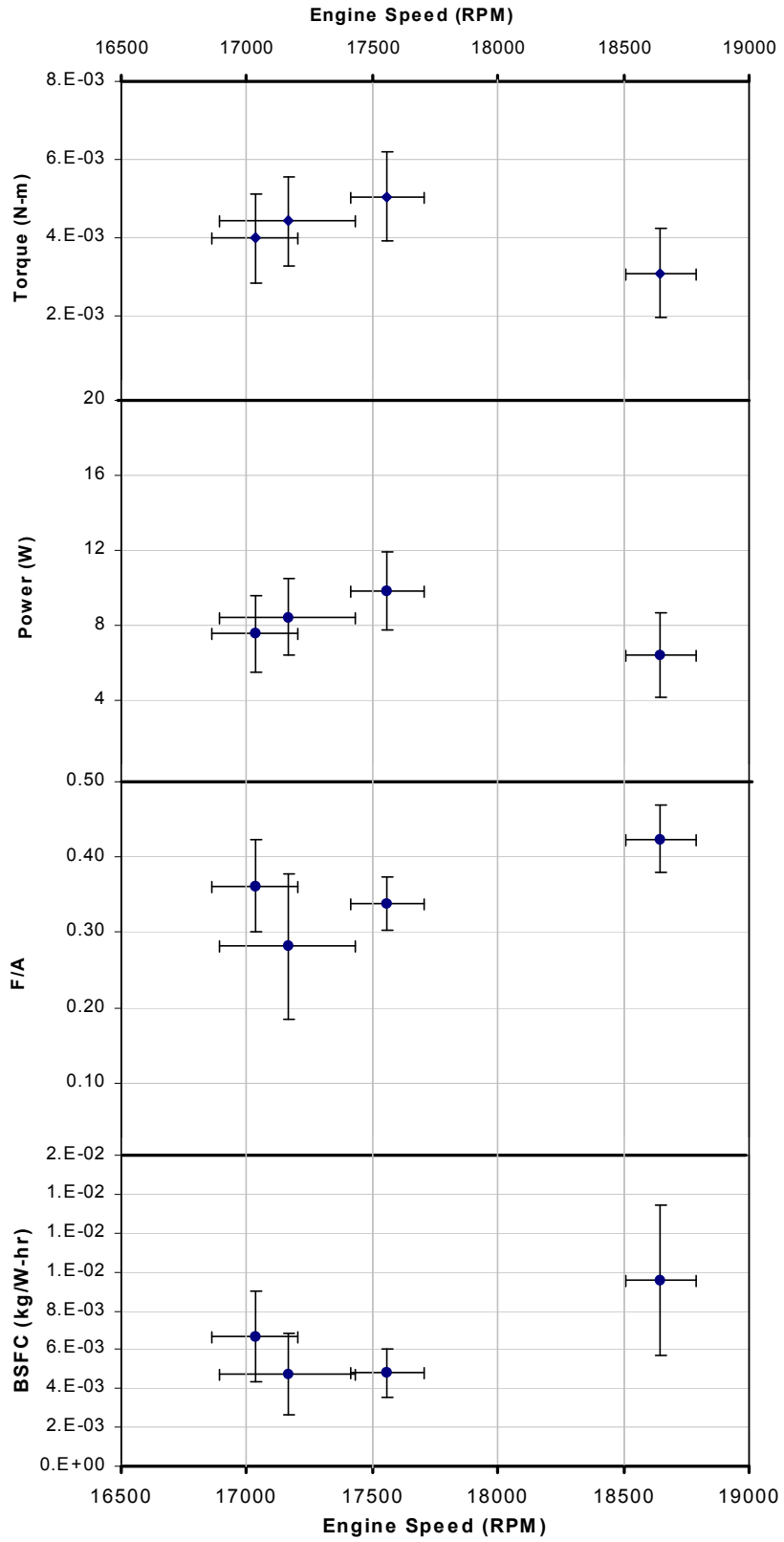


Figure 3.20

Overall, the performance of this engine was consistent with the Original Cox engine while operating at slightly higher speeds. Figure 3.21 reiterates the overall lack of clear performance trends via the set of stacked plots depicting torque, power, fuel/air ratio, and BSFC for the modified Micro-Flite “Engine A”.



Micro-Flite Tee Dee "Engine A" Stacked Performance Plots  
Figure 3.21

### 3.3.3 Modified Micro-Flite Tee Dee 0.010 Engine B

The averaged measurements for the Micro-Flite Tee Dee “Engine B” are shown in Table 3.7. Unlike the Micro-Flite “Engine A”, the measurements for this engine were taken at various throttle settings. Because it was difficult to determine the extent at which the exhaust ports were covered at each throttle setting, a qualitative representation of throttle was defined as 0 at full open throttle, -1 as some closure, -2 as more closure than -1, and -3 as even more closure and almost completely closed. Note that two full throttle measurements were taken and that only one valid temperature measurement was obtained.

Micro-Flite Tee Dee 0.010 "Engine B" Measured Data					
Throttle Setting (from full at 0)	Speed (RPM)	Torque (N-m)	Temperature (C)	Airflow (kg/s)	Fuel Flow (kg/s)
0	19711	3.087E-03	--	4.293E-05	1.346E-05
-1	20106	2.784E-03	--	4.160E-05	1.639E-05
-2	19265	1.564E-03	--	3.866E-05	1.493E-05
-3	17930	2.671E-03	--	3.623E-05	1.282E-05
0	19574	1.785E-03	100.09	4.320E-05	2.000E-05

Table 3.7

For the Micro-Flite “Engine B”, the power was corrected for atmosphere as described in Section 3.3.1 using a relative humidity of 0.76, atmospheric pressure of 100.8 kPa [61], temperature of 27.64 °C, and saturated water vapor pressure of 0.0718 kPa [52]. Equations 3.3, 3.7, 3.8, 3.9, and 3.10 were then applied to find the corresponding computed performance values as shown in Table 3.8.

Micro-Flite Tee Dee 0.010 "Engine B" Calculated Performance							
Speed (RPM)	Fuel/Air Mixture	Vol. Efficiency	Power (W)	Efficiency (IO)	Efficiency (BO)	BSFC (kg/W-hr)	Power Density (W/kg)
19711	0.314	0.664	6.88	0.0303	0.0229	7.05E-03	529
20106	0.394	0.631	6.25	0.0226	0.0171	9.45E-03	480
19265	0.386	0.612	3.37	0.0134	0.0101	1.59E-02	260
17930	0.354	0.616	5.34	0.0247	0.0186	8.64E-03	411
19574	0.463	0.673	3.90	0.0116	0.0087	1.85E-02	300

Table 3.8

Figure 3.22 shows the speed data for this engine plotted against approximate throttle setting. The plot shows an apparent peak RPM with a slight closing of the throttle and then a clear expected trend of decreasing engine speed with decreasing throttle. Error bars for all plots of this engine are derived from calculations described in Section 3.4. Note that since the throttle setting was manually applied, error bars are not included in Figure 3.22 for the qualitative throttle representation.

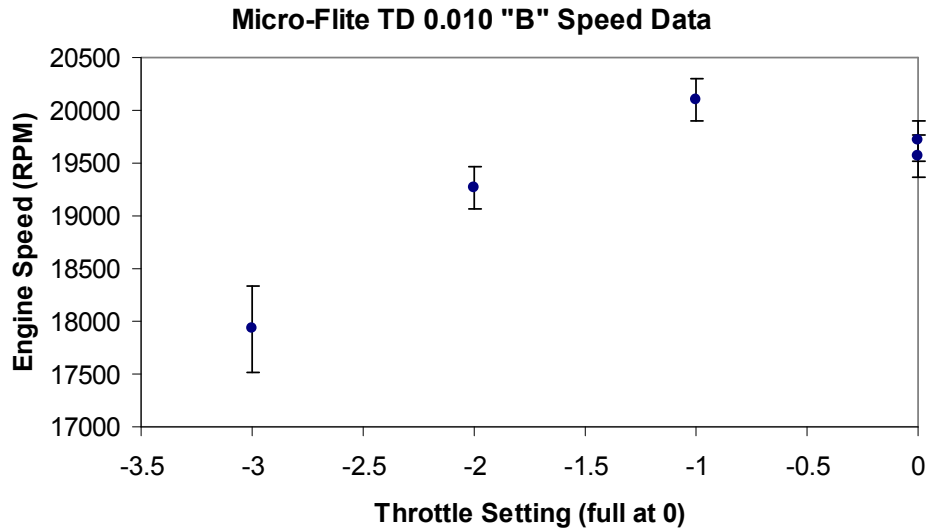


Figure 3.22

Figure 3.23 shows the mass flow rates versus engine speed with labeled throttle settings (where T: 0, T: -1, T: -2, and T: -3 correspond to the throttle settings shown in Figure 3.22). As with the other two engines, the both rates appear to be relatively consistent over the range of the test.

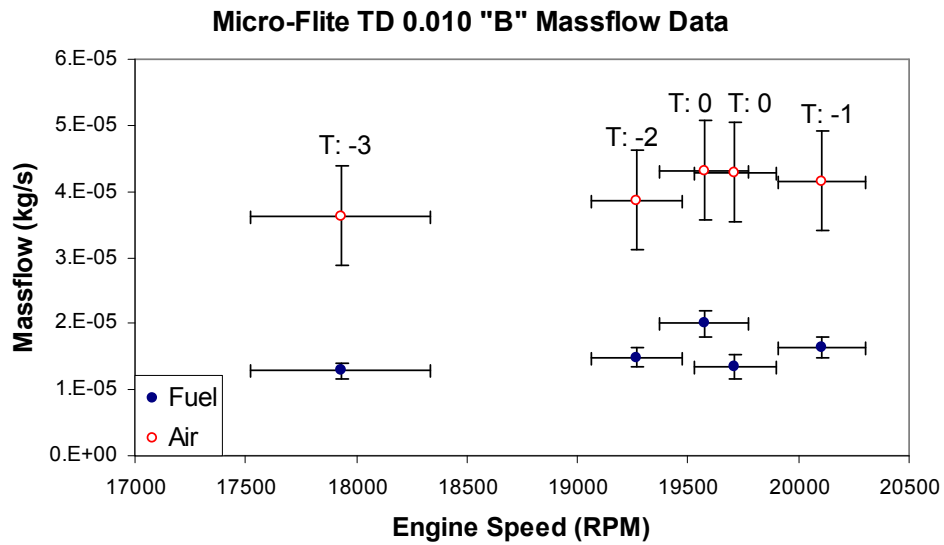


Figure 3.23

Figure 3.24 shows that the volumetric efficiency values of this engine are consistent with the range of values from the other two engines while once again reflecting the relatively flat nature across the operating range.

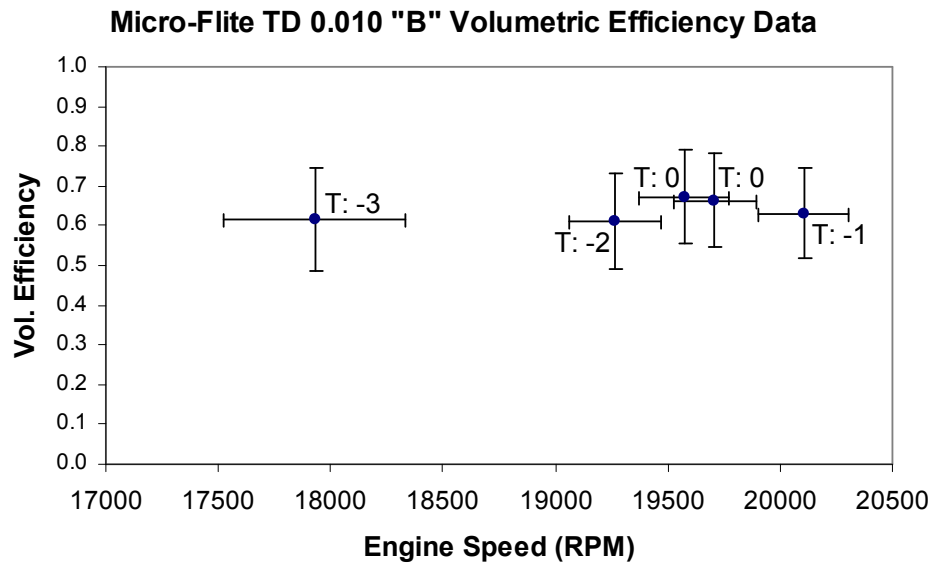


Figure 3.24

As shown in Figure 3.25, no clear trend in efficiency can also be seen for this engine over the throttle range of the test.

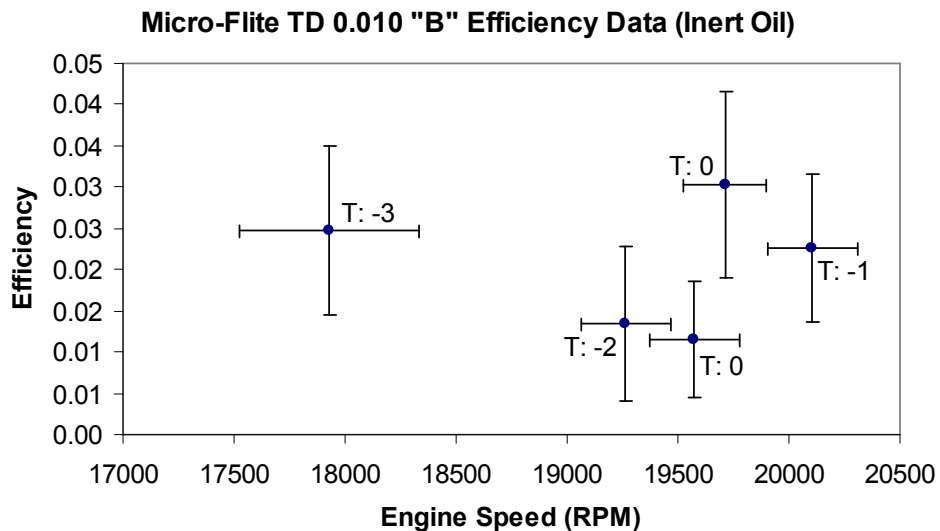


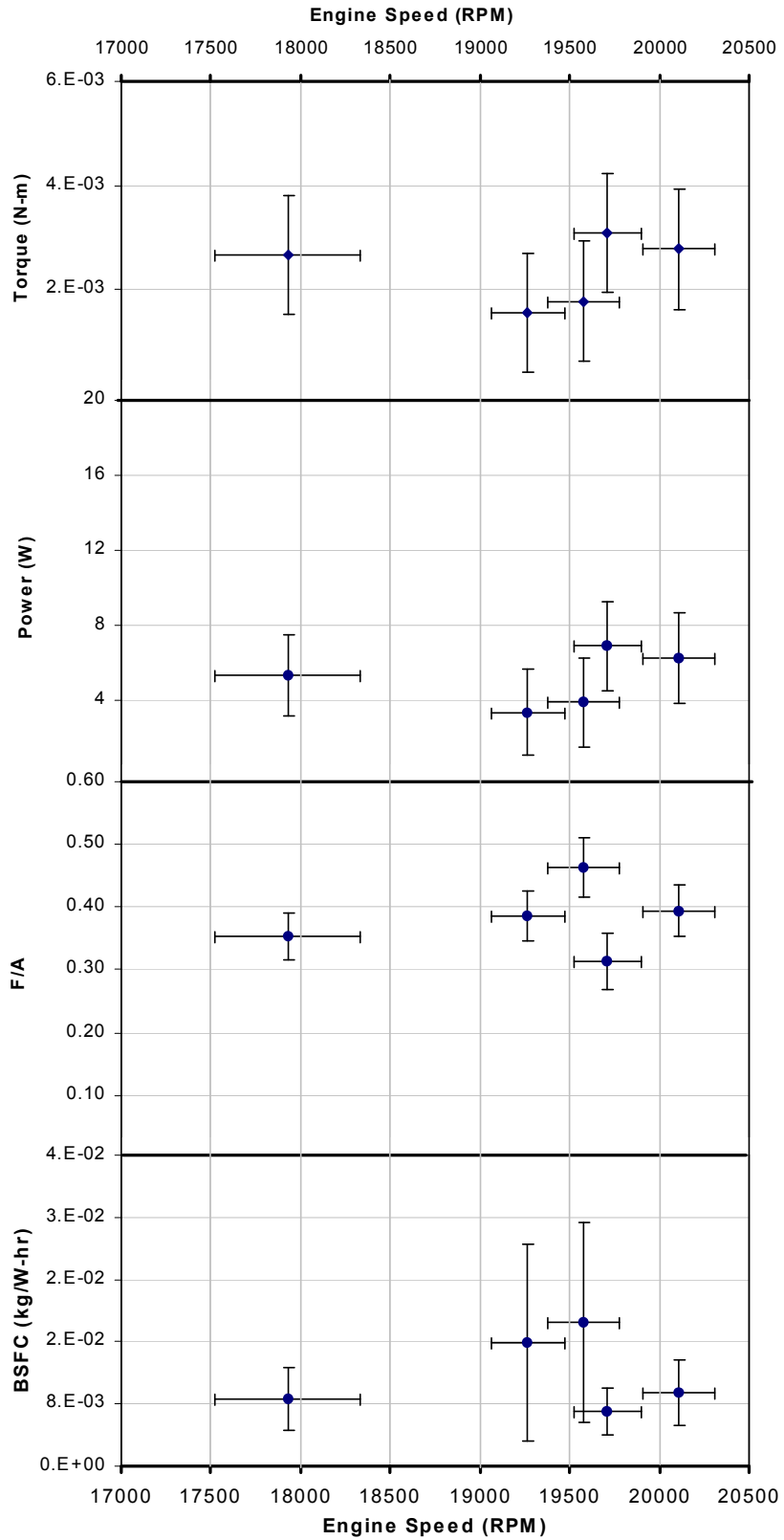
Figure 3.25

Figure 3.26 once again demonstrates the lack of performance trends over the throttle settings of the test via the set of stacked plots depicting torque, power, fuel/air ratio, and BSFC for the modified Micro-Flite "Engine B".

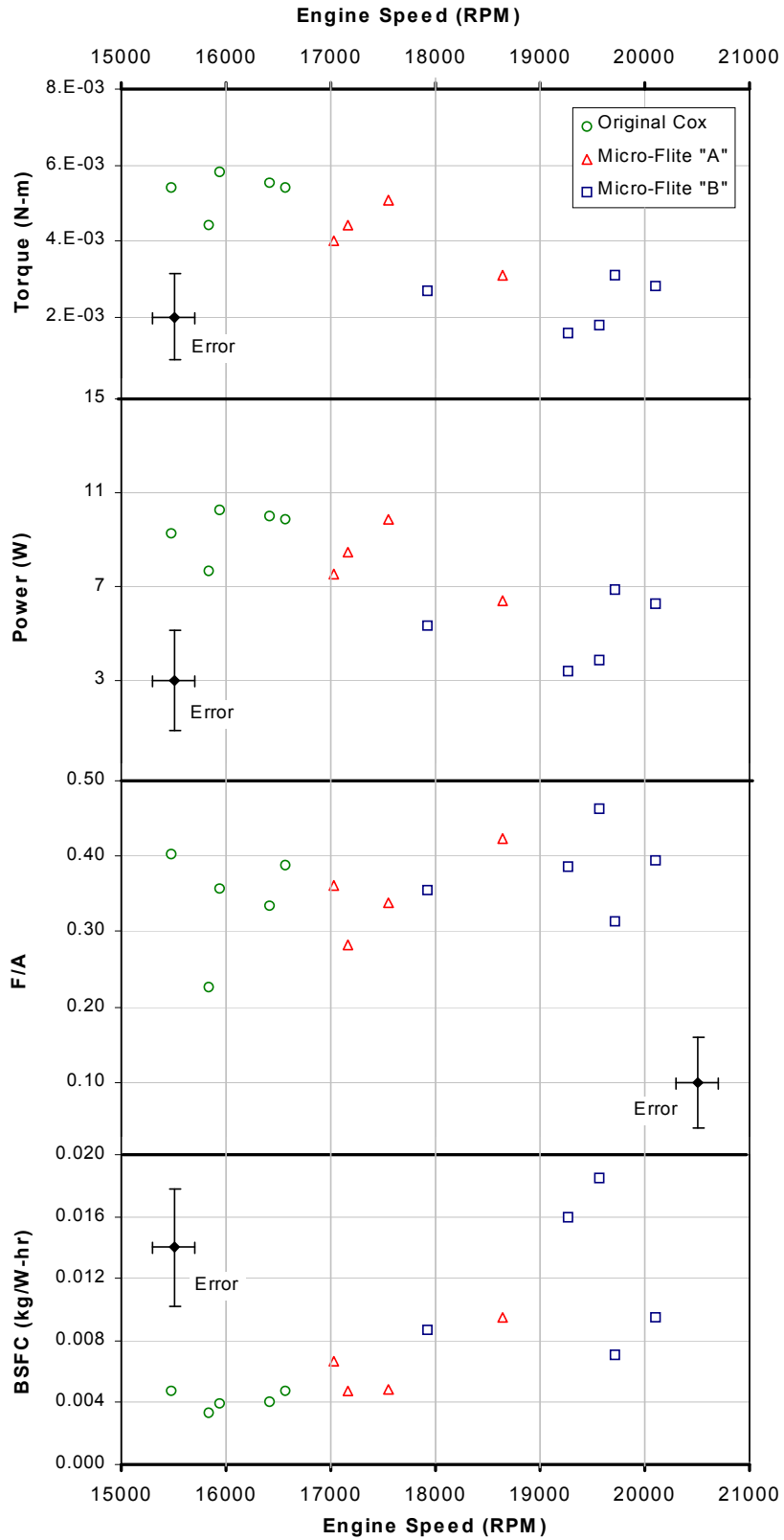
Overall, while this engine achieved the highest RPM of all three engines and demonstrated the ability to adjust its speed with the custom Micro-Flite throttle

sleeve, its performance range closely mirrored the flat nature of the other two engines.

Summarizing the performance of all three engines tested, the stacked plots of Figure 3.27 shows a slight decrease in power of the Micro-Flite engines with respect to the Original Cox engine. This may be a result of the Micro-Flite throttle mechanism inhibiting the maximum performance of the engine despite claims to the contrary by the manufacturer [26].



Micro-Flite Tee Dee "Engine B" Stacked Performance Plots  
Figure 3.26



Cox Tee Dee 0.010 Stacked Performance Plots  
Figure 3.27

### 3.4 Error Analysis

Using standard procedures [45], the error,  $\delta m$ , for each measurement,  $m$ , was calculated via Equation 3.11 where  $B$  is the total systematic uncertainty of the measurement and  $S_x$  is the contribution to uncertainty from random processes.

$$\delta m = 2\sqrt{\left(\frac{B}{2}\right)^2 + (S_x)^2} \quad (\text{Eq. 3.11})$$

The total systematic uncertainty,  $B$ , was calculated with Equation 3.12 where  $b_1..b_m$  are the individual contributions of uncertainty in the measurement device. For this experiment, all measurements taken through the computer DAQ device had a  $b_1$  contribution of 0.005 V from the DAQ and a  $b_2$  contribution from the uncertainty of the actual measuring instrument as listed in Table 3.2.

$$B = \sqrt{(b_1)^2 + (b_2)^2 + \dots + (b_m)^2} \quad (\text{Eq. 3.12})$$

The uncertainty from random processes,  $S_x$ , was determined with Equation 3.13 where  $M$  is the total number of measurements,  $x_k$  is the  $k^{\text{th}}$  measurement and  $\bar{x}$  is the average of  $M$  measurements.

$$S_{\bar{x}} = \frac{1}{\sqrt{M}} \sqrt{\sum_{k=1}^M \frac{(x_k - \bar{x})^2}{M-1}} \quad (\text{Eq. 3.13})$$

The error of a computed function (such as power),  $\delta X$ , was calculated via Equation 3.14 where  $(\partial X / \partial \bar{p}_j)$  represents the partial derivative of the function  $X$  with respect to the  $j^{\text{th}}$  variable and  $m_j$  is the total uncertainty of the  $j^{\text{th}}$  variable.

$$\delta X = \sqrt{\left(\frac{\partial X}{\partial \bar{p}_1} \delta m_1\right)^2 + \dots + \left(\frac{\partial X}{\partial \bar{p}_j} \delta m_j\right)^2} \quad (\text{Eq. 3.14})$$

Table 3.9 lists total uncertainty,  $\delta m$ , for each measurement taken on the original Cox Tee Dee 0.010 engine as determined via Equation 3.11. Table 3.10 lists the corresponding computed uncertainty,  $\delta X$ , for each performance value as computed via Equation 3.14. Note that only inert oil efficiency was calculated and the large error in fuel flow rate on the last measurement is a result of a very small time sampling when the engine cut off before the desired time interval was reached.

Original Cox Tee Dee 0.010 Measurement Uncertainty					
Speed (RPM)	d(Speed) (RPM)	d(Airflow) (kg/s)	d(Fuel Flow) (kg/s)	d(Temperature) (C)	d(Torque) (N-m)
15935	115	7.527E-06	1.131E-06	0.138	1.1362E-03
15470	156	7.525E-06	1.229E-06	0.093	1.1366E-03
16567	199	7.531E-06	1.327E-06	0.429	1.1362E-03
16417	369	7.530E-06	1.131E-06	0.403	1.1370E-03
15839	179	7.526E-06	7.161E-06	0.210	1.1363E-03

Table 3.9

Original Cox Tee Dee 0.010 Performance Uncertainty						
Speed (RPM)	d(F/A)	d(Vol. Eff.)	d(Power) (W)	d(Efficiency)	d(BSFC) (kg/W-hr)	d(Power Density) (W/kg)
15935	0.037	0.144	1.90	0.0113	9.157E-04	146
15470	0.042	0.148	1.84	0.0099	1.165E-03	142
16567	0.040	0.139	1.97	0.0099	1.180E-03	152
16417	0.034	0.141	1.97	0.0115	9.828E-04	151
15839	0.234	0.145	1.89	0.0628	3.647E-03	145

Table 3.10

Table 3.11 lists total uncertainty,  $\delta m$ , for each measurement taken on the modified Micro-Flite Tee Dee 0.010 “Engine A” as determined via Equation 3.11. Table 3.12 lists the corresponding computed uncertainty,  $\delta X$ , for each performance value as computed via Equation 3.14.

Micro-Flite Tee Dee 0.010 "Engine A" Measurement Uncertainty					
Speed (RPM)	d(Speed) (RPM)	d(Airflow) (kg/s)	d(Fuel Flow) (kg/s)	d(Temperature) (C)	d(Torque) (N-m)
18648	141	7.543E-06	1.719E-06	0.174	1.1393E-03
17558	147	7.540E-06	1.327E-06	--	1.1391E-03
17034	171	7.540E-06	2.348E-06	0.162	1.1390E-03
17163	272	7.542E-06	3.726E-06	0.340	1.1390E-03

Table 3.11

Micro-Flite Tee Dee 0.010 "Engine A" Performance Uncertainty						
Speed (RPM)	d(F/A)	d(Vol. Eff.)	d(Power) (W)	d(Efficiency)	d(BSFC) (kg/W-hr)	d(Power Density) (W/kg)
18648	0.044	0.123	2.23	0.0081	3.859E-03	171
17558	0.035	0.131	2.10	0.0103	1.259E-03	161
17034	0.062	0.135	2.03	0.0100	2.339E-03	156
17163	0.096	0.134	2.05	0.0180	2.125E-03	158

Table 3.12

Table 3.13 lists total uncertainty,  $\delta m$ , for each measurement taken on the modified Micro-Flite Tee Dee 0.010 “Engine B” as determined via Equation 3.11. Table 3.14 lists the corresponding computed uncertainty,  $\delta X$ , for each performance value as computed via Equation 3.14.

Micro-Flite Tee Dee 0.010 "Engine B" Measurement Uncertainty					
Speed (RPM)	d(Speed) (RPM)	d(Airflow) (kg/s)	d(Fuel Flow) (kg/s)	d(Temperature) (C)	d(Torque) (N-m)
19711	186	7.549E-06	1.940E-06	--	1.1502E-03
20106	200	7.546E-06	1.661E-06	--	1.1503E-03
19265	206	7.540E-06	1.509E-06	--	1.1504E-03
17930	406	7.535E-06	1.293E-06	--	1.1503E-03
19574	201	7.550E-06	2.040E-06	0.031	1.1503E-03

Table 3.13

Micro-Flite Tee Dee 0.010 "Engine B" Performance Uncertainty						
Speed (RPM)	d(F/A)	d(Vol. Eff.)	d(Power) (W)	d(Efficiency)	d(BSFC) (kg/W-hr)	d(Power Density) (W/kg)
19711	0.046	0.117	2.37	0.0112	3.039E-03	183
20106	0.041	0.115	2.42	0.0090	4.284E-03	186
19265	0.040	0.119	2.32	0.0093	1.264E-02	179
17930	0.036	0.129	2.16	0.0103	4.077E-03	166
19574	0.048	0.118	2.36	0.0071	1.284E-02	181

Table 3.14

## 4. Simulation With MATLAB

Of the piston engine simulation programs that are publicly available, very few are capable of or suitable for simulating engines on the scale of small model aircraft engines.

A survey found two commercial programs, MOTA<sup>®</sup> [69] (\$189.55 USD per license) and Virtual Engines Virtual 2-Stroke<sup>®</sup> [48] (\$2,000 USD per year for an academic license), which hold potential for the task. The MOTA website states that the program “Accepts 3.5cc To 500cc Engines”, which excludes the 0.163cc Tee Dee 0.010, but the developers speculate it may still be able to simulate smaller engines [70]. The developers of Virtual Engines assert that it can simulate a Tee Dee 0.010-sized engine [30], but a more thorough review of the program’s usefulness is needed before making the commitment to such an expensive license. Both of these programs were avoided for this work due to uncertainty of capabilities and cost justification.

Instead, an initial attempt to model the Tee Dee 0.010 was made using the non-commercial ESP (Engine Simulation Program) developed at Stanford University [58]. While ESP is designed for four-stroke engines, the thinking was that modifying the valve timing might enable it to simulate two-stroke engines as well. In the end this proved not to be correct as ESP did not produce sensible results for the Tee Dee or any two-stroke engine (see Appendix B).

Due to the poor results obtained from the ESP simulation, a secondary method of modeling the Tee Dee’s performance was examined for this work. This alternate approach is based on a work-in-progress MATLAB code first developed by Dr. Christopher Cadou and recently improved by Shyam Menon of the Micro-Reacting Flow Laboratory of the University of Maryland.

While this model is currently far less sophisticated than ESP, it is designed specifically for small engine research. As a result, it includes models for two-stroke mechanisms such as crankcase compression and transfer porting that must be incorporated when simulating two-stroke engines like the Tee Dee 0.010.

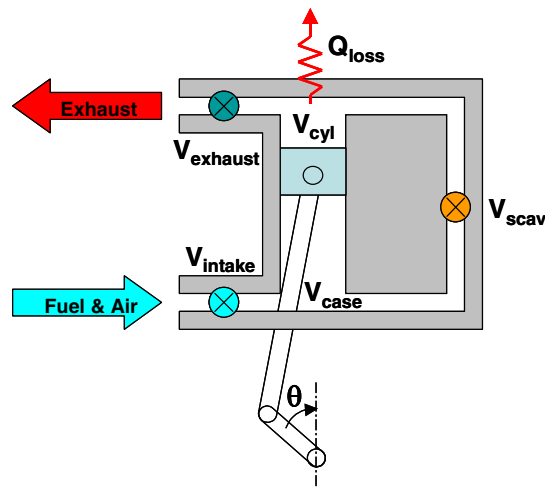
It should be emphasized, however, that this simulation is a “first cut” model of the actual Tee Dee operation. The model does not include a detailed combustion model, nor does it account for such mechanisms such as heat loss or piston blow-by. The results of this section only represent what the performance of the engine “might” be given a basic zero-dimensional model calibrated with performance measurements over a very limited speed range.

### 4.1 Algorithm Description

The simulation is comprised of a set of 20 MATLAB-executable text scripts called ‘m-files’ that are included in Appendix A. When the main m-file, TD\_model.m, is

called from within MATLAB, the script executes line-by-line (while also calling the other m-files), the performance solutions are tabulated, and the resulting plots are displayed within the MATLAB environment.

The code is designed to simulate a small two-stroke engine by modeling the conditions of two control volumes (cylinder as  $V_{cyl}$  and crankcase as  $V_{case}$ ) and three valves (intake as  $V_{intake}$ , transfer as  $V_{scav}$ , and exhaust as  $V_{exhaust}$ ) relative to crank position (angle as  $\theta$ ) as depicted in Figure 4.1. The timings for each valve can be independently defined to match the two-stroke operation of the Tee Dee (including the use of the transfer valve for scavenging) as described in Section 2. At the time of writing, an appropriate heat loss model (shown as  $Q_{loss}$ ) was still being developed and was therefore not included in this preliminary examination.



(Source: Christopher Cadou)  
 MATLAB Engine Model  
 Figure 4.1

During execution, the simulation solves a set of ordinary differential equations (ODE) that define the zero-dimensional state of the control volumes at each crank position interval. This is represented in Figure 4.2 as a matrix of equations solved for each volume at each interval with MATLAB's 'ode45' differential equation solver function [44] (where  $\omega$  represents engine speed).

The first equation is the thermodynamic equation of state (for an ideal gas) where  $V$  is volume,  $R$  is the universal gas constant,  $T$  is the temperature,  $p$  is pressure, and  $m$  is mass. The second equation is the conservation of mass simply represented as the change in mass of the mixture in the control volume,  $m$ , from the massflow in,  $\dot{m}_{in}$ , and massflow out,  $\dot{m}_{out}$ . The third equation is the conservation of energy represented as the change in heat energy  $Q$  from the energy flux in (or work in),  $\dot{Q}_{in}$ , and the energy flux out,  $\dot{Q}_{out}$ . (Because the heat loss model was excluded, the  $\dot{Q}_{out}$  term was assumed to be zero in this simulation. Also note that work out is not calculated here, but for this particular simulation, work is found rather by calculating the area inside

the computed P-V diagram as explained in Section 4.3.) The fourth equation is the forcing element of the matrix that represents how the change in volume,  $V$ , is driven by the crank position  $A(\theta)$ . The fifth equation represents the 1<sup>st</sup> law of thermodynamics which relates the change of internal energy (given by mass,  $m$ , specific heat at constant volume  $C_v$ , and temperature  $T$ ) to work and energy transfers of the system given by  $W$  and  $Q$  respectively. Finally, the sixth equation of the matrix is the 2<sup>nd</sup> law of thermodynamics which defines the entropy change,  $S$ , to the system as a result of heat transfer,  $Q$  at temperature  $T$  [32: pg. 27-32].

<b>State</b>	$V$	$-RT$	$0$	$p$	$-mR$	$0$	$\frac{d}{d\theta}$	$Q$	$= \frac{1}{\omega}$	$\begin{bmatrix} 0 \\ \dot{m}_{in} - \dot{m}_{out} \\ \dot{Q}_{in} - \dot{Q}_{out} \\ \omega A(\theta) \\ 0 \\ 0 \end{bmatrix}$			
<b>Mass cons.</b>	$0$	$1$	$0$	$0$	$0$	$0$					$p$	$m$	$0$
<b>Work in</b>	$0$	$0$	$1$	$0$	$0$	$0$					$Q$	$\dot{Q}_{in} - \dot{Q}_{out}$	$0$
<b>Forcing</b>	$0$	$0$	$0$	$1$	$0$	$0$					$V$	$\omega A(\theta)$	$0$
<b>1<sup>st</sup> law</b>	$0$	$0$	$-1$	$0$	$mC_v$	$0$					$T$	$0$	$0$
<b>2<sup>nd</sup> law</b>	$0$	$0$	$-1/T$	$0$	$0$	$1$					$S$	$0$	$0$

(Source: Christopher Cadou)

Matrix of differential equations solved by MATLAB

Figure 4.2

The combustion model for the simulation (used to describe work in) is based on a simple heat release function,  $HR$ , described by Equation 4.1 where  $\dot{m}_{air}$  is the mass flow of air,  $\phi$  is the equivalence ratio,  $f_{stoich}$  is the stoichiometric fuel/air ratio,  $Q_r$  is the lower heating value of the fuel,  $\theta_{rel}$  is the number of crank angle degrees through which the heat is released, and  $\eta_{comb}$  is the combustion efficiency. For this simulation,  $\theta_{rel}$  was set at 9 degrees so that the heat of combustion was released during 4.5 degrees of crank angle surrounding TDC. (Note that fixing ignition at TDC is a poor assumption, but it is done here since a detailed cylinder pressure or chemical reaction model is not incorporated into this simulation.) The value for combustion efficiency was determined by fitting the overall power output of the model to measured results as described in Section 4.2.

$$HR = \dot{m}_{air} \cdot \phi \cdot f_{stoich} \cdot \left( \frac{Q_r}{\theta_{rel}} \right) \cdot \eta_{comb} \quad (\text{Eq. 4.1})$$

The MATLAB code integrates this coupled set of ODEs over each portion of the cycle. The portions of the cycle are separated by the valve events as shown in Figure 2.18. At each interval of the simulation, these variables are solved and used as initial conditions for the succeeding interval. The values of the performance variables are tabulated with respect to crank angle, and the plots are then displayed automatically within the MATLAB application.

To test a range of inputs, the simulation allows for the solving of several engine configuration cases at once. The code reads a list of engine speeds, equivalence ratios, and intake valve efficiencies from an Excel spreadsheet (TestCases.xls) then computes the results for each case over the desired amount of cycles and archives the results into a single MATLAB array.

#### 4.2 Parameter Configuration

To configure the simulation for the Tee Dee 0.010, the following parameters were modified in the m-files:

*TD\_model.m* (main program script):

##### **Engine:**

***b=0.00602;***      % bore                      (m)  
***lc=0.01;***      % connecting rod length      (m)  
***S=0.00574;***      % stroke                      (m)  
***R\_ratio = lc/(0.007/2);*** % Ratio of connecting rod length to radius of crank.  
 (from approximate hand measurements)

***r=8.11;***      % compression ratio      (unitless)  
 (as determined by Equation B.1 in Appendix B)

***RPM=30000;***      % engine speed              (RPM)  
 (for this particular run, 30,000 RPM was chosen, however other speeds were additionally tested as shown in Section 4.3)

##### **Fuel/combustion:**

***Qr=16.86e6;***      % heating value of (inert oil) fuel (J/Kg)  
***f\_stoich=0.278;*** % stoichiometric fuel/air ratio (mass basis, unitless, neglect oil)  
***n\_stoich=0.179;*** % stoichiometric fuel/air ratio (mole basis, unitless, neglect oil)  
***MW\_f=35.7843;*** % molecular weight of fuel (45% methanol, 35% nitromethane)  
 (as determined in Section 2.4.2)

##### **Timing:**

***th\_0=180;***      % BDC                              (deg)  
***th\_1=220\*pi/180;*** % Angle at which transfer port closes (deg)  
***th\_2=240\*pi/180;*** % Angle at which exhaust port closes (deg)  
 (as depicted in Figure 2.18)

##### **Ports:**

***Exhaustportht = 0.001;*** % (m)  
***Transferportht = 0.001;*** % (m)  
***Exhportwidth = 2\*0.005;*** % multiplied by two to account for the two ports (m)  
***Tranportwidth = 2\*0.003;*** % multiplied by two to account for the two ports (m)

**Inletportlength** = 0.002; % (m)  
(from approximate hand measurements)

**Flow:**

**D\_rv**=0.002; % Diameter of rotary valve orifice (m)  
(from approximate hand measurements)

**Volumes:**

**V\_BDCc**=(0.013\*pi\*(D\_rv/2)^2)+(0.002\*pi\*(0.007/2)^2)+(0.005\*pi\*(b/2)^2);  
(approximation based on the volume of the hollow crankshaft, the volume of the cylinder-shaped gap between the crankshaft and the crankcase wall, and the volume of the hollow piston)

**Cycle Execution:**

**num\_cycles**=10; % the number of cycles to compute for each test case  
(This value represents how many Tee Dee cycles are executed for each case in order to achieve convergence. Only the results from the last converged cycle are tabulated.)

**[T1,Y1]=ode45(@rhs1,[180:d\_th:220],Y0,options,omega);**  
**[T2,Y2]=ode45(@rhs2,[221:d\_th:240],Y0,options,omega);**  
**[T3,Y3]=ode45(@rhs3,[241:d\_th:250],Y0,options,omega);**  
**[T4,Y4]=ode45(@rhs4,[251:d\_th:355],Y0,options,omega);**  
**[T5,Y5]=ode45(@rhs5,[356:d\_th:365],Y0,options,omega);**  
**[T6,Y6]=ode45(@rhs6,[366:d\_th:390],Y0,options,omega);**  
**[T7,Y7]=ode45(@rhs7,[391:d\_th:480],Y0,options,omega);**  
**[T8,Y8]=ode45(@rhs8,[481:d\_th:500],Y0,options,omega);**  
**[T9,Y9]=ode45(@rhs1,[501:d\_th:540],Y0,options,omega);**

(These commands call the MATLAB integrator function for each segment of the cycle separated by the valve events described in Section 2.3.)

*mdotincc.m* (defines the intake mass flow):

**Intake opening and closing geometry:**

(based on engine geometry described in Section 2.3)

**if(t<=310)**

(310 is the crank angle at which the intake valve is fully open)

**Inletportwidth** = (t-250)\*0.03333\*1e-3;

(250 is angle at which the intake valve begins to open and 0.03333\*1e-3 is the slope of the linear curve defining the width of the intake opening with respect to crank angle assuming the max width is 0.002 m)

**elseif ((t>330)&&(t<=390))**

(330 is the angle at which the intake valve begins to close and 390 is the angle at which it is fully closed)

**Inletportwidth** = (2.0-(t-330)\*0.03333)\*1e-3;

(2.0\*1e-3 is the maximum width of the intake opening, 330 is the angle at which

the valve begins to close, and  $0.03333 \times 10^{-3}$  is the slope of the linear curve defining the width of the intake opening with respect to crank angle)

*TestCases.xls* (contains a table of input parameters for several cases):

<b>Speed(Rpm)</b>	<b>Eqv. Ratio</b>	<b>Intake Efficiency</b>
$\omega_1$	$\phi_1$	$\eta_1$
.	.	.
.	.	.
.	.	.
$\omega_n$	$\phi_n$	$\eta_n$

(Each row of the spreadsheet describes a different test case where  $\omega_1 \dots \omega_n$  represent the engine speeds (in RPM),  $\phi_1 \dots \phi_n$  represent the equivalence ratios, and  $\eta_1 \dots \eta_n$  represent the intake valve efficiencies (in percentage). When the simulation is executed, the code takes the parameters from the first row, computes the desired number of cycles, archives the results, and continues onto the next case until the last row of the spreadsheet is read.

To determine the values for equivalence ratio ( $\phi_1 \dots \phi_n$ ), the measured Original Cox Tee Dee data from Section 3.3.1 was first fit to a linear curve, as shown in Figure 4.3. The resulting line's equation was then used to predict the equivalence ratios for a wide range of speeds as shown in Section 4.3.

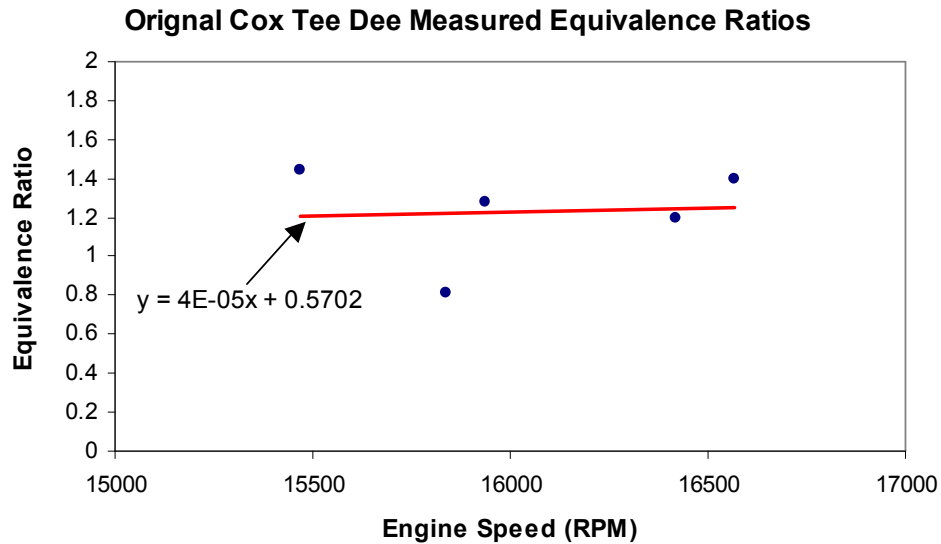


Figure 4.3

To determine the proper intake efficiencies ( $\eta_1 \dots \eta_n$ ), an attempt was initially made to optimize the values (with the same method used to determine combustion efficiency) until the calculated volumetric efficiencies fit the measured results. The volumetric airflow,  $Q_{air}$ , was found using Equation 4.2 where  $\dot{m}$  is the total mass

flow,  $\phi$  is the equivalence ratio,  $f_{stoich}$  is the stoichiometric fuel/air ratio, and  $\rho_{air}$  is the density of air. Finally, volumetric efficiency was computed using Equation 3.7.

$$Q_{air} = \frac{\dot{m}}{1 + \phi f_{stoich}} - \frac{1}{\rho_{air}} \quad (\text{Eq. 4.2})$$

Unfortunately, when the intake efficiency was set to 100%, the resulting volumetric efficiency was still smaller than the measured results as shown in Section 4.4. While this apparently demonstrates a fundamental error in the model, the valve efficiency for each run was left at 100% for the closest approximation possible.)

*heat\_rel.m (describes the heat release calculation for combustion):*

***hr=m\_air\*phi\*f\_stoich\*Qr/9\* 0.16;***

(Unlike ESP, since a heat loss model was not included this simulation, heat energy loss for the cycle was approximated by specifying only a combustion efficiency.

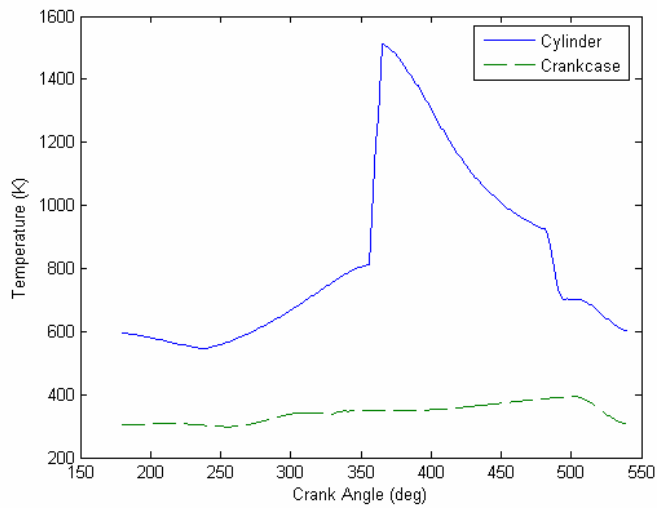
This calculation represents Equation 4.1 where  $\theta_{rel}$  is 9 degrees and  $\eta_{comb}$  is 0.16.

To determine a proper combustion efficiency value, the simulation was run at the five speeds and equivalence ratios corresponding to the Original Cox Tee Dee experiments in Section 3. [Note that the modified Tee Dee engines were not included in this comparison because the model does not have any accounting for a throttle mechanism.] The resulting power values were then compared to the measured values by taking the average of the difference between each simulated and measured value. The combustion efficiency in the simulation was continuously adjusted until the average difference between the two was minimized. Through this method, the best-fit combustion efficiency,  $\eta_{comb}$ , was determined to be 16%.)

### 4.3 Results and Analysis

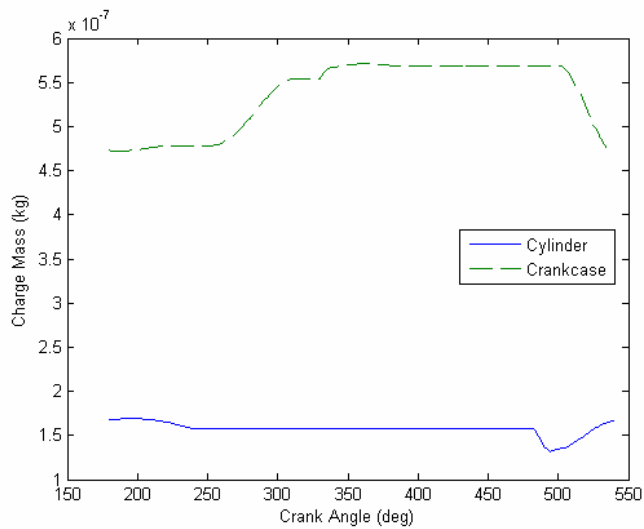
The following results were computed by the MATLAB Tee Dee 0.010 model for the 30,000 RPM case with an equivalence ratio of 1.77 and combustion efficiency of 16% as derived in Section 4.2.

Figure 4.4 shows crankcase and cylinder temperature throughout the cycle as computed by the MATLAB model. Predictably, the temperature in the cylinder spikes at ignition (360°), drops steadily during expansion, then sharply drops again when the exhaust port opens at 480°. The crankcase temperature can also be seen slightly rising during crankcase compression then dropping after the transfer port opens at 500°.



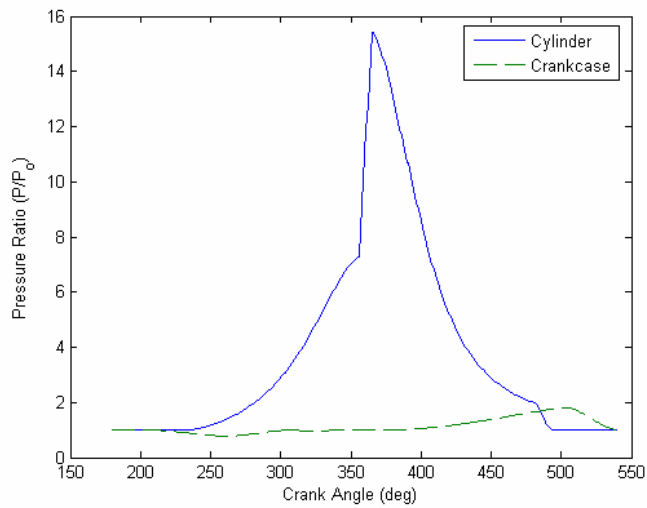
MATLAB Tee Dee 0.010 Temperatures  
Figure 4.4

Figure 4.5 shows the mass contained in the cylinder and crankcase through the cycle. As expected, the mass within the cylinder is constant in between the transfer and exhaust port events. The mass within the crankcase increases as the rotary valve opens and then drops when the transfer port opens.



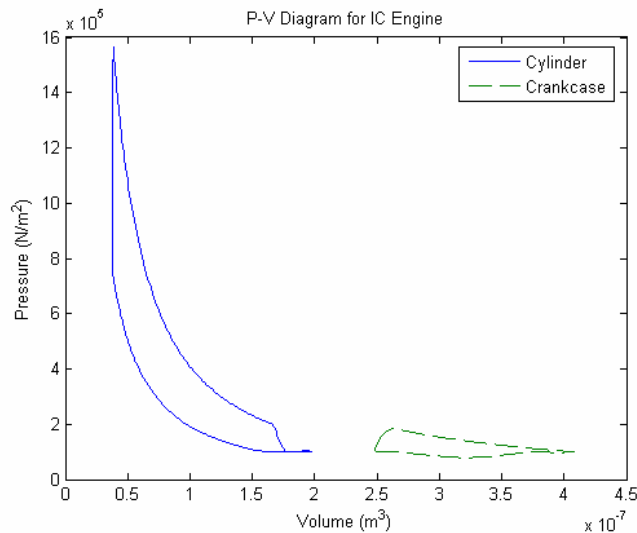
MATLAB Tee Dee 0.010 Masses  
Figure 4.5

As seen in the plot of pressure ratios in Figure 4.6, the cylinder pressure increases through the compression stroke and ignition, and then drops during the expansion stroke.



MATLAB Tee Dee 0.010 Pressures  
Figure 4.6

The P-V diagrams for both control volumes are shown in Figure 4.7. From the standard definition [42, et al], the area within the cylinder P-V trace represents the work output of the power stroke and the area within the crankcase P-V trace represents the pumping work. The net work output of the cycle is the cylinder work minus the pumping work.



MATLAB Tee Dee 0.010 P-V Diagrams  
Figure 4.7

Equation 4.3 represents the standard definition of power [42] where  $mep$  is the mean effective pressure,  $V_d$  is engine displacement,  $N$  is crankshaft rotations per unit time/seconds (RPM/60), and  $X$  is the number of revolutions per power stroke ( $X=1$  for a two-stroke engine).

$$P = (mep)V_d \frac{N}{X} \quad (\text{Eq. 4.3})$$

The power output of this simulation can be found by adapting Equation 4.3 so that the term representing work per cycle,  $(mep)V_d$ , is replaced simply by the area of the polygon plotted on the P-V diagram. Once configured with the equivalence ratios and efficiencies measured in Section 3, work for each speed setting was calculated using MATLAB's 'polyarea' function then entered into the equation for the power output.

The simulation results for a wide range of speeds are listed in Table 4.1 along with the corresponding plots of volumetric efficiency and power in Figures 4.8 and 4.9 respectively.

Speed (RPM)	Equiv. Ratio	Vol. Efficiency (%)	Power (W)
6000	0.81	57.72	3.52
9000	0.93	54.19	5.74
12000	1.05	51.63	7.87
15000	1.17	50.18	9.54
18000	1.29	48.91	11.14
21000	1.41	48.06	12.75
24000	1.53	47.45	14.38
27000	1.65	46.64	15.87
30000	1.77	46.24	17.48
33000	1.89	45.76	19.02
36000	2.01	45.41	20.58

MATLAB Tee Dee 0.010 Results

Table 4.1

The plot of volumetric efficiency in Figure 4.8 demonstrates an expected drop in the Tee Dee's ability to inhale enough air at higher speeds, however, the low magnitudes reflect the inaccuracy witnessed during model optimization in Section 4.2.

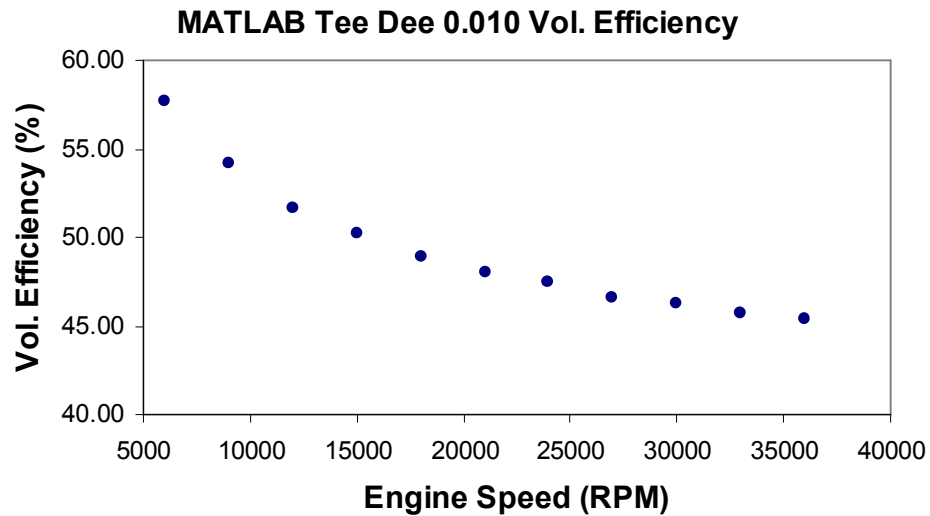


Figure 4.8

Figure 4.9 shows the MATLAB-derived power curve along with the measured power values of the Original Cox Tee Dee and the previously published power curve from Aeromodeller (taken from Figure 2.20). From the comparison, it is clear the simulated curve does not show the decrease one expects near the higher speeds seen in the Aeromodeller curve, however, this may simply reflect the inaccuracy of the model's volumetric efficiency. While the MATLAB-derived slope is slightly lower than the Aeromodeller curve and the measured results only cover a small speed range, overall, the datum sets seem to agree well.

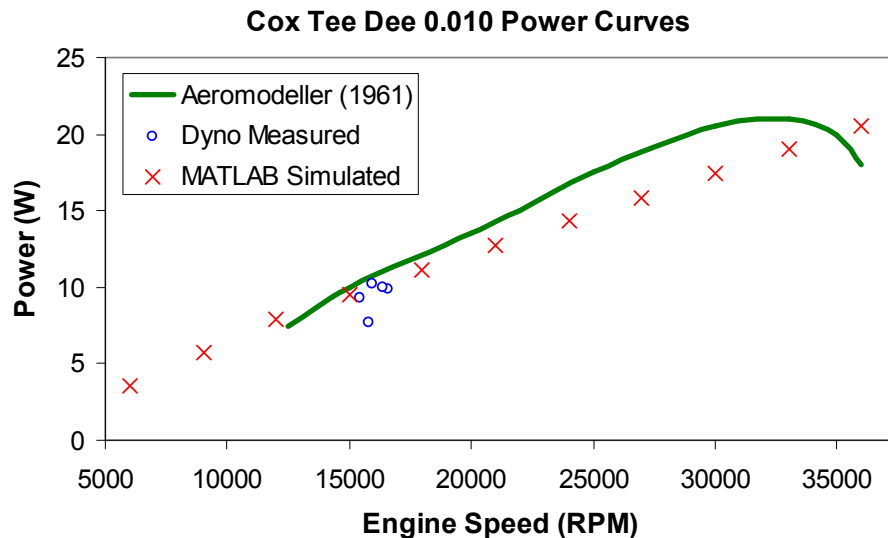


Figure 4.9

#### 4.4 Error Analysis

Table 4.2 lists the power output of the MATLAB model next to the measured power output of the Original Cox Tee Dee at each speed along with the percentage difference from the measured value. Note that the combustion efficiency was adjusted in order to minimize the average error of these power values as described in Section 4.2.

RPM	MATLAB: P (W)	Meas: P (W)	Diff (W)	%Diff
15470	9.83	9.26	0.57	6
15839	8.28	7.70	0.58	8
15935	10.05	10.24	-0.19	2
16417	10.31	10.00	0.30	3
16567	10.39	9.89	0.51	5

MATLAB and Measured Power Comparison

Table 4.2

Tables 4.3 and 4.4 list the airflow and volumetric efficiency of the MATLAB model respectively. While the error percentages are relatively small, since the intake efficiency was set to the unrealistic value of 100%, the results here demonstrate a fundamental error in the model as discussed in Section 4.2. (A future work task includes reevaluating the valve and volumetric efficiency algorithms in order to rectify this shortcoming of the simulation.) Additional performance values such as BSFC and thermal efficiency were not calculated and compared because they are derived from the same power and mass flow values analyzed here.

RPM	MATLAB: Airflow (kg/s)	Meas: Airflow (kg/s)	Diff (kg/s)	%Diff
15470	2.963E-05	3.037E-05	-7.4E-07	2
15839	3.120E-05	3.145E-05	-2.4E-07	1
15935	3.031E-05	3.151E-05	-1.2E-06	4
16417	3.110E-05	3.368E-05	-2.6E-06	8
16567	3.136E-05	3.386E-05	-2.5E-06	7

MATLAB and Measured Airflow Comparison

Table 4.3

RPM	MATLAB: Vol Efficiency	Meas: Vol Efficiency	Diff	%Diff
15470	0.5013	0.5985	-0.10	16
15839	0.5157	0.6053	-0.09	15
15935	0.4979	0.6029	-0.10	17
16417	0.4959	0.6255	-0.13	21
16567	0.4956	0.6231	-0.13	20

MATLAB and Measured Volumetric Efficiency Comparison

Table 4.4

Overall, while the MATLAB results were produced without advanced loss modeling, the values are still closer to the measured values than the results from ESP (seen in Appendix B). Additionally, because of the inclusion of two-stroke mechanisms, the

performance diagrams in Section 4.3 depict expected behavior and yield a very basic, but valid description of the events of the Tee Dee's operation.

## 5. Conclusion

### 5.1 Findings

The principal contribution of this thesis is to report the first scientifically rigorous measurements of the performance of the Cox Tee Dee 0.010 glow fuel engine. The results show that the engine is capable of producing 10.2 W with an overall efficiency of 6.4%. This corresponds to a power density of 788 W/kg and a specific fuel consumption of  $3.95 \times 10^{-3}$  kg/W-hr. The Tee Dee's power output is more than twice that produced by the UC Berkeley meso-scale rotary engine and matches the most optimistic projections of the MIT microturbine project. While its efficiency and power density are well below that of the University of Michigan's meso-scale swing engine, the Tee Dee is much smaller (13 g for the Tee Dee vs. 31 g for the swing engine) and its unidirectional shaft rotation makes it much better suited for propeller-based propulsion. Other important findings are as follows:

- The specialized dynamometer developed to measure the performance of hobby-scale model engines had to be modified to accommodate the diminutive Cox Tee Dee 0.010. The 800 W hysteresis brake had too much friction and could not be driven by the Tee Dee. Therefore, it was replaced with a DC motor that was used to apply a load by operating it in reverse as a generator. It was also found that the engine would not run properly unless the tension applied to the crankshaft by the propeller was simulated on the dynamometer. This was accomplished by using a specific type of shaft coupler.
- Detailed measurements of power, thermodynamic efficiency, and volumetric efficiency of the original Cox engine are consistent with reports in the hobby literature (as shown in Figure 2.20).
- Detailed measurements of power, thermodynamic efficiency, and volumetric efficiency for two Cox Tee Dee engines that were modified by Micro-Flite Inc. so that they are throttleable show that the modifications reduce performance. The Micro-Flite engines produced, at best, 9.85 W at an efficiency of 3.4%. The results conflict with claims in the Micro-Flite literature [26] that suggest that the presence of the throttle mechanism does not inhibit full-throttle performance.
- The speed range tested for this work is too small to detect any clear trend of power output and efficiency with speed. A smaller absorber with lower friction coupled with higher potency fuel may need to be implemented in order to test the engine over a wider operating range.
- An investigation of the Stanford Engine Simulation Program (ESP) indicated that it cannot be adapted for use in two-stroke engines by modifying the valve timing. A highly simplified MATLAB simulation was used instead. The power curve produced was consistent with the experimental measurements within their error boundaries and with a power curve published in the hobby literature. The results also suggest that the Tee Dee has very low combustion efficiency.

## 5.2 Capability Assessment

After decades of production and extensive use in the hobby industry, the Cox Tee Dee 0.010 has already proven itself as an effective and reliable model aircraft powerplant. While the Tee Dee's surprisingly noisy operation excludes its use in some environments, its small size and high power density make it an attractive choice for small-scale power applications. Its thermal efficiency of 6.4% enables it to surpass the endurance of batteries for emerging MAV power applications. It is not clear, however, whether material wear and fatigue would limit endurance below the theoretical value since the laboratory tests of this work did not exceed 30 minutes of continuous operation.

## 5.3 Future Work

### 5.3.1 Measurement Tasks

There are a number of improvements to the experiments that are required in order to fully characterize the performance of the Tee Dee 0.010 engine. First, the brushed DC motor should be replaced with a direct-drive brushless motor so as to reduce baseline frictional loading on the engine. Second, the thrust when the engine is operating with its standard propeller should be measured and a coupling designed to produce comparable levels of crankshaft pre-load. Taken together, these two steps would enable the engine to operate at a wider range of speeds. Since preliminary results from the engine simulation indicate that combustion efficiency is extremely low because of oxygen starvation, a third strategy is to try operating on fuels with higher nitromethane contents. Finally, endurance tests should be performed in order to establish how long the engine can operate without performance degradation.

### 5.3.2 Simulation Tasks

The MATLAB simulation needs to be improved in order to provide proper matching between the predicted and experimentally observed air flow rates through the engine. Also, the model for the combustion process needs a lot of improvement. A first step would be to impose a pressure-crank angle profile similar to that found in larger engines. However, this will probably not work well because the combustion process in the Tee Dee 0.010 is very different than that occurring in larger engines because of the unusually high nitromethane content and surface area/volume ratio. A second step is to use CANTERA to simulate the combustion process itself using finite rate multi-step chemistry. It might also be necessary to incorporate a turbulence model although turbulent processes should be less important in this engine because Reynolds numbers will be smaller. Finally, it may be useful to experiment with commercial programs for simulating two-stroke engines like as MOTA<sup>®</sup> or Virtual Engines' Virtual 2-Stroke<sup>®</sup>. However, the quality of the combustion models in these codes is unknown.

## Appendix A: MATLAB Simulation Code

### TD Model.m:

```

%% EngineCycle
%% Computes p-V, T-S diagrams for a compression ignition engine
% %
clc;
clear all;
global R cp cv Vo b S lc P_o T_o f_stoich phi Qr t_comb flag th_1 th_2 th_3 th_4 gamma_u Exhaustportht ...
    Transferportht Inletportlength Inletportwidth Exhportwidth Tranportwidth Cd Cd_t areafalg Cd_in RPM ...
    k_wall d_wall h_en diff_g_theta Spbar k_gas nu_gas c1 c2 g_theta omega R_ratio V_BDC rho_air mair mfuel;

%USER ADJUSTABLE PARAMETERS
% Engine
b = 0.00602; %bore (m)
lc = 0.01; %connecting rod length (m)
S = 0.00574; %stroke (m)
R_ratio = lc/(0.007/2); % Ratio of connecting rod length to radius of crank.
r = 8.11; %compression ratio (unitless)
% Fuel/combustion
Qr = 16.86e6; %heating value of (inert oil) fuel (J/Kg)
f_stoich = 0.278; %stoichiometric fuel/air ratio (mass basis, unitless, neglect oil)
n_stoich = 0.179; %stoichiometric fuel/air ratio (mole basis, unitless, neglect oil)
MW_f = 35.7843; %molecular weight of fuel (45% methanol, 35% nitromethane, neglect oil)
MW_a = 28.84; %molecular weight of air
Cp_u = 1004; %heat capacity of unburned fuel-air mixture (J/kgK)

t_del = 0.5e-3; %ignition delay (s)
t_comb = 1;
Cd = 1;
Cd_t = 1;

% Timing
th_0 = 180; %BDC (deg)
th_1 = 220*pi/180; %Angle at which transfer port closes (deg)
th_2 = 240*pi/180; %Angle at which exhaust port closes (deg)
% th_3 = 405*pi/180; %Angle at which intake port closes (deg)
% th_4 = 472*pi/180; %Angle at which exhaust port opens (deg)
% th_5 = 481*pi/180; %Angle at which transfer port opens (deg)
% %
Exhaustportht = 0.001; % (m)
Transferportht = 0.001; % (m)
Exhportwidth = 2*0.005; % multiplied by two to account for the two ports (m)
Tranportwidth = 2*0.003; % multiplied by two to account for the two ports (m)
Inletportlength = 0.002; % (m)
% Flow
D_rv = 0.002; %Diameter of rotary valve orifice (m)
C_rv = 1; %Loss coefficient of rotary valve orifice (unitless)
% Environment
P_o = 101324; %Atmospheric pressure (N/m2)
T_o = 300; %Atmospheric temperautre (K)
T_o1 = 300;
rho_air = 1.23;
P_s = 1.25*P_o; %Scavenging pressure (N/m^2)
T_s = T_o1*(1.1)^((1.4-1)/1.4); %Scavenging temperature (K)
% Calculation
d_th = 1; %Angle increment for calculation (deg)
R_univ = 8314; %Gas constant for air (J/kgK)

h_en = 1e-15; %HT coefficient for environment. (W/m2K)
k_wall = 1e-15; %Conductivity of wall. (W/mK)
d_wall = 5e-3; %Thickness of wall.(m)
k_gas = 0.05e-15; %Thermal conductivity of gas. (W/mK)
nu_gas = 62.53e-6; %Kinematic viscosity of gas.(m2/s)
c1 = 0.76;% Calibration constant for 2/4 stroke engine.
c2 = 0.64;% Calibration constant for 2/4 stroke engine.

```

```

%
% % Computed Engine Parameters
Vo=pi*b*b*S/(4*(r-1)); %cylinder dead volume (m^3)
V_BDC=Vo+(pi*b*b*S/4); %cylinder volume at BDC (m^3)
V_BDCC=(0.013*pi*(D_rv/2)^2)+(0.002*pi*(0.007/2)^2)+(0.005*pi*(b/2)^2); %crankcase volume at BDC from shaft vol, case
vol, and piston vol (m^3)

%
% Computed thermodynamic parameters
MW_u=MW_a; %assume working fluid is pure air
R=R_univ/MW_u; %gas constant for fuel-air mixture
cv=Cp_u-R;
gamma_u=Cp_u/cv;
%
%integrate DEs over one engine cycle
theta_span=linspace(180,540,359)*pi/180;
%
options=odeset('Mass',@mass_mat3,'RelTol',1e-3,'AbsTol',1e-3);
areafalg=0;

% Cycle Execution

num_cycles=10; % the number of cycles to compute for each case

%First section.
Ncase = 0;
Testcases = xlsread('Testcases.xls');
Nc = size(Testcases);
j = Nc(1);
while (Ncase < j)
    Ncase = Ncase + 1
    RPM = Testcases(Ncase,1); %engine speed (RPM)
    omega = RPM*2*pi/60; %angular speed (rad/s)
    Spbar = 2 * lc * omega;
    Ncycle = 0;
    phi=Testcases(Ncase,2); %equivalence ratio (unitless)
    Cd_in = Testcases(Ncase,3)/100;

    %%CYLINDER%%
    Y0(1)=P_o; %pressure
    Y0(2)=(1+(f_stoich*phi))*(P_o*V_BDC)/(R*T_o); %charge mass
    Y0(3)=0; %work of compression (isentropic)
    Y0(4)=V_BDC; %charge volume
    Y0(5)=T_o1; %initial charge temperature
    Y0(6)=0; %initial entropy
    %%CRANKCASE%%
    Y0(7)=P_s; %pressure
    Y0(8)=(1+(f_stoich*phi))*(P_s*V_BDCC)/(R*T_s); %charge mass
    Y0(9)=0; %heat content (after isentropic compression)
    Y0(10)=V_BDCC; %charge volume
    Y0(11)=T_s; %initial charge temperature
    Y0(12)=0;

    while (Ncycle<num_cases)
        Ncycle = Ncycle + 1;
        options=odeset('Mass',@mass_mat3,'RelTol',1e-3,'AbsTol',1e-3);
        [T1,Y1]=ode45(@rhs1,[180:d_th:220],Y0,options,omega);
        a=size(Y1);
        Y0 = Y1(a(1),:);
        Y0(3)=0;
        Y0(9)=0;
        [T2,Y2]=ode45(@rhs2,[221:d_th:240],Y0,options,omega);
        a=size(Y2);
        Y0 = Y2(a(1),:);
        Y0(3)=0;
        Y0(9)=0;
        %Second section.
        [T3,Y3]=ode45(@rhs3,[241:d_th:250],Y0,options,omega);
        a=size(Y3);
        Y0 = Y3(a(1),:);

```

```

Y0(3)=0;
Y0(9)=0;
[T4,Y4]=ode45(@rhs4,[251:d_th:355],Y0,options,omega);
a=size(Y4);
Y0 = Y4(a(1),:);
Y0(3)=0;
Y0(9)=0;
x = Y0(2);
y = f_stoich * phi;
mair = x / (1 + y);
mfuel = y * mair;
[T5,Y5]=ode45(@rhs5,[356:d_th:365],Y0,options,omega);
a=size(Y5);
Y0 = Y5(a(1),:);
Y0(3)=0;
Y0(9)=0;
[T6,Y6]=ode45(@rhs6,[366:d_th:390],Y0,options,omega);
a=size(Y6);
Y0 = Y6(a(1),:);
Y0(3)=0;
Y0(9)=0;
[T7,Y7]=ode45(@rhs7,[391:d_th:480],Y0,options,omega);
a=size(Y7);
Y0 = Y7(a(1),:);
Y0(3)=0;
Y0(9)=0;
[T8,Y8]=ode45(@rhs8,[481:d_th:500],Y0,options,omega);
a=size(Y8);
Y0 = Y8(a(1),:);
Y0(3)=0;
Y0(9)=0;
[T9,Y9]=ode45(@rhs1,[501:d_th:540],Y0,options,omega);
a=size(Y9);
Y0 = Y9(a(1),:);
Y0(3)=0;
Y0(9)=0;
Tcomb=[T1',T2',T3',T4',T5',T6',T7',T8',T9'];
for j=1:12
    Ycomb(j,:)=(Y1(:,j))',(Y2(:,j))',(Y3(:,j))',(Y4(:,j))',(Y5(:,j))',(Y6(:,j))',(Y7(:,j))',(Y8(:,j))',(Y9(:,j))');
end
Tvec(1:length(Tcomb'),Ncycle)=Tcomb';
sizeY = size(Ycomb');
Yvec(1:sizeY(1),1:sizeY(2),Ncycle)=Ycomb';
end
T_complete = Tvec(:,1);
Y_complete = Yvec(:,1);
if Ncycle>1
    T_complete = [Tvec(:,1);360+Tvec(:,2)];
    Y_complete = [Yvec(:,1);Yvec(:,2)];
end
if (Ncycle>2)
    for j = 3:Ncycle
        T_complete_new = [T_complete;360*(j-1)+Tvec(:,j)];
        T_complete = T_complete_new;
        Y_complete_new = [Y_complete;Yvec(:,j)];
        Y_complete = Y_complete_new;
    end
end
end
%Save the results vector for post processing.
Yres = Yvec(:,Ncycle);
Tres = Tvec(:,Ncycle);
vol = CyIVol(Vo,b,S,lc,Tres*pi/180);
Results(Ncase,:)=postprocess(Yres,Tres,vol);
end

%%%%%%%%%%
figure
plot(Tvec(:,Ncycle),Yvec(:,4,Ncycle),Tvec(:,Ncycle),Yvec(:,10,Ncycle));
xlabel('Crank Angle (deg)');
ylabel('Cylinder Volume (m^3)');

```

```

legend('Cylinder volume','Crank case volume');

figure
plot(Tvec(:,Ncycle),Yvec(:,1,Ncycle)/P_o,Tvec(:,Ncycle),Yvec(:,7,Ncycle)/P_o);
%plot(T_complete,Y_complete(:,1)/P_o,T_complete,Y_complete(:,7)/P_o);
xlabel('Crank Angle (deg)');
ylabel('Pressure Ratio (P/P_o)');
legend('Cylinder','Crankcase');

figure
plot(Tvec(:,Ncycle),Yvec(:,2,Ncycle),Tvec(:,Ncycle),Yvec(:,8,Ncycle));
%plot(T_complete,Y_complete(:,2),T_complete,Y_complete(:,8));
xlabel('Crank Angle (deg)');
ylabel('Charge Mass (kg)');
legend('Cylinder','Crankcase');

figure
plot(Tvec(:,Ncycle),Yvec(:,5,Ncycle),Tvec(:,Ncycle),Yvec(:,11,Ncycle));
%plot(T_complete,Y_complete(:,5),T_complete,Y_complete(:,11));
xlabel('Crank Angle (deg)');
ylabel('Temperature (K)');
legend('Cylinder','Crankcase');

figure
plot(Yvec(:,4,Ncycle),Yvec(:,1,Ncycle),Yvec(:,10,Ncycle),Yvec(:,7,Ncycle));
%plot(Y_complete(:,4),Y_complete(:,1),Y_complete(:,10),Y_complete(:,7));
xlabel('Volume (m^3)');
ylabel('Pressure (N/m^2)');
title('P-V Diagram for IC Engine');
legend('Cylinder','Crankcase');

figure
plot(Tvec(:,Ncycle),Yvec(:,3,Ncycle),Tvec(:,Ncycle),Yvec(:,9,Ncycle));
%plot(T_complete,Y_complete(:,3),T_complete,Y_complete(:,9));
xlabel('Crank Angle (deg)');
ylabel('Heat Content (J)');
legend('Cylinder','Crankcase');

figure
plot(Tvec(:,Ncycle),Yvec(:,2,Ncycle).*cv.*Yvec(:,5,Ncycle),Tvec(:,Ncycle),Yvec(:,8,Ncycle).*cv.*Yvec(:,11,Ncycle));
%plot(T_complete(:,Y_complete(:,2).*cv.*Y_complete(:,5)),T_complete(:,Y_complete(:,8).*cv.*Y_complete(:,11)));
xlabel('Crank Angle (deg)');
ylabel('Internal energy (J)');
legend('Cylinder','Crankcase');

```

### **CylVol.m:**

```

function t=CylVol(Vo,b,S,lc,th)
% computes the cylinder volume as a function of crank angle theta
% Th=0 corresponds to TDC
% Vo: cylinder dead volume
% b: cylinder bore
% S: stroke
% lc: connecting rod length
% th: crank angle (theta)

A1=S*(1-cos(th))./2;
A2=lc-(((lc^2)-(S*sin(th)./2).^2).^(1/2));
t=Vo + (pi*b*b/4).*(A1+A2);

```

### **D CylVol Dtheta.m:**

```

function t=D_CylVol_Dtheta(Vo,b,S,lc,th)
% computes the rate of change of cylinder volume with crank angle theta
% Th=0 corresponds to TDC
% Vo: cylinder dead volume (m^3)
% b: cylinder bore (m)

```

```

% S: stroke (m)
% lc: connecting rod length (m)
% th: crank angle (theta) (rad)
%
% A1=1/sqrt((lc*lc)-(S*S*sin(th)*sin(th)/4));
% A2=1+(S*A1*cos(th)/2);

dA1= S/2*sin(th);
dA2 = -1/2*(lc^2-((S*sin(th))/2)^2)^(-1/2)*(-2*S^2*sin(th)^2*cos(th)/4);

% t=(pi*b*b/4)*(S/2)*sin(th)*A2;
t=(pi*b*b/4)*(dA1+dA2);

```

### **heat\_rel.m:**

```

function hr=heat_rel1(th,m_air,f_stoich,phi,Qr,t_comb,om)
global flag mair mfuel;
% computes the heat release rate associated with combustion
if(phi>1)
    hr = (mfuel/phi*Qr/9)*0.16;
elseif (phi<=1)
    hr = (mfuel * Qr / 9)*0.16;
end

```

### **heat\_transfer.m:**

```

function hr=heat_transfer(m_air,T1,T2)
global cp;
% computes the heat release rate associated with mass transfer processes.
if (m_air)>0
    hr=m_air*cp*T1;
elseif (m_air)<0
    hr=m_air*cp*T2;
else
    hr = 0;
end

```

### **mass\_mat3.m:**

```

% function M=mass_mat3(t,Y,R,cv,Vo,b,S,lc,om,P_o,T_o,D_rv,C_rv)
function M=mass_mat3(t,Y,om)
global R cv Vo b S lc P_o T_o k_wall d_wall h_en omega R_ratio nu_gas k_gas c1 c2 RPM;
% computes the mass matrix for the system of ODEs describing
% the IC engine

% Y Vector of state variables
% Cylinder
% Y(1) cylinder pressure
% Y(2) mass of gas in cylinder
% Y(3) heat transfer
% Y(4) cylinder volume
% Y(5) gas temperature
% Y(6) entropy
% Crankcase
% Y(7) crank case pressure
% Y(8) mass of gas in crank case
% Y(9) enthalpy
% Y(10) crank case volume
% Y(11) gas temperature
% Y(12) entropy

M = zeros(12,12); %create mass matrix

```

```

%%CYLINDER%%
%Equation 1 (state)
M(1,1)=Y(4);
M(1,2)=-R*Y(5);
M(1,4)=Y(1);
M(1,5)=-Y(2)*R;
%Equation 2 (cons. mass)
M(2,2)=1;
%Equation 3 (energy input)
M(3,3)=1;
% M(3,13)=-1/(RPM /60 * 360);
%Equation 4 (forcing (volume change))
M(4,4)=1;
%Equation 5 (1st law)
M(5,3)=-1;
M(5,4)=Y(1);
M(5,5)=Y(2)*cv;
%Equation 6 (2nd law)
M(6,3)=-1/Y(5);
M(6,6)=1;

```

```

%%CRANKCASE%%
%Equation 1 (state)
M(7,7)=Y(10);
M(7,8)=-R*Y(11);
M(7,10)=Y(7);
M(7,11)=-Y(8)*R;
%Equation 2 (cons. mass)
M(8,8)=1;
%Equation 3 (energy input)
M(9,9)=1;
%Equation 4 (forcing (volume change))
M(10,10)=1;
%Equation 5 (1st law)
M(11,9)=-1;
M(11,10)=Y(7);
M(11,11)=Y(8)*cv;
%Equation 6 (2nd law)
M(12,9)=-1/Y(11);
M(12,12)=1;

```

### **mdotexcyl.m:**

```

function marealex=mdotperarea(th,P1,T1)
global Vo b S lc th_1 th_2 th_3 th_4 P_o T_o cp R Cd Cd_t Exhaustportht Exhporthtwidth Tranporthtwidth Transferportht
gamma_u areaflag;
% Computes mass flow rate per unit area given:
% P_1 upstream pressure (pressure in volume under consideration) (N/m^2)
% P_2 downstream static pressure (pressure outside volume under consideration) (N/m^2)
% rho_o upstream total density (kg/m^3)
% T_o upstream total temperature (K)
% cp heat capacity of gas (J/kgK)
% C_orifice loss coefficient for orifice (unitless)
%
% -----\
% \-----
% rho_o, T_o, P_o --> mdot P
% /-----
% -----/
P2 = P_o;
%Find critical pressure ratio.
CPR = (2/(gamma_u+1))^(gamma_u/(gamma_u-1));
loc = (PistDisp(th)-PistDisp(th_2));
if (loc>=0)
    Exhportht = loc;
    if(Exhportht>Exhaustportht)
        A_ex = Exhporthtwidth * Exhaustportht;
    else

```

```

    A_ex = Exhportwidth * Exhportht;
end
Pratio=P2/P1;
if (Pratio)<=1
    if (Pratio) <= CPR
        marealex = -(Cd * A_ex * P1 / (sqrt(R * T1))) * gamma_u^0.5 * (2 / (gamma_u + 1)) ^ ((gamma_u + 1) / (2 * (gamma_u - 1)));
    else
        marealex = -(Cd * A_ex * P1 / (sqrt(R * T1))) * (Pratio) ^ (1 / gamma_u) * (2 * gamma_u / (gamma_u - 1)) * (1 - (P2 / P1) ^ ((gamma_u - 1) / gamma_u)) ^ 0.5;
    end
else
    T1 = T_o;
    Ptemp = P2;
    P2 = P1;
    P1 = Ptemp;
    Pratio = (P2 / P1);
    if (Pratio) <= CPR
        marealex = (Cd * A_ex * P1 / (sqrt(R * T1))) * gamma_u^0.5 * (2 / (gamma_u + 1)) ^ ((gamma_u + 1) / (2 * (gamma_u - 1)));
    else
        marealex = (Cd * A_ex * P1 / (sqrt(R * T1))) * (Pratio) ^ (1 / gamma_u) * (2 * gamma_u / (gamma_u - 1)) * (1 - (P2 / P1) ^ ((gamma_u - 1) / gamma_u)) ^ 0.5;
    end
end
end
marealex=0;
end
end

```

### **mdotincc.m:**

```

function mareain=mdotincc(th,P2,T2)
global th_1 th_2 th_3 th_4 P_o T_o cp R Cd Cd_t Cd_in Inletportlength Inletportwidth areaflag gamma_u RPM;
% Computes mass flow rate per unit area given:
% P_1 upstream pressure (pressure in volume under consideration) (N/m^2)
% P_2 downstream static pressure (pressure outside volume under consideration) (N/m^2)
% rho_o upstream total density (kg/m^3)
% T_o upstream total temperature (K)
% cp heat capacity of gas (J/kgK)
% C_orifice loss coefficient for orifice (unitless)
%
% -----\
% \-----
% rho_o, T_o, P_o --> mdot P
% /-----
% -----/

%Find critical pressure ratio.
P1 = P_o;
T1 = T_o;
CPR = (2 / (gamma_u + 1)) ^ (gamma_u / (gamma_u - 1));
t = th * 180 / pi;

% intake opening and closing geometry
if(t<=310)
    Inletportwidth = (t-250)*0.03333*1e-3;
elseif ((t>330)&&(t<=390))
    Inletportwidth = (2.0-(t-330)*0.03333)*1e-3;
else
    Inletportwidth = 0;
end

if(Inletportwidth>0)
    A_in = Inletportwidth * Inletportlength;
    Pratio=P2/P1;
    if (Pratio)<=1
        if (P2/P1) <= CPR
            mareain = (Cd_in * A_in * P1 / (sqrt(R * T1))) * gamma_u^0.5 * (2 / (gamma_u + 1)) ^ ((gamma_u + 1) / (2 * (gamma_u - 1)));
        else

```

```

        mareain = (Cd_in * A_in * P1 / (sqrt(R * T1))) * (P2/P1)^(1/gamma_u) * (2*gamma_u/(gamma_u-1)) * (1 -
(P2/P1)^((gamma_u-1)/gamma_u))^0.5;
    end
    else
        Ptemp = P2;
        P2 = P1;
        P1 = Ptemp;
        Ttemp = T2;
        T2 = T1;
        T1 = Ttemp;
        if (P2/P1) <= CPR
            mareain = -(Cd_in * A_in * P1 / (sqrt(R * T1))) * gamma_u^0.5 * (2/(gamma_u+1))^(gamma_u+1) / (2*(gamma_u-1));
        else
            mareain = -(Cd_in * A_in * P1 / (sqrt(R * T1))) * (P2/P1)^(1/gamma_u) * (2*gamma_u/(gamma_u-1)) * (1 -
(P2/P1)^((gamma_u-1)/gamma_u))^0.5;
        end
    end
end
else
    mareain = 0;
end
end

```

### **mdotrcc.m:**

```

function mareatr =mdotrcc(th,P1,T1,P2,T2)
global Vo b S lc th_1 th_2 th_3 th_4 P_c T_o cp R Cd_t Transferportht Tranportwidth gamma_u areaflag;
% Computes mass flow rate per unit area given:
% P_1 upstream pressure (pressure in volume under consideration) (N/m^2)
% P_2 downstream static pressure (pressure outside volume under consideration) (N/m^2)
% rho_o upstream total density (kg/m^3)
% T_o upstream total temperature (K)
% cp heat capacity of gas (J/kgK)
% C_orifice loss coefficient for orifice (unitless)
%
% -----\
% \-----
% rho_o, T_o, P_o --> mdot P
% /-----
% -----/

%Find critical pressure ratio.
CPR = (2/(gamma_u+1))^(gamma_u/(gamma_u-1));
loctran = (PistDisp(th)-PistDisp(th_1));
if(loctran>0)
    Tranportht = loctran;
    if (Tranportht>Transferportht)
        A_t = Tranportwidth * Transferportht;
    else
        A_t = Tranportwidth * Tranportht;
    end
    Pratio=P2/P1;
    if (Pratio)<=1
        if (P2/P1) <= CPR
            mareatr = -(Cd_t * A_t * P1 / (sqrt(R * T1))) * gamma_u^0.5 * (2/(gamma_u+1))^(gamma_u+1) / (2*(gamma_u-1));
        else
            mareatr = -(Cd_t * A_t * P1 / (sqrt(R * T1))) * (P2/P1)^(1/gamma_u) * (2*gamma_u/(gamma_u-1)) * (1 -
(P2/P1)^((gamma_u-1)/gamma_u))^0.5;
        end
    end
    else
        Ptemp = P2;
        P2 = P1;
        P1 = Ptemp;
        Ttemp = T2;
        T2 = T1;
        T1 = Ttemp;
        if (P2/P1) <= CPR
            mareatr = (Cd_t * A_t * P1 / (sqrt(R * T1))) * gamma_u^0.5 * (2/(gamma_u+1))^(gamma_u+1) / (2*(gamma_u-1));
        else

```

```

        mareatr = (Cd_t * A_t * P1 / (sqrt(R * T1))) * (P2/P1)^(1/gamma_u) * (2*gamma_u/(gamma_u-1)) * (1-(P2/P1)^((gamma_u-1)/gamma_u))^0.5;
    end
end
else
    mareatr=0;
end

```

### mdottreyl.m:

```

function mareatr=mdotperarea(th,P2,T2,P1,T1)
global Vo b S lc th_1 th_2 th_3 th_4 P_o T_o cp R Cd Cd_t Exhaustportht Exhportwidth Tranportwidth Transferportht
gamma_u areaflag;
% Computes mass flow rate per unit area given:
% P_1 upstream pressure (pressure in volume under consideration) (N/m^2)
% P_2 downstream static pressure (pressure outside volume under consideration) (N/m^2)
% rho_o upstream total density (kg/m^3)
% T_o upstream total temperature (K)
% cp heat capacity of gas (J/kgK)
% C_orifice loss coefficient for orifice (unitless)
% -----\
%          \-----
% rho_o, T_o, P_o --> mdot P
%          /-----
% -----/
%Find critical pressure ratio.
CPR = (2/(gamma_u+1))^(gamma_u/(gamma_u-1));
%-----
loctran = (PistDisp(th)-PistDisp(th_1));
if (loctran>0)
    Tranportht = loctran;
    if (Tranportht>Transferportht)
        A_t = Tranportwidth * Transferportht;
    else
        A_t = Tranportwidth * Tranportht;
    end
    Pratio=P2/P1;
    if (Pratio)<=1
        if (P2/P1) <= CPR
            mareatr = (Cd_t * A_t * P1 / (sqrt(R * T1))) * gamma_u^0.5 * (2/(gamma_u+1))^((gamma_u+1)/(2*(gamma_u-1)));
        else
            mareatr = (Cd_t * A_t * P1 / (sqrt(R * T1))) * (P2/P1)^(1/gamma_u) * (2*gamma_u/(gamma_u-1)) * (1-(P2/P1)^((gamma_u-1)/gamma_u))^0.5;
        end
    else
        Ptemp = P2;
        P2 = P1;
        P1 = Ptemp;
        Ttemp = T2;
        T2 = T1;
        T1 = Ttemp;
        if (P2/P1) <= CPR
            mareatr = -(Cd_t * A_t * P1 / (sqrt(R * T1))) * gamma_u^0.5 * (2/(gamma_u+1))^((gamma_u+1)/(2*(gamma_u-1)));
        else
            mareatr = -(Cd_t * A_t * P1 / (sqrt(R * T1))) * (P2/P1)^(1/gamma_u) * (2*gamma_u/(gamma_u-1)) * (1-(P2/P1)^((gamma_u-1)/gamma_u))^0.5;
        end
    end
end
else
    mareatr = 0;
end

```

## PistDisp.m:

```
function d=PistDisp(th)
global Vo b S lc;
% computes the cylinder volume as a function of crank angle theta
% Th=0 corresponds to TDC
% Vo: cylinder dead volume
% b: cylinder bore
% S: stroke
% lc: connecting rod length
% th: crank angle (theta)

A1=S*(1-cos(th))/2;
A2=lc-(((lc^2)-(S*sin(th)/2).^2).^(1/2));
d=(A1+A2);
```

## rhs1.m:

```
% function dY=rhs3(t,Y,R,cv,Vo,b,S,lc,om,P_o,T_o,D_rv,C_rv,phi)
function dY=rhs1(t,Y,om)
global R cp cv Vo b S lc P_o T_o f_stoich phi Qr t_comb flag gamma_u Exhaustportht ...
Exhportht Transportwidth Cd_t Cd th_1 th_2 th_3 th_4 areaflag RPM diff_g_theta ...
Spbar k_wall d_wall nu_gas c1 c2 g_theta omega R_ratio h_en;
% computes the right hand side (rhs) for the system of ODEs describing
% the IC engine

% Y Vector of state variables
% Y(1) cylinder pressure
% Y(2) mass of gas in cylinder
% Y(3) enthalpy
% Y(4) cylinder volume
% Y(5) gas temperature
% Y(6) entropy

dY=zeros(12,1); %set up a column vector
th=t*pi/180; %compute crank angle in radians
cp=cv+R;
%%CYLINDER%%
% Equation 1 (state)
dY(1,1)=0;
% Equation 2 (cons. mass)
m1 = mdotexcyl(th,Y(1),Y(5))/(6*RPM);
% m1 = 0;
m2 = mdottrecyl(th,Y(1),Y(5),Y(7),Y(11))/(6*RPM);
dY(2,1)= m1 + m2;
% Equation 3 (energy input)
h1 = heat_transfer(m1,T_o,Y(5));
h2 = heat_transfer(m2,Y(11),Y(5));
dY(3,1) = h1 + h2;
% dY(3,1) = 0;
% Equation 4 (forcing (volume change))
dY(4,1)=D_CylVol_Dtheta(Vo,b,S,lc,th)*pi/180;
% Equation 5 (1st law)
dY(5,1)=0;
% Equation 6 (2nd law)
dY(6,1)=0;

%%CRANKCASE%%
% Equation 1 (state)
dY(7,1)=0;
% Equation 2 (cons. mass)
dY(8,1)=mdottrcc(th,Y(7),Y(11),Y(1),Y(5))/(6*RPM);
% Equation 4 (energy input)
dY(9,1)=heat_transfer(dY(8,1),Y(5),Y(11));
% dY(9,1)=0;
% Equation 5 (forcing (volume change))
dY(10,1)=-D_CylVol_Dtheta(Vo,b,S,lc,th)*pi/180;
```

```

% Equation 6 (1st law)
dY(11,1)=0;
% Equation 7 (2nd law)
dY(12,1)=0;

```

## rhs2.m:

```

% function dY=rhs3(t,Y,R,cv,Vo,b,S,lc,om,P_o,T_o,D_rv,C_rv,phi)
function dY=rhs2(t,Y,om)
global R cp cv Vo b S lc P_o T_o f_stoich phi Qr t_comb flag gamma_u Cd Cd_in Exhaustportht ...
Exhportwidthth_1 th_2 th_3 th_4 areafalg RPM diff_g_theta Spbar k_wall d_wall h_en nu_gas c1 c2 g_theta omega R_ratio;
% computes the right hand side (rhs) for the system of ODEs describing
% the IC engine

% Y Vector of state variables
% Y(1) cylinder pressure
% Y(2) mass of gas in cylinder
% Y(3) enthalpy
% Y(4) cylinder volume
% Y(5) gas temperature
% Y(6) entropy

dY=zeros(12,1); %set up a column vector
th=t*pi/180; %compute crank angle in radians
cp=cv+R;
%%CYLINDER%%
% Equation 1 (state)
dY(1,1)=0;
% Equation 2 (cons. mass)
m1 = mdotexcyl(th,Y(1),Y(5))/(6*RPM);
m2 = 0;
dY(2,1)= m1 + m2;
% Equation 3 (energy input)
h1 = heat_transfer(m1,T_o,Y(5));
h2 = heat_transfer(m2,Y(11),Y(5));
dY(3,1) = h1 + h2;
% dY(3,1)=0;
% Equation 4 (forcing (volume change))
dY(4,1)=D_CylVol_Dtheta(Vo,b,S,lc,th)*pi/180;
% Equation 5 (1st law)
dY(5,1)=0;
% Equation 6 (2nd law)
dY(6,1)=0;

%%CRANKCASE%%
% Equation 1 (state)
dY(7,1)=0;
% Equation 2 (cons. mass)
m1 = mdotincc(th,Y(7),Y(11))/(6*RPM);
m2 = 0;
dY(8,1)= m1 + m2;
% dY(8,1) = mdotincc(th,Y(7),Y(11))/(6*RPM);
% dY(8,1)=0;
% Equation 4 (energy input)
% dY(9,1)=heat_transfer(dY(8,1),T_o,Y(11));
h1 = heat_transfer(m1,T_o,Y(11));
h2 = heat_transfer(m2,Y(5),Y(11));
dY(9,1) = h1 + h2;
% dY(3,1)=0;
% dY(9,1)=0;
% Equation 5 (forcing (volume change))
dY(10,1)=-D_CylVol_Dtheta(Vo,b,S,lc,th)*pi/180;
% Equation 6 (1st law)
dY(11,1)=0;
% Equation 7 (2nd law)
dY(12,1)=0;

```

### rhs3.m:

```
% function dY=rhs3(t,Y,R,cv,Vo,b,S,lc,om,P_o,T_o,D_rv,C_rv,phi)
function dY=rhs3(t,Y,om)
global R cp cv Vo b S lc P_o T_o f_stoich phi Qr t_comb flag gamma_u Cd Cd_in Exhaustportht ...
Exhportwidthth_1 th_2 th_3 th_4 areafalg RPM diff_g_theta Spbar k_wall d_wall h_en nu_gas c1 c2 g_theta omega R_ratio;
% computes the right hand side (rhs) for the system of ODEs describing
% the IC engine

% Y Vector of state variables
% Y(1) cylinder pressure
% Y(2) mass of gas in cylinder
% Y(3) enthalpy
% Y(4) cylinder volume
% Y(5) gas temperature
% Y(6) entropy

dY=zeros(12,1); %set up a column vector
th=t*pi/180; %compute crank angle in radians
cp=cv+R;
%%CYLINDER%%
% Equation 1 (state)
dY(1,1)=0;
% Equation 2 (cons. mass)
dY(2,1)=0;
% Equation 3 (energy input)
dY(3,1)=heat_transfer(dY(2,1),T_o,Y(5));
% dY(3,1)=0;
% Equation 4 (forcing (volume change))
dY(4,1)=D_CylVol_Dtheta(Vo,b,S,lc,th)*pi/180;
% Equation 5 (1st law)
dY(5,1)=0;
% Equation 6 (2nd law)
dY(6,1)=0;

%%CRANKCASE%%
% Equation 1 (state)
dY(7,1)=0;
% Equation 2 (cons. mass)
dY(8,1)=0;
% dY(8,1)=0;
% Equation 4 (energy input)
dY(9,1)=heat_transfer(dY(8,1),T_o,Y(11));
% dY(9,1)=0;
% Equation 5 (forcing (volume change))
dY(10,1)=D_CylVol_Dtheta(Vo,b,S,lc,th)*pi/180;
% Equation 6 (1st law)
dY(11,1)=0;
% Equation 7 (2nd law)
dY(12,1)=0;
```

### rhs4.m:

```
% function dY=rhs3(t,Y,R,cv,Vo,b,S,lc,om,P_o,T_o,D_rv,C_rv,phi)
function dY=rhs4(t,Y,om)
global R cp cv Vo b S lc P_o T_o f_stoich phi Qr t_comb flag gamma_u RPM diff_g_theta Spbar k_gas nu_gas c1 c2 g_theta ...
omega R_ratio k_wall d_wall h_en;
% computes the right hand side (rhs) for the system of ODEs describing
% the IC engine

% Y Vector of state variables
% Y(1) cylinder pressure
% Y(2) mass of gas in cylinder
% Y(3) work
% Y(4) enthalpy
% Y(5) cylinder volume
% Y(6) gas temperature
```

```

% Y(7) entropy

dY=zeros(12,1); %set up a column vector
th=t*pi/180; %compute crank angle in radians
cp=cv+R;

%%CYLINDER%%
% Equation 1 (state)
dY(1,1)=0;
% Equation 2 (cons. mass)
dY(2,1)=0;
% Equation 3 (energy input)
dY(3,1)=0;
% dY(3,1)=0;
% Equation 4 (forcing (volume change))
dY(4,1)=D_CylVol_Dtheta(Vo,b,S,lc,th)*pi/180;
% Equation 5 (1st law)
dY(5,1)=0;
% Equation 6 (2nd law)
dY(6,1)=0;

%%CRANKCASE%%
% Equation 1 (state)
dY(7,1)=0;
% Equation 2 (cons. mass)
dY(8,1)=mdotincc(th,Y(7),Y(11))/(6*RPM);
% dY(8,1)=0;
% Equation 4 (energy input)
dY(9,1)=heat_transfer(dY(8,1),T_o,Y(11));
% dY(9,1)=0;
% Equation 5 (forcing (volume change))
dY(10,1)=-D_CylVol_Dtheta(Vo,b,S,lc,th)*pi/180;
% Equation 6 (1st law)
dY(11,1)=0;
% Equation 7 (2nd law)
dY(12,1)=0;

```

### **rhs5.m:**

```

% function dY=rhs3(t,Y,R,cv,Vo,b,S,lc,om,P_o,T_o,D_rv,C_rv,phi)
function dY=rhs5(t,Y,om)
global R cv Vo b S lc P_o T_o f_stoich phi Qr t_comb flag gamma_u RPM ...
diff_g_theta Spbar k_gas nu_gas c1 c2 g_theta omega R_ratio k_wall d_wall h_en mair mfuel;
% computes the right hand side (rhs) for the system of ODEs describing
% the IC engine

% Y Vector of state variables
% Y(1) cylinder pressure
% Y(2) mass of gas in cylinder
% Y(3) work
% Y(4) enthalpy
% Y(5) cylinder volume
% Y(6) gas temperature
% Y(7) entropy

dY=zeros(12,1); %set up a column vector
th=t*pi/180; %compute crank angle in radians
cp=cv+R;

%%CYLINDER%%
% Equation 1 (state)
dY(1,1)=0;
% Equation 2 (cons. mass)
dY(2,1)=0;
% Equation 3 (energy input)
dY(3,1)=heat_rel(t,Y(2),f_stoich,phi,Qr,t_comb,om);
% dY(3,1)=0;
% Equation 4 (forcing (volume change))

```

```

dY(4,1)=D_CylVol_Dtheta(Vo,b,S,lc,th)*pi/180;
% Equation 5 (1st law)
dY(5,1)=0;
% Equation 6 (2nd law)
dY(6,1)=0;

%%CRANKCASE%%
% Equation 1 (state)
dY(7,1)=0;
% Equation 2 (cons. mass)
dY(8,1)=mdotincc(th,Y(7),Y(11))/(6*RPM);
% dY(8,1)=0;
% Equation 4 (energy input)
dY(9,1)=heat_transfer(dY(8,1),T_o,Y(11));
% dY(9,1)=0;
% Equation 5 (forcing (volume change))
dY(10,1)=-D_CylVol_Dtheta(Vo,b,S,lc,th)*pi/180;
% Equation 6 (1st law)
dY(11,1)=0;
% Equation 7 (2nd law)
dY(12,1)=0;

```

### **rhs6.m:**

```

% function dY=rhs3(t,Y,R,cv,Vo,b,S,lc,om,P_o,T_o,D_rv,C_rv,phi)
function dY=rhs6(t,Y,om)
global R cv Vo b S lc P_o T_o f_stoich phi Qr t_comb flag gamma_u RPM ...
diff_g_theta Spbar k_gas nu_gas c1 c2 g_theta omega R_ratio k_wall d_wall h_en;
% computes the right hand side (rhs) for the system of ODEs describing
% the IC engine

% Y Vector of state variables
% Y(1) cylinder pressure
% Y(2) mass of gas in cylinder
% Y(3) work
% Y(4) enthalpy
% Y(5) cylinder volume
% Y(6) gas temperature
% Y(7) entropy

dY=zeros(12,1); %set up a column vector
th=t*pi/180; %compute crank angle in radians
cp=cv+R;

%%CYLINDER%%
% Equation 1 (state)
dY(1,1)=0;
% Equation 2 (cons. mass)
dY(2,1)=0;
% Equation 3 (energy input)
dY(3,1)=0;
% dY(3,1)=0;
% Equation 4 (forcing (volume change))
dY(4,1)=D_CylVol_Dtheta(Vo,b,S,lc,th)*pi/180;
% Equation 5 (1st law)
dY(5,1)=0;
% Equation 6 (2nd law)
dY(6,1)=0;

%%CRANKCASE%%
% Equation 1 (state)
dY(7,1)=0;
% Equation 2 (cons. mass)
dY(8,1)=mdotincc(th,Y(7),Y(11))/(6*RPM);
% dY(8,1)=0;
% Equation 4 (energy input)
dY(9,1)=heat_transfer(dY(8,1),T_o,Y(11));
% dY(9,1)=0;

```

```

% Equation 5 (forcing (volume change))
dY(10,1)=-D_CylVol_Dtheta(Vo,b,S,lc,th)*pi/180;
% Equation 6 (1st law)
dY(11,1)=0;
% Equation 7 (2nd law)
dY(12,1)=0;

```

### **rhs7.m:**

```

% function dY=rhs3(t,Y,R,cv,Vo,b,S,lc,om,P_o,T_o,D_rv,C_rv,phi)
function dY=rhs7(t,Y,om)
global R cp cv Vo b S lc P_o T_o f_stoich phi Qr t_comb flag gamma_u Exhaustportht Exhportwidth ...
Cd th_1 th_2 th_3 th_4 areaflag RPM diff_g_theta Spbar k_gas nu_gas c1 c2 g_theta omega R_ratio k_wall d_wall h_en;
% computes the right hand side (rhs) for the system of ODEs describing
% the IC engine

% Y Vector of state variables
% Y(1) cylinder pressure
% Y(2) mass of gas in cylinder
% Y(3) enthalpy
% Y(4) cylinder volume
% Y(5) gas temperature
% Y(6) entropy

dY=zeros(12,1); %set up a column vector
th=t*pi/180; %compute crank angle in radians
cp=cv+R;
tranflag = 1;
%%CYLINDER%%
% Equation 1 (state)
dY(1,1)=0;
% Equation 2 (cons. mass)
dY(2,1)=0;
% Equation 3 (energy input)
dY(3,1)=0;
% dY(3,1)=0;
% Equation 4 (forcing (volume change))
dY(4,1)=D_CylVol_Dtheta(Vo,b,S,lc,th)*pi/180;
% Equation 5 (1st law)
dY(5,1)=0;
% Equation 6 (2nd law)
dY(6,1)=0;

%%CRANKCASE%%
% Equation 1 (state)
dY(7,1)=0;
% Equation 2 (cons. mass)
dY(8,1)=0;
% Equation 4 (energy input)
dY(9,1)=0;
% Equation 5 (forcing (volume change))
dY(10,1)=-D_CylVol_Dtheta(Vo,b,S,lc,th)*pi/180;
% Equation 6 (1st law)
dY(11,1)=0;
% Equation 7 (2nd law)
dY(12,1)=0;

```

### **rhs8.m:**

```

% function dY=rhs3(t,Y,R,cv,Vo,b,S,lc,om,P_o,T_o,D_rv,C_rv,phi)
function dY=rhs8(t,Y,om)
global R cp cv Vo b S lc P_o T_o f_stoich phi Qr t_comb flag gamma_u Exhaustportht ...
Exhportwidth Cd th_1 th_2 th_3 th_4 areaflag RPM diff_g_theta Spbar k_gas nu_gas c1 c2 g_theta R_ratio omega k_wall
d_wall h_en;
% computes the right hand side (rhs) for the system of ODEs describing
% the IC engine

```

```

% Y Vector of state variables
% Y(1) cylinder pressure
% Y(2) mass of gas in cylinder
% Y(3) enthalpy
% Y(4) cylinder volume
% Y(5) gas temperature
% Y(6) entropy

dY=zeros(12,1); %set up a column vector
th=t*pi/180; %compute crank angle in radians
cp=cv+R;
%%CYLINDER%%
% Equation 1 (state)
dY(1,1)=0;
% Equation 2 (cons. mass)
dY(2,1)=mdotexcycl(th,Y(1),Y(5))/(6*RPM);
% dY(2,1)=mdotperarea(th,tranflag,Y(1),Y(5),Y(7),Y(11))/(6*RPM);
% Equation 3 (energy input)
dY(3,1)=heat_transfer(dY(2,1),T_o,Y(5));
% dY(3,1)=0;
% Equation 4 (forcing (volume change))
dY(4,1)=D_CylVol_Dtheta(Vo,b,S,lc,th)*pi/180;
% Equation 5 (1st law)
dY(5,1)=0;
% Equation 6 (2nd law)
dY(6,1)=0;

%%CRANKCASE%%
% Equation 1 (state)
dY(7,1)=0;
% Equation 2 (cons. mass)
dY(8,1)=0;
% Equation 4 (energy input)
% dY(9,1)=heat_transfercc(dY(8,1),Y(5),Y(11));
dY(9,1)=0;
% Equation 5 (forcing (volume change))
dY(10,1)=D_CylVol_Dtheta(Vo,b,S,lc,th)*pi/180;
% Equation 6 (1st law)
dY(11,1)=0;
% Equation 7 (2nd law)
dY(12,1)=0;

```

## Appendix B: Simulation with the Stanford ESP

### **Background**

ESP was initially developed by Professor W.C. Reynolds in the spring of 1987 for use by students and researchers in the Mechanical Engineering Department at Stanford University [42]. Over the years, the software package gained functionality and interface improvements culminating in a Microsoft Windows-based graphical user interface last updated in 2001 [58]. Since then, Professor Reynolds has passed away and no further development work on the program has been publicly released.

ESP's simulation method is based on solving a set of algebraic relations and ordinary differential equations that describe the conditions within the engine cylinder and valves for each stage of the cycle. The user inputs the engine geometry, fuel components, and engine operating conditions along with a set of thermodynamic model factors (such as Stanton number and combustion efficiency). ESP then solves for one cycle at a time using a second-order Runge-Kutta integration and a time step equal to one crank angle degree [42].

Four stages are calculated for each cycle: compression, combustion, expansion, and gas exchange. The compression, expansion, and gas exchange results are determined while assuming a homogeneous zone of gas, but the combustion stage is calculated assuming a separate zone for burned and unburned gases. The simulation also allows for backpressure in the valves and incorporates a basic turbulence model for heat exchange and combustion calculations [42].

An in-depth description of each segment and calculation method of ESP is included in John Lumley's book on engine design [42] as well as in the help documentation of the software program [58], so a detailed explanation will be withheld here.

### **Parameter Configuration**

As ESP was intended to simulate large four-stroke engines, certain parameters were manipulated in order to "trick" the program into simulating a small two-stroke engine. John Lumley has suggested that the manifold portion of the program is too entrenched in four-stroke architecture to successfully modify, but that the piston and cylinder portion may be able to handle the small two-stroke adaptations for the Tee Dee 0.010 [41]. For this reason, ESP will be executed for this work without the manifold modeling portion.

The latest version of ESP for Windows additionally comes with two pre-processing programs which help configure the main ESP code: ESPJAN and ESPCAM. ESPJAN is a version of the STANJAN (Stanford University's JANAAF) thermodynamic properties database for ESP and is used to define the chemical reaction properties at each stage of the simulation. ESPCAM is used to specify valve-opening curves. These two programs produce parameter files that are then input into the main ESP

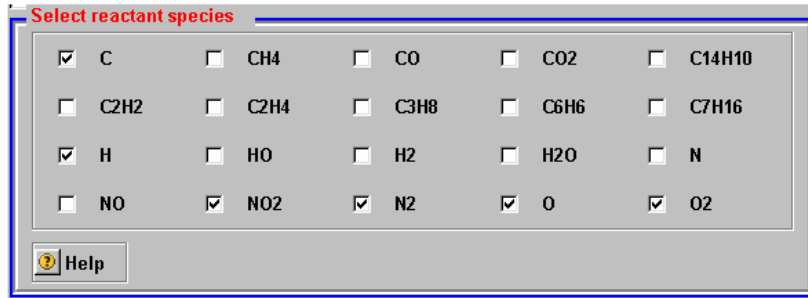
program along with the other user-specified parameters before executing the code. Below is a description of the entire ESP configuration including ESPJAN and ESPCAM along with explanations of how they were adapted to simulate the Tee Dee 0.010 where appropriate.

## ESPJAN

*Input: User Values*

*Output: (.ESJ) Fuel Parameter File*

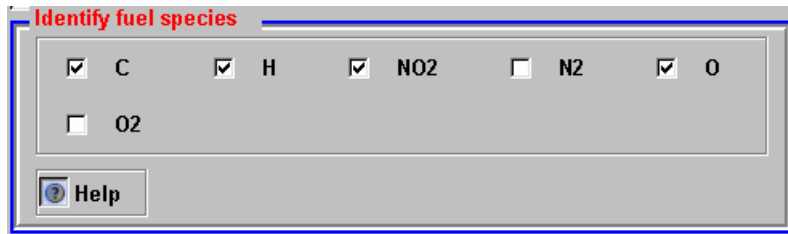
The first window of ESPJAN is the reactant selection section. While the exact molecules of methanol and nitromethane are not included in the list, the individual atoms that make up each of the reactants of the reaction described in Section 2.4 were selected (as shown in the partial screenshot in Figure B.1).



ESPJAN Reactant Selection Window  
Figure B.1

***Reactant Species: C, H, NO2, N2, O, O2***

In the next window, “Identify fuel species”, the atoms composing the fuel elements of methanol and nitromethane were selected (as shown in Figure B.2). Even though nitromethane effectively acts as an oxidizer in the reaction (because it also burns during the reaction while releasing energy), it was considered a fuel component.

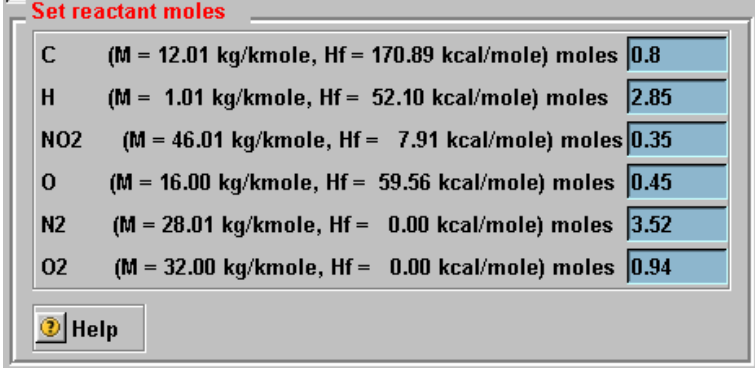


ESPJAN Reactant Selection Window  
Figure B.2

***Fuel Species: C, H, NO2, O***

The moles of the reactants were selected in the next window, “Set reactant moles”, based on Equations 2.4 and 2.5 in Section 2.4 as shown in Figure B.3 (when oil is

inert). (Note that ESPJAN must be run separately for each case of inert and burned oil.)



The image shows a software window titled "Set reactant moles". It contains a table with six rows, each representing a chemical species. Each row lists the species name, its molecular weight (M) in kg/kmole, its heat of formation (Hf) in kcal/mole, and the number of moles specified. The moles values are entered in blue input boxes. At the bottom left of the window is a "Help" button with a question mark icon.

Species	M (kg/kmole)	Hf (kcal/mole)	moles
C	12.01	170.89	0.8
H	1.01	52.10	2.85
NO2	46.01	7.91	0.35
O	16.00	59.56	0.45
N2	28.01	0.00	3.52
O2	32.00	0.00	0.94

ESPJAN Reactant Moles Specification Window  
Figure B.3

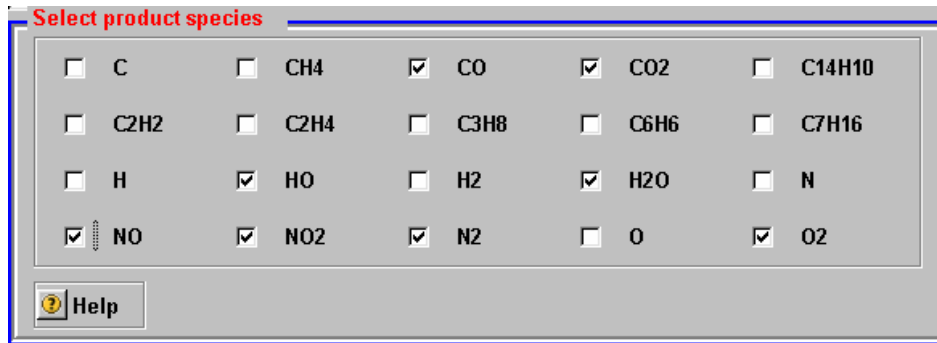
***Reactant Mols (inert oil):***

***C: 0.8***  
***H: 2.85***  
***NO2: 0.35***  
***O: 0.45***  
***N2: 3.52***  
***O2: 0.94***

***Reactant Mols (burned oil):***

***C: 4.4***  
***H: 9.65***  
***NO2: 0.35***  
***O: 1.05***  
***N2: 22.36***  
***O2: 5.94***

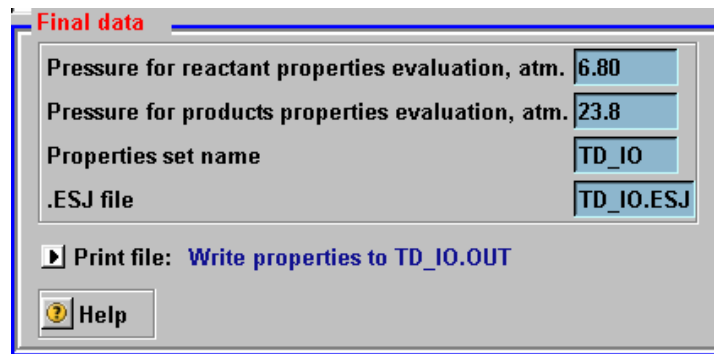
In the last window, "Select product species", the major and minor products were selected as shown in Figure B.4. The major products were selected from Equation 2.4 and the minor products of CO, NO, NO<sub>2</sub>, and HO were assumed from known typical hydrocarbon exhaust.



ESPJAN Product Selection Window  
Figure B.4

***Product Species: CO, CO2, HO, H2O, O2, NO, NO2, N2***

In the final window, “Final data”, the pressure used to evaluate the reactant and product properties are entered as shown in Figure B.5. Without accurate pressure sensor readings for the intake or exhaust gases of this engine, an approximation for both values was taken from a generic pressure plot given in Gierke’s model aircraft engine book [28: pg. 18]. This window is also used to name the (.ESJ) output file that will be created and later imported into the main ESP program.



ESPJAN Pressure Specification Window  
Figure B.5

***Reactants Pressure, atm: 6.80***

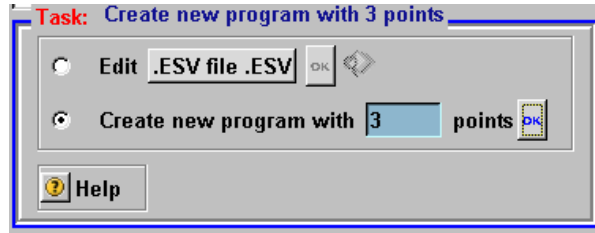
***Products Pressure, atm: 23.8***

## ESPCAM

*Input: User Values*

*Output: (.ESV) Valve Opening Parameter File*

In the first window of ESPCAM, the number of points used to describe the valve-opening curve is selected as shown in Figure B.6. Based on the measurements of the Tee Dee 0.010, a basic 3-point curve was defined for the effective exhaust and intake valve openings. (Note that ESPCAM must be run separately for each valve.)

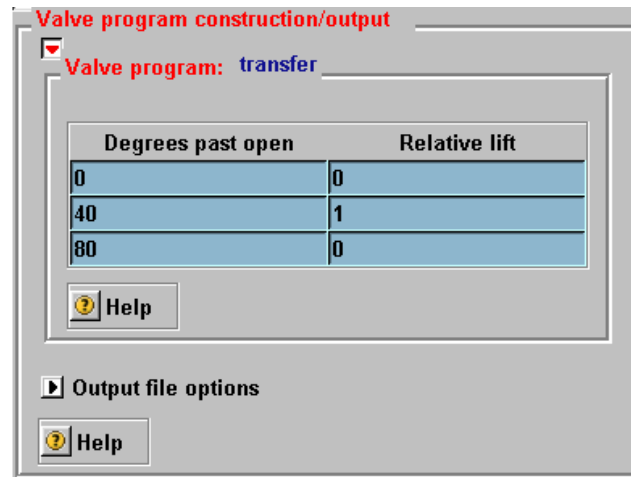


ESPCAM Program Setup Window  
Figure B.6

***Program Points (exhaust): 3***

***Program Points (intake): 3***

In the last window of the ESPCAM configuration, the points defining the opening of the valve relative to crankshaft angle is entered where a relative lift of 1 is fully open and a relative lift of 0 is fully closed. **In this case, since only the cylinder and piston are modeled, the transfer port was considered the intake valve.** Based on approximate measurements of valve timings described in Section 2.3, the values for a 3-point curve for the exhaust and intake/transfer valves were entered as shown in Figure B.7 (for intake/transfer). (Figures B.8 and B.9 show plots of the transfer and exhaust port curves respectively.) This window is also used to name the (.ESV) output file that will be created and later imported into the main ESP program.



ESPCAM Valve Lift Specification Window  
Figure B.7

***Valve Program: Transfer (intake)***

***Degrees past open: 0***

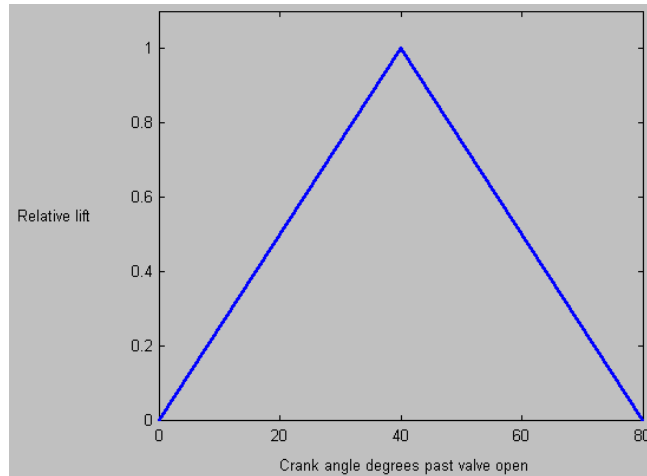
***Degrees past open: 40***

***Degrees past open: 80***

***Relative lift: 0***

***Relative lift: 1***

***Relative lift: 0***



Tee Dee 0.010 Transfer Port Opening Curve  
Figure B.8

***Valve Program: Exhaust***

***Degrees past open: 0***

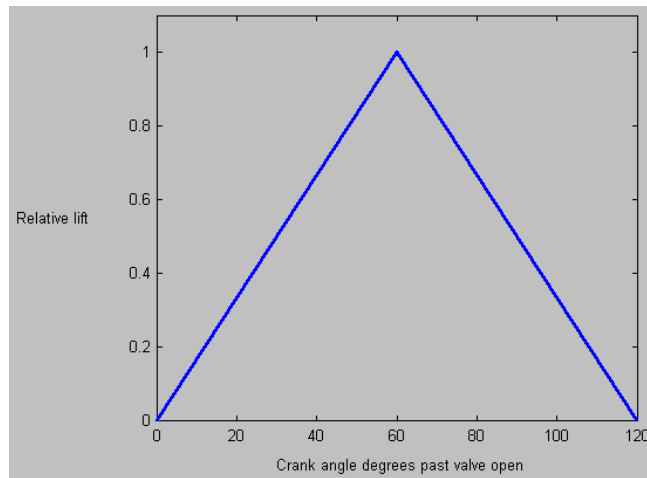
***Relative lift: 0***

***Degrees past open: 60***

***Relative lift: 1***

***Degrees past open: 120***

***Relative lift: 0***



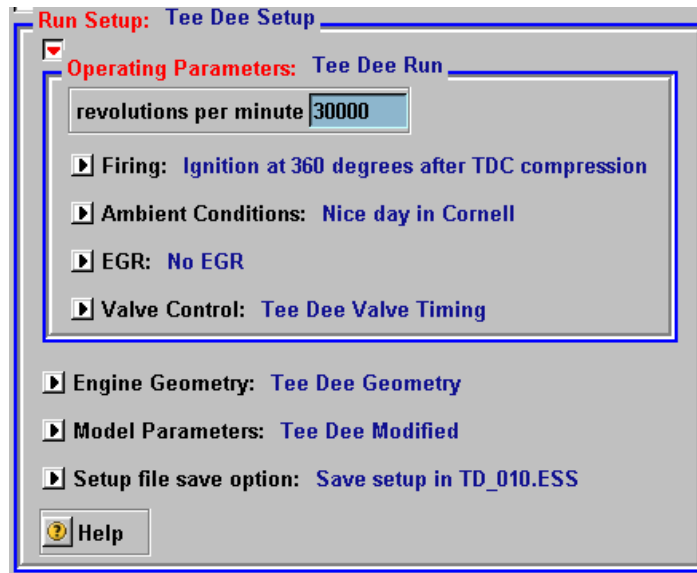
Tee Dee 0.010 Exhaust Port Opening Curve  
Figure B.9

**ESP**

*Input: User Values, (.ESJ) Fuel File, (.ESV) Valve File*

*Output: Computation Results, Plots*

The first window of the main ESP program contains the “Run Setup” panel which has a set of sub-panels used to configure the engine simulation as shown in Figure B.10. Based on the predetermined Tee Dee 0.010 values, each sub-panel field was filled as described below. For parameters where the Tee Dee value could not be determined, the default (based on a large four-stroke engine) was used as an approximation.



ESP Main Setup Window  
Figure B.10

***Operating Parameters:***

***revolutions per minute: 30000***

(Various sources have cited the peak power output of the engine to occur between 27,000 [26] and 33,000 [31], so an average value of 30,000 was chosen for this parameter.)

***Firing: Ignition at 360 degrees after TDC compression***

(This is one place where the program was “tricked” into simulating a two-stroke engine. The default value here is 710 deg after TDC- appropriate for a four-stroke engine firing only once every two revolutions, but the number was changed to 360 deg (as an ideal approximation) to force it to ignite after every revolution.)

***Ambient Conditions:***

(all default values)

***intake ambient pressure: 1 atm***

***exhaust ambient pressure: 1 atm***

***ambient temperature: 300 K***

***EGR:***

***mass percent EGR: 0 (default)***

(Exhaust Gas Re-circulation (EGR) is a process often used in larger four-stroke engines to reduce emissions and increase efficiency by re-burning the exhaust. In this case of a two-stroke simulation, the default of no EGR was chosen. Future work may consider experimenting with

this parameter for a two-stroke to attempt simulating scavenging losses.)

**EGR return temperature: 300 K (default)**

**Valve Control:**

(all from approximate measurements)

**crank degrees after compression TDC where intake opens: 140**

**crank degrees after compression TDC where intake closes: 220**

**crank degrees after compression TDC where exhaust opens: 120**

**crank degrees after compression TDC where exhaust closes: 240**

**max. intake valve flow area % of reference: 100**

**max. exhaust valve flow area % of reference: 100**

**Engine Geometry:**

**Intake Valve Program: Use TRANSFER.ESV**

(This is the file created in ESPCAM)

**Exhaust Valve Program: Use EXHAUST.ESV**

(This is the file created in ESPCAM)

**Valve Reference Areas:**

(all from approximate measurements)

**reference flow area of intake valve (full open), m<sup>2</sup>: 0.00001**

**reference flow area of exhaust valve (full open), m<sup>2</sup>: 0.000003**

**Piston/Cylinder:**

**cylinder bore, m: 0.00602**

**volume compression ratio: 8.11**

(The volume at the start of cylinder compression is (stroke minus the exhaust port height) x (pi\*(bore/2)<sup>2</sup>) + (volume of conical cylinder head). The volume at the end of compression is simply the volume of the conical head. The compression ratio is then (start volume) / (end volume). This calculation is described in Equation B.1 where  $s$  is stroke,  $b$  is bore,  $h_e$  is exhaust port height, and  $h_h$  is height of cylinder head. Based on measurements, the height of the conical cylinder head is 2 mm and the exhaust port height is 1 mm, so the compression ratio used was 8.11. If the exhaust port is ignored, the ratio is 9.61.)

$$\text{compression ratio} = \frac{(s - h_e)\pi\left(\frac{b}{2}\right)^2 + \frac{1}{3}\pi h_h\left(\frac{b}{2}\right)^2}{\frac{1}{3}\pi h_h\left(\frac{b}{2}\right)^2} \quad (\text{Eq. B.1})$$

**piston compression stroke, m: 0.00574**

(Even though actual compression only happens in the length of stroke minus the exhaust port height as described in the compression ratio

calculation, it was assumed that ESP is asking here simply for the total travel distance of the piston in one stroke.)

***Piston Program:***

***Conventional; connecting rod length: 0.01 m***  
(from approximate measurement)

***Model Parameters:***

***Gas Properties: Use TD\_IO.ESJ (or TD\_BO.ESJ)***

(This is the file created in ESPJAN. Note that a separate file must be used for each case of inert oil and burned oil.)

***Valve Flow Model:***

(all default values)

***discharge coefficient for intake valve: .645***

***discharge coefficient for intake valve backflow: .868***

***discharge coefficient for exhaust valve: .868***

***discharge coefficient for intake valve backflow: .645***

(These values describe the performance of the valves by defining the ratio of actual flow to ideal isentropic flow for each condition. Because no information on the Tee Dee's valve efficiency is known, all default values were chosen.)

***Heat Transfer Model:***

(all default values)

***Stanton number during compression: 0.0356***

***Stanton number during burn for unburned gas: 0.0356***

***Stanton number during burn for burned gas: 0.0356***

***Stanton number during expansion: 0.0356***

***Stanton number for in-cylinder heat trans. during gas exch.: 0.0356***

***Stanton number for heat transfer from inlet valve flow: 0.00237***

***Stanton number for heat transfer from exhaust valve flow: 0.00237***

***(heat transfer area above piston at TDC)/(bore area): 1.37***

***(heat transfer area for intake jet flow)/(bore area): 0.05***

***(heat transfer area for exhaust jet flow)/(bore area): 0.05***

***temperature of liner/piston/head heat transfer area, K: 400***

***temperature of intake valve-flow heat transfer area, K: 400***

***temperature of exhaust valve-flow heat transfer area, K: 400***

(The Stanton number is a ratio that describes the amount of heat transferred to a fluid flow relative to the heat capacity of the flow [42]. Together with the area ratios and temperatures from the list above, ESP uses the Stanton numbers to determine heat transfer results at each stage of the simulation. Once again, because these values are not known for the specific case of the Tee Dee 0.010, default values were used.)

***Turbulence Model:***

(all default values)

***(inlet flow turb. kinetic energy)/(mean flow kinetic energy): 0.2***

***(exhaust bkflow. turb. energy)/(mean bkflo. kinetic energy): 0.2***

***factor in turbulence dissipation during compression: 0.298***

***factor in turbulence dissipation during burn: 0.05***

***factor in turbulence dissipation during expansion: 0.298***

***factor in turbulence dissipation during gas exchange: 0.298***

***factor in turbulence production during compression: 0.00502***

***factor in turbulence production during burn: 0.03***

***factor in turbulence production during expansion: 0.00502***

***factor in turbulence production during gas exchange: 0.00502***

(These factors configure ESP's turbulence model by defining the extent to which turbulence influences the flow conditions at each stage in the calculation. As with the previous thermodynamic model parameters, default values were kept in lieu of specific Tee Dee values.)

***Flame Geometry Model: Cylindrical Burn***

(Because no information on flame geometry for the Tee Dee is available and the ignition method and fuel type is very different than the default engine, the approximated cylindrical burn option was selected.)

***Flame Propagation Model:***

***fraction of mass ignited at ignition: 0.02 (default)***

***laminar flame speed, m/s: 0.4***

(approximation based on methanol with a rich fuel/air ratio [64] as measured during high speed Tee Dee operation in Section 3)

***ratio of turbulent flame speed to turbulence velocity: 1.5 (default)***

***fraction of reactants burned (combustion efficiency): 0.985 (default)***

(Combustion efficiency of a small two-stroke engine is assumed to be less than the default engine, but because no exact value is known, the default value was used.)

***Intake Manifold Model: No manifold (default)***

***Exhaust Manifold Model: No manifold (default)***

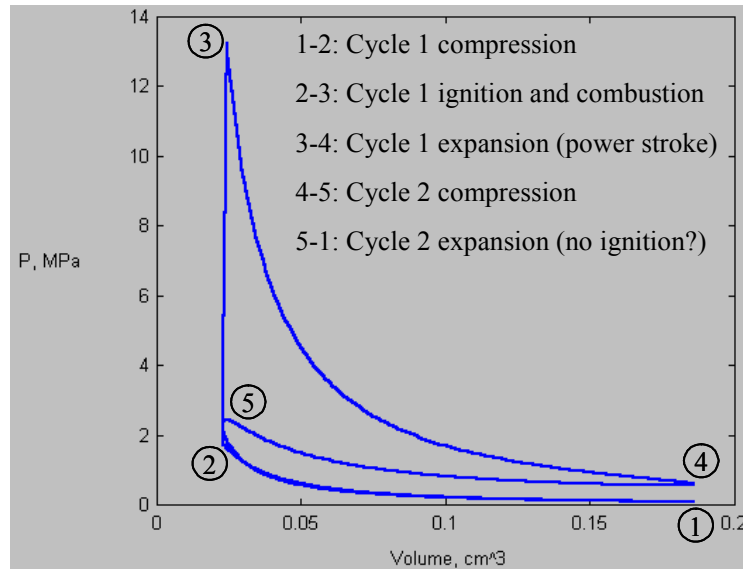
**Results and Analysis**

For this simulation, ESP was run with the described configurations for only one cycle. The results after computing additional cycles of ESP in either the inert oil or burned oil configuration included implausible output such as negative work and negative exhaust temperatures and were therefore discarded. Note also that because ESP was intended for four-stroke engines, one cycle is actually two revolutions, or two cycles of the two-stroke Tee Dee 0.010 (1 ESP Cycle = 2 Tee Dee Cycles).

Inert Oil Configuration:

***P-V Diagram:***

Figure B.11 shows the pressure-volume (P-V) diagram for the engine over the first two Tee Dee cycles (four strokes total) with key events labeled. The lack of pressure rise during the second cycle suggests ESP may not be performing the ignition and combustion routines at the directed times. Since that is consistent with four-stroke operation, it may indicate that ESP is incapable of departing from its four-stroke architecture. From the standard definition [42, et al], the area within the curve represents the work output of the engine.

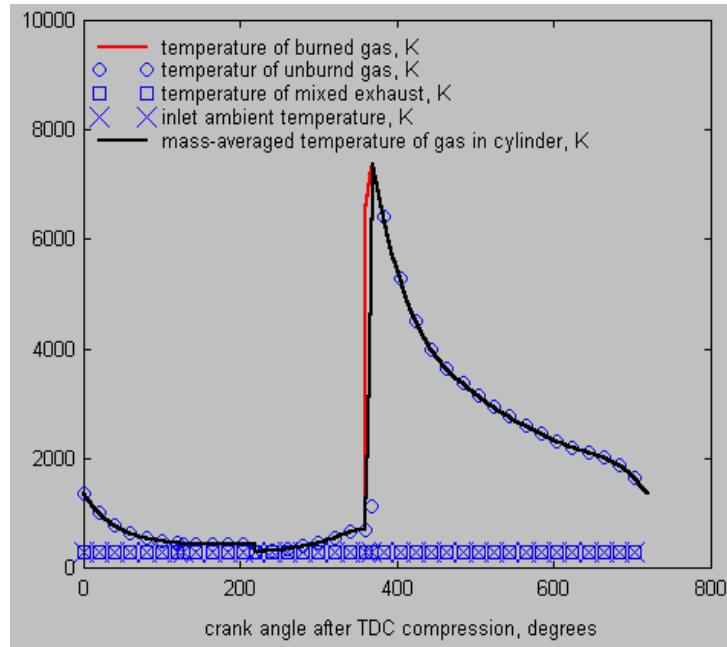


ESP Tee Dee 0.010 Inert Oil P-V Diagram

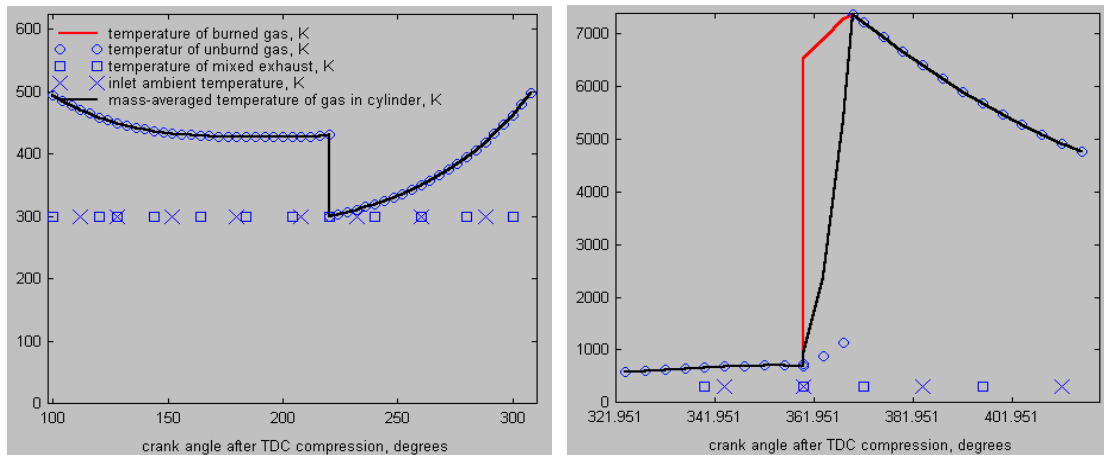
Figure B.11

***Temperatures:***

Figure B.12 shows multiple gas temperature curves over the first two cycles. Figure B.13 shows zoomed areas including the temperature activity near combustion at TDC (on the right) and the transfer port activity near 200° (on the left). Predictably, the plot shows the balance shift of temperatures from the burned (in red) to unburned gases (in open circles) as charge combustion occurs. Evidence of the simulation's inability to correctly model a two-stroke process (or a significant cycle lag) may be seen in the left side of Figure B.12 where the curve of 0° to 360° is not closely repeated from 360° to 720°.



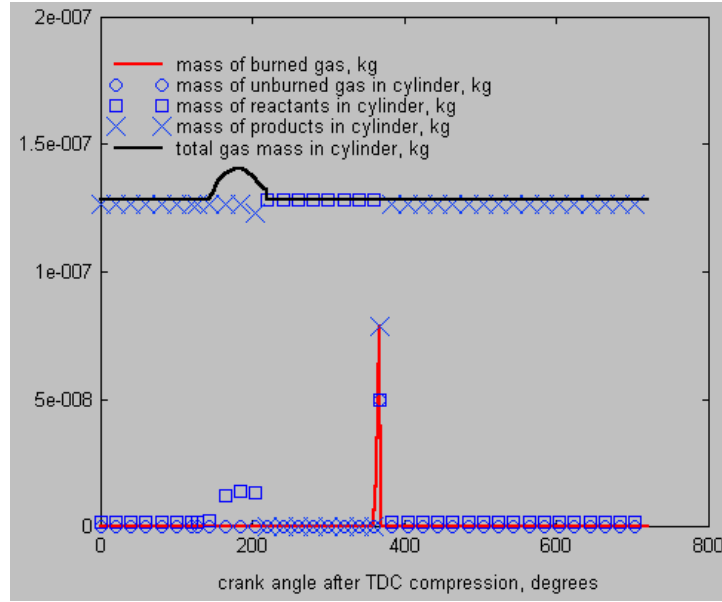
ESP Tee Dee 0.010 Inert Oil Cycle Temperatures  
Figure B.12



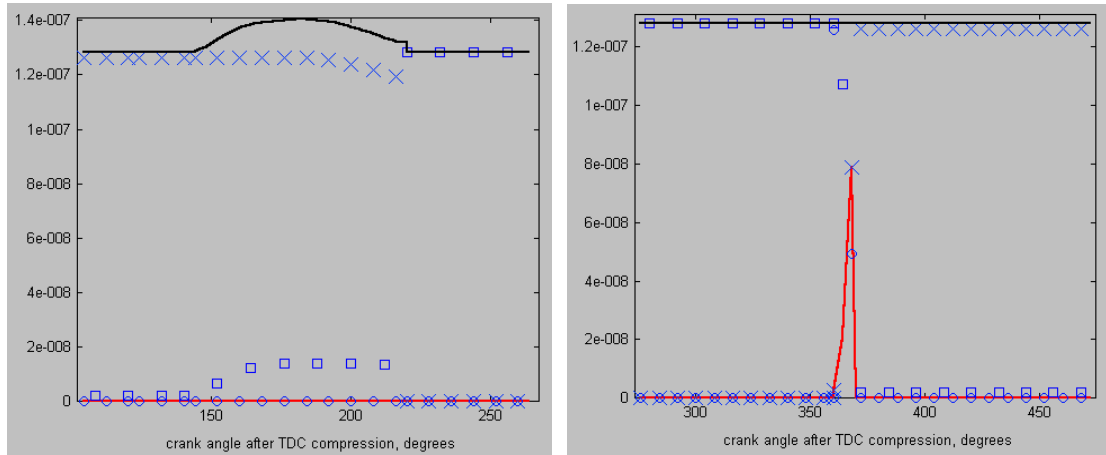
ESP Tee Dee 0.010 Inert Oil Cycle Temperatures (Zoomed)  
Figure B.13

**Masses:**

Figure B.14 shows the in-cylinder mass amounts during the first two cycles. Shown on the zoomed left plot of Figure B.15, near BDC, the total cylinder mass increases as the transfer port opens (at 140° as shown in Figure 2.18). The mass of products is also seen dropping at this time as the exhaust port remains open until 240° after TDC. The right plot in Figure B.15 shows the increase of products and decrease of reactants consistent with combustion near TDC. Here again, the pattern activity of the first cycle (0°-360°) does not seem to be repeated at the proper time in the second cycle (360°-720°).



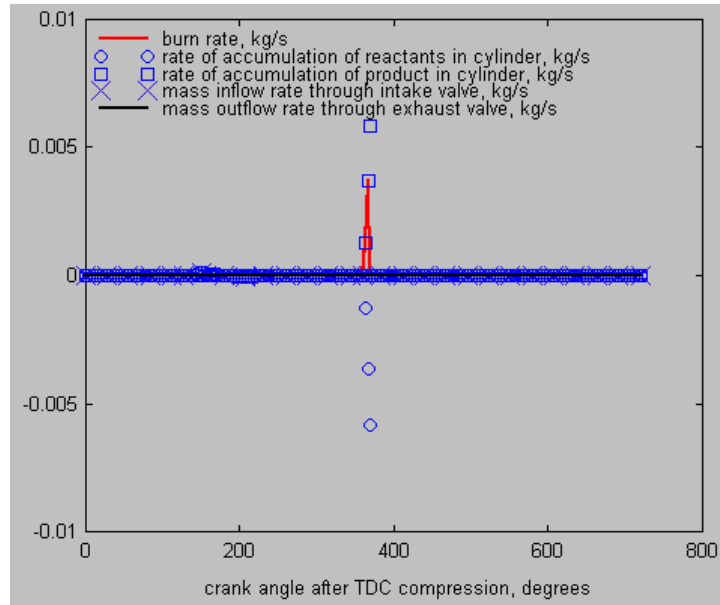
ESP Tee Dee 0.010 Inert Oil Cycle Masses  
Figure B.14



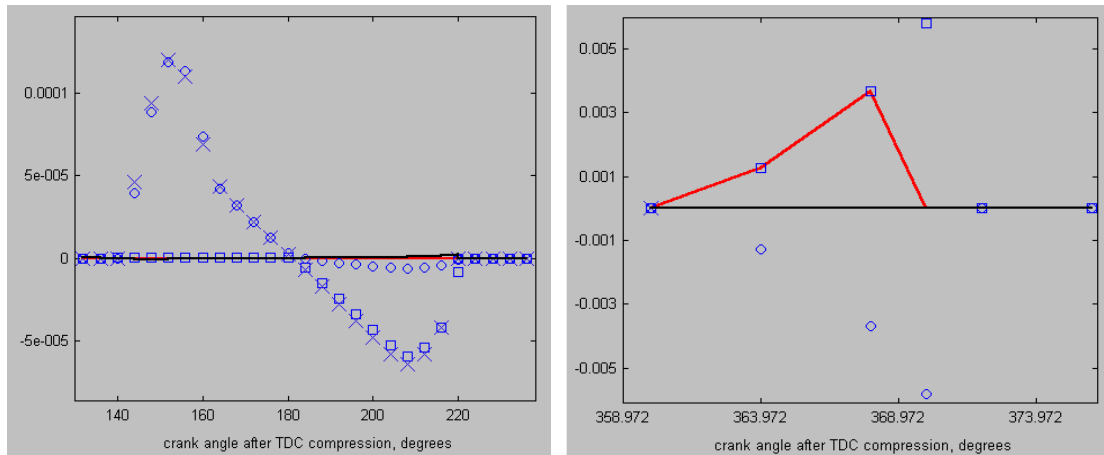
ESP Tee Dee 0.010 Inert Oil Cycle Masses (Zoomed)  
Figure B.15

**Mass Flows:**

Figure B.16 shows the relatively large spike in mass flow rates near TDC (360°) where combustion causes a quick exchange of mass between reactants and products (as shown by the zoomed region in the left plot of Figure B.17). The activity seen near BDC (showed zoomed in the right plot of Figure B.17) is a result of the opening and closing of the transfer port.



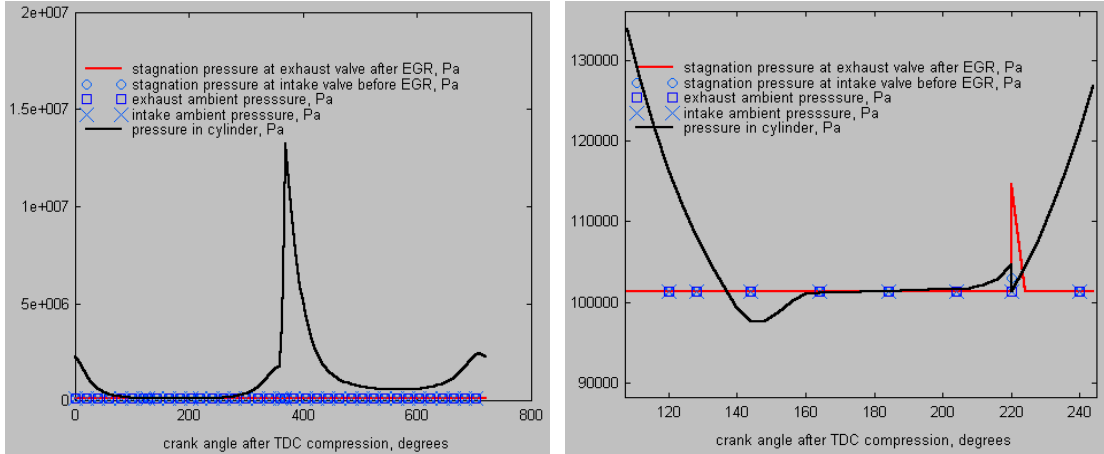
ESP Tee Dee 0.010 Inert Oil Cycle Mass Flows  
Figure B.16



ESP Tee Dee 0.010 Inert Oil Cycle Mass Flows (Zoomed)  
Figure B.17

**Pressures:**

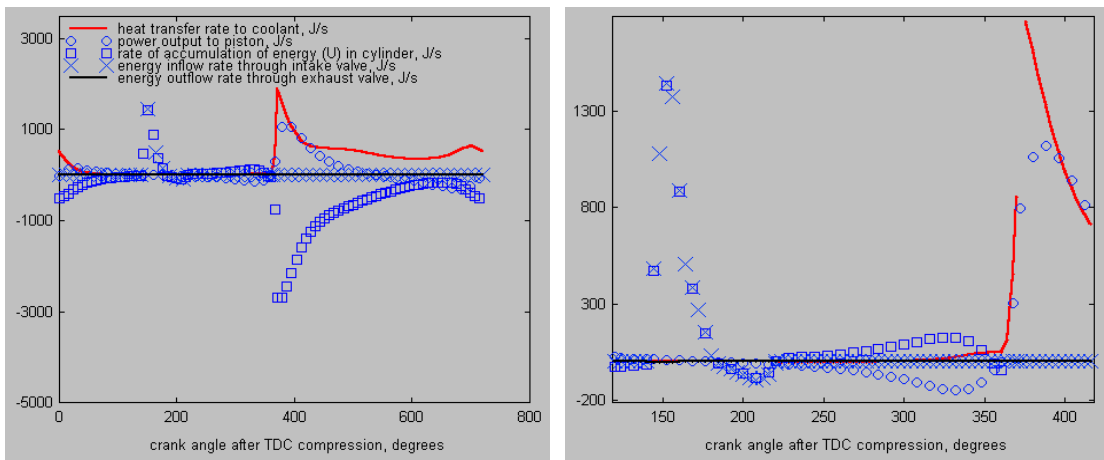
Figure B.18 shows the cyclical increase in cylinder pressure as the piston moves toward TDC during the compression stroke and large drop of pressure during the power (expansion) stroke. Sharper increases might be expected, however, around the TDC points of surrounding compression strokes at  $0^\circ$  and  $720^\circ$ . The zoomed region shown in the right plot shows a flattened pressure curve during the time when both the transfer (intake) and exhaust ports are open. Since no EGR conditions were used in the simulation, the minor activity seen around  $220^\circ$  may be artifacts of the computations around the transfer (intake) port closure.



ESP Tee Dee 0.010 Inert Oil Cycle Pressures  
Figure B.18

**Energy Transfer Rates:**

Figure B.19 shows the various energy rates during two Tee Dee cycles simulated by ESP. (The energy values are determined from the thermochemical state of the flow after ESP shifts the data so that pure products have zero internal energy at 300 K [58].) As shown in the zoomed region on the right plot, an increase of intake energy flow is seen during the opening of the transfer ports along with a decrease in energy accumulation as the combustion reaction releases energy and the piston accordingly produces power after TDC. Since this engine has no coolant, the red curve is assumed to represent heat losses to the cylinder walls and atmosphere. Once again suggesting a significant inaccuracy in the two-stroke model, the intake activity seen around 150° is not seen again where it is expected at 500°.

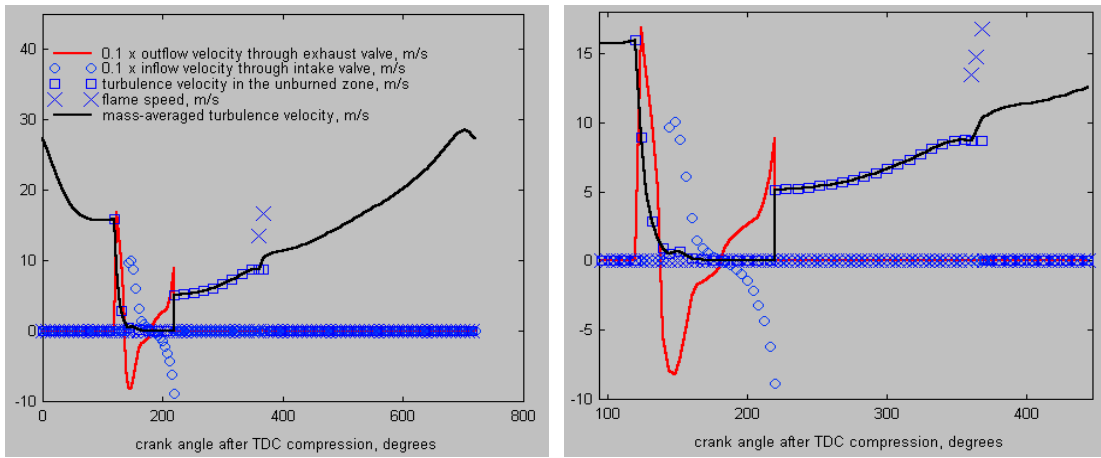


ESP Tee Dee 0.010 Inert Oil Cycle Energy Transfer Rates  
Figure B.19

**Velocities:**

Figure B.20 shows the various gas velocities during the two Tee Dee cycles simulated by ESP. The flame speed curve (represented with cross symbols) shows a predictable spike around ignition and large fluctuations of the exhaust and intake gases can be

seen around the port opening and closing events. This plot also demonstrates the very apparent inaccuracy of the two-stroke ESP model seen previously as the abundant activity during the first two strokes is not seen again in the last two strokes.



ESP Tee Dee 0.010 Inert Oil Cycle Flow Velocities  
Figure B.20

**Performance Summary:**

Table B.1 shows the list of values output by ESP that summarize the performance data computed during the first ESP cycle for the inert oil case.

Performance Output	Value	Units
net indicated work output/displacement	1.626E+06	Pa
mass of fuel/indicated work output	3.144E-09	kg/J
flow mass/displacement mass at mixed charge density	3.133E-02	--
heat transfer/net indicated work output	4.637	--
average polytropic exponent for compression	1.383	--
average polytropic exponent for expansion	1.202	--
cycle peak pressure	130.4	atm
crank angle at maximum pressure	370	degrees
crank angle at end of burn	370	degrees
mixed exhaust temperature at valve exit	523	K

ESP Tee Dee 0.010 Inert Oil Performance Summary  
Table B.1

Additionally, the power output of the simulated engine can be determined from the standard definition of power as described by Equation 4.3 where  $mep$  is the mean effective pressure given in the first line of Table B.1. **Note that the  $mep$  given in Table B.1 must be divided by two to account for the fact that the net work produced during one ESP cycle is actually the net work produced during two Tee Dee cycles.** Even as the results suggest ignition may only happen during the first Tee Dee cycle, there is no way to have ESP calculate work for only the first two strokes.

Table B.2 lists the other performance values calculated for the computed ESP cycle. Note that the fuel mass flow was determined by multiplying the fuel/mixture ratio

without the presence of oil (given in Section 2.4.2 as 0.218) by the maximum intake flow in the mass flows diagram (0.00012 kg/s).

Calculated Performance (Inert Oil)	Value	Units
Power	66.666	W
Power Density	5128.2	W/kg
Efficiency	0.1512	--
BSFC	0.0014	kg/W-hr

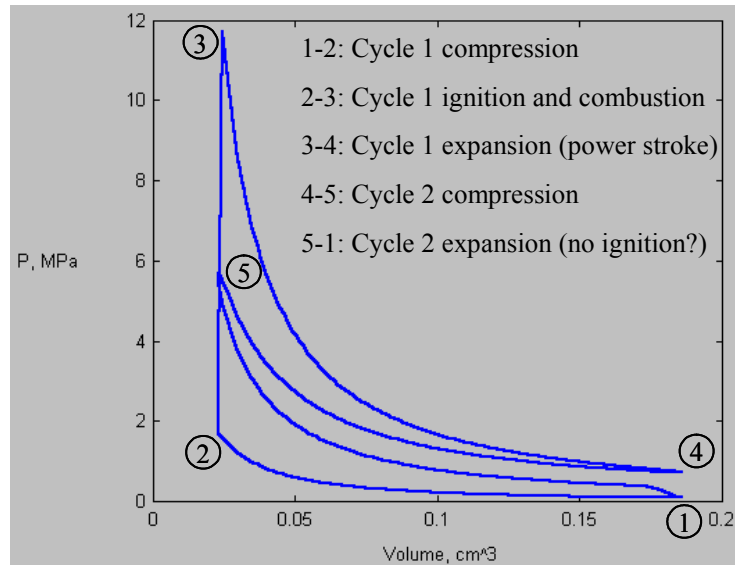
ESP Derived Inert Oil Performance Values  
Table B.2

From Table B.2, it is evident that the power and efficiency values for the ESP simulation are well above the expected peak capability of the Tee Dee 0.010. These elevated values are most likely a result of the inability of ESP to model the specific loss mechanisms associated with two-stroke engines and small-scale combustion. Additionally, ESP uses a turbulence model that is probably not appropriate for these scales.

#### Burned Oil Configuration

##### ***P-V Diagram:***

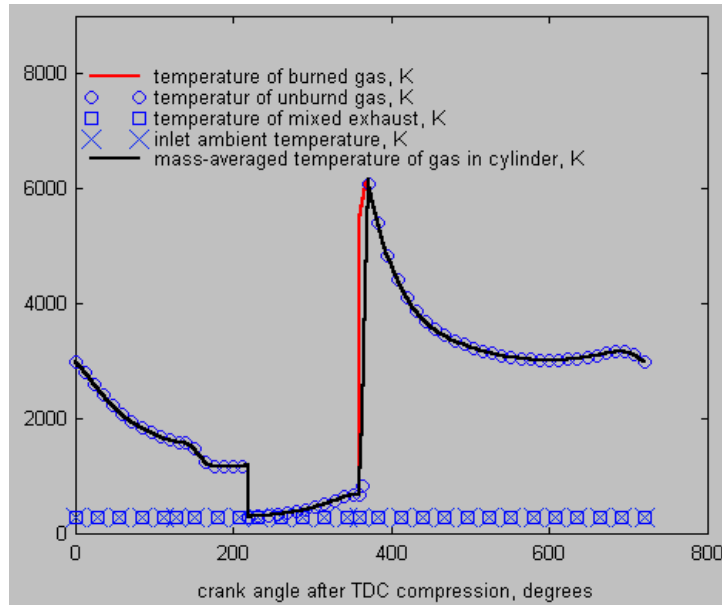
The P-V diagram for the burned oil case, shown in Figure 3.21, is similar in shape to the ESP output of the inert oil case (Figure B.11). While the pressure rise during both cycles is larger than the inert oil case (most likely because of the increased energy content of the charge), the relative dramatic drop in pressure during the second cycle once again suggests ESP is not performing combustion as directed for two-stroke operation.



ESP Tee Dee 0.010 Burned Oil P-V Diagram  
Figure B.21

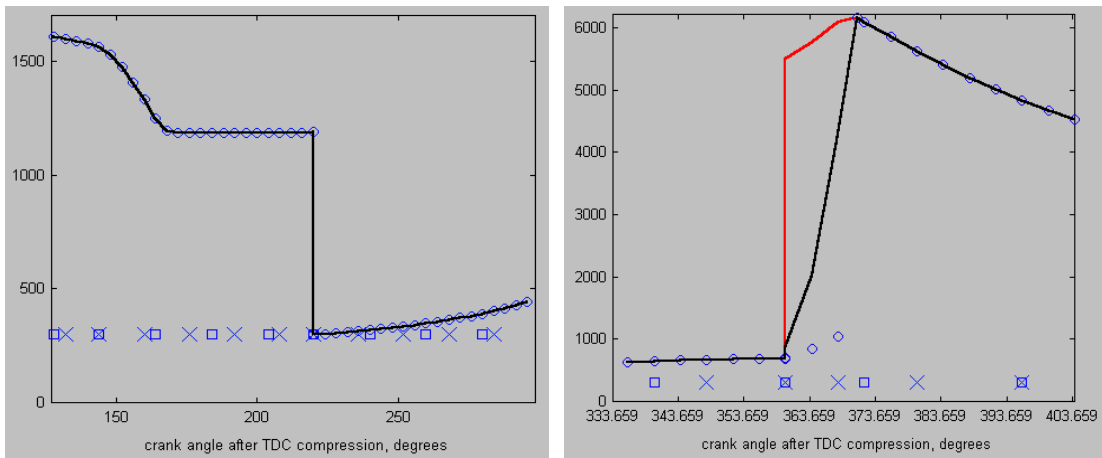
**Temperatures:**

The plot of temperatures for the burned oil case (shown in Figure B.22) closely mirrors the inert oil case, but has a lower overall magnitude and a more dramatic drop in pressure near the port events (shown in the zoomed left plot of Figure B.23) of the first Tee Dee cycle.



ESP Tee Dee 0.010 Burned Oil Cycle Temperatures

Figure B.22

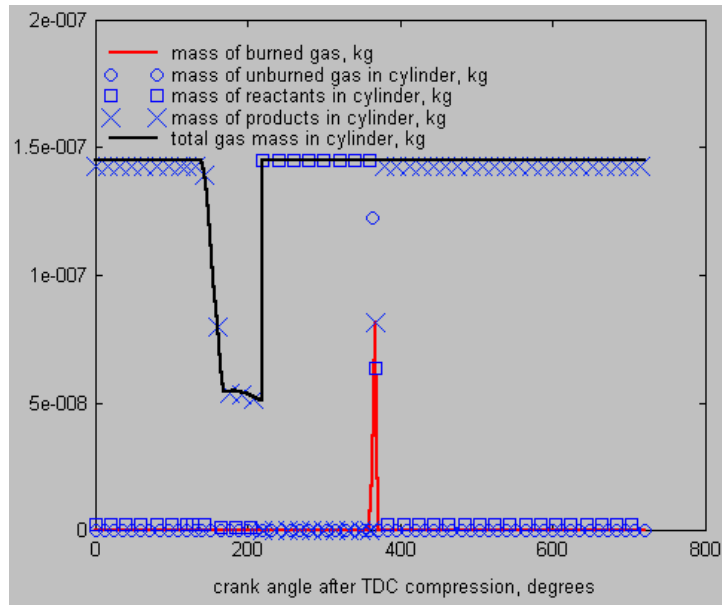


ESP Tee Dee 0.010 Inert Oil Cycle Temperatures (Zoomed)

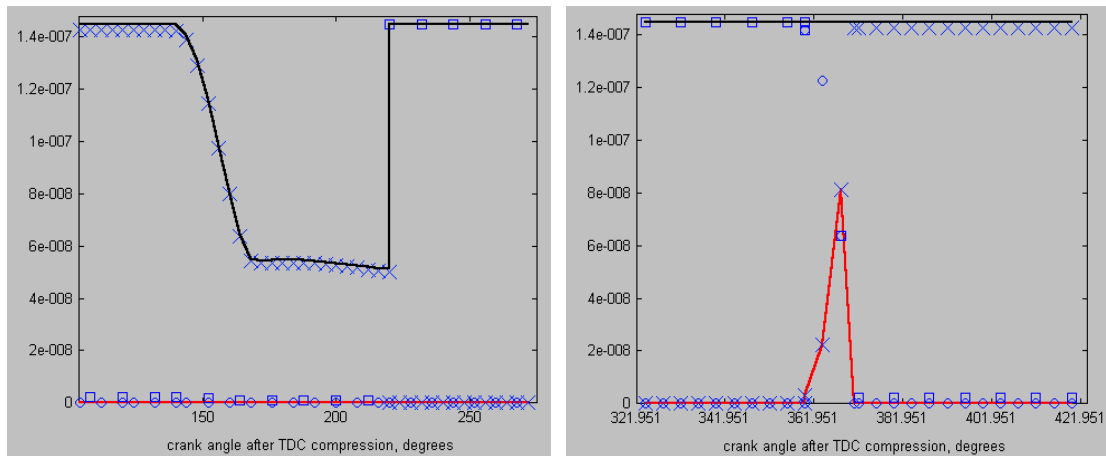
Figure B.23

**Masses:**

In the burned oil case (Figure B.24), the overall mass drops rather than rises near the port events, but the pattern near TDC (shown in the zoomed right plot in Figure B.25) and combustion is similar to the inert oil ESP cycle (Figure B.15).



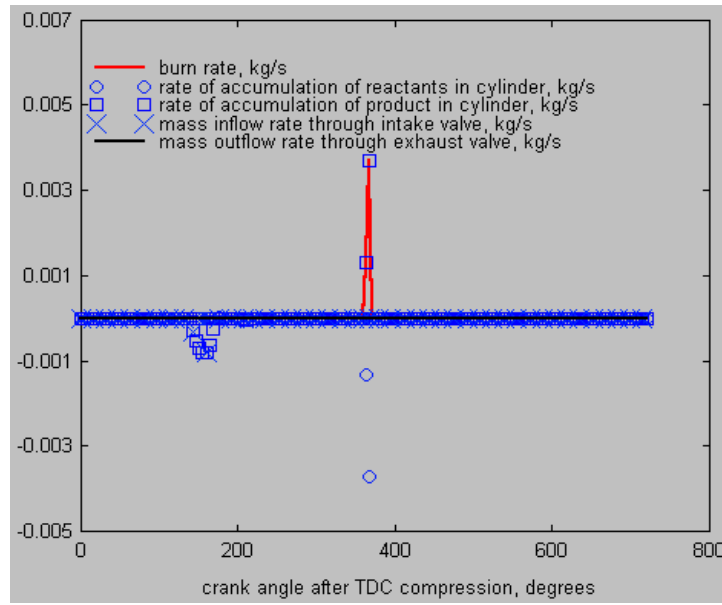
ESP Tee Dee 0.010 Burned Oil Cycle Masses  
Figure B.24



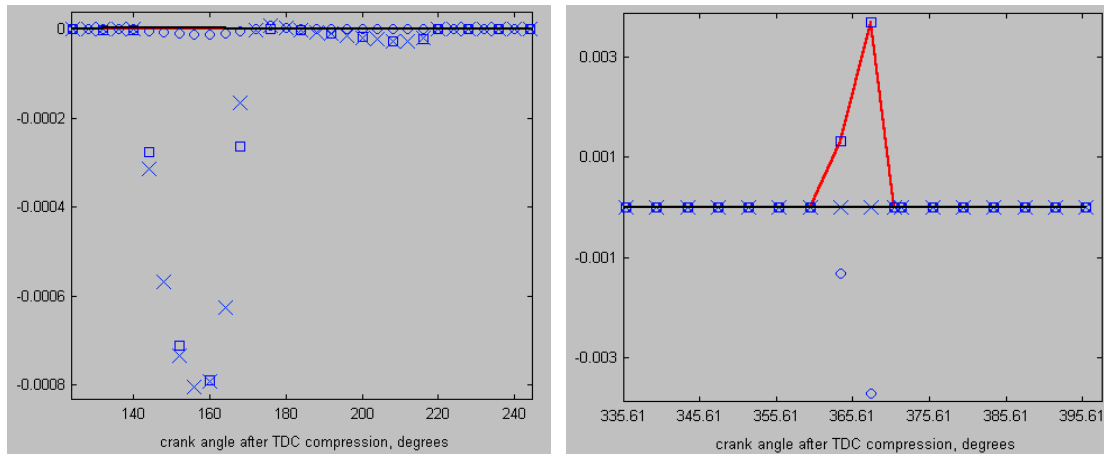
ESP Tee Dee 0.010 Burned Oil Cycle Masses (Zoomed)  
Figure B.25

**Mass Flows:**

While the burn rate of the burned oil case (Figure B.26) is similar to the inert oil case (Figure B.16), the maximum rates of accumulations (shown in the zoomed left plot of Figure B.27) are lower. Additionally, the mass flow rates during the intake/transfer port events (shown in the zoomed right plot of Figure B.27) are an order of magnitude larger than in the inert oil case.



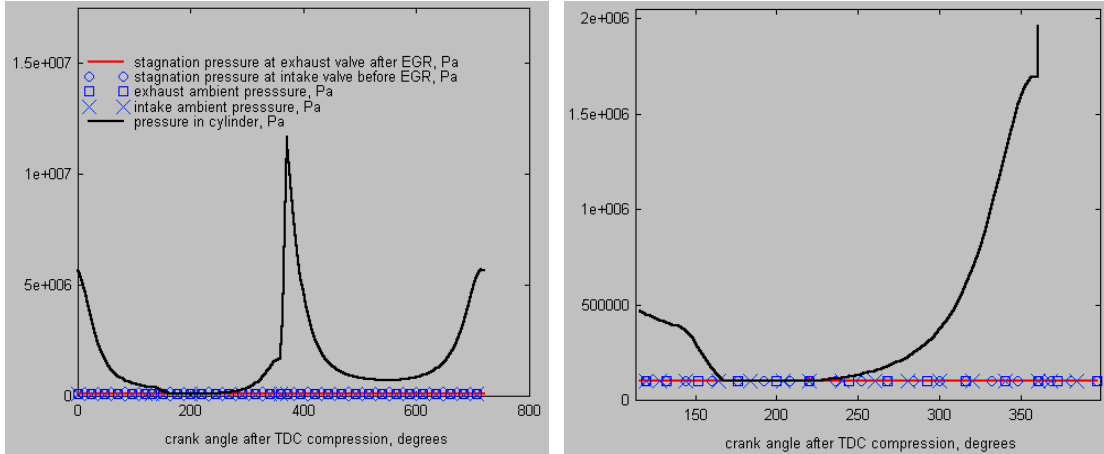
ESP Tee Dee 0.010 Burned Oil Cycle Mass Flows  
Figure B.26



ESP Tee Dee 0.010 Burned Oil Cycle Mass Flows (Zoomed)  
Figure B.27

**Pressures:**

While the max pressure at TDC is slightly lower, the patterns of pressures in the burned oil case (Figure B.28) are similar to the patterns in the inert oil case (Figure B.18). This case also displays slightly more symmetry around the TDC events.

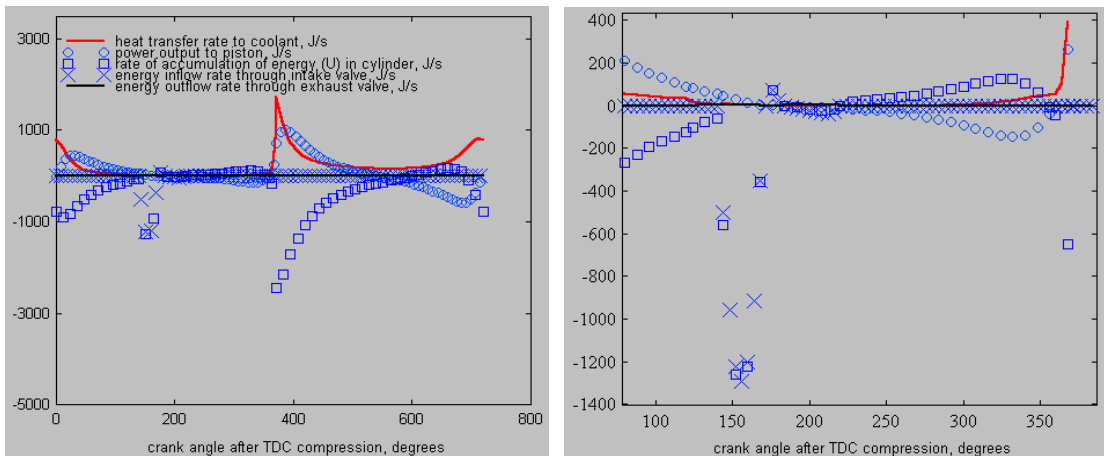


ESP Tee Dee 0.010 Burned Oil Cycle Pressures

Figure B.28

**Energy Transfer Rates:**

The pattern of energy rates in the burned oil case (Figure B.29) is similar to the inert oil case (Figure B.19), however the spike of intake valve activity (shown in the zoomed region on the right plot) is reversed.

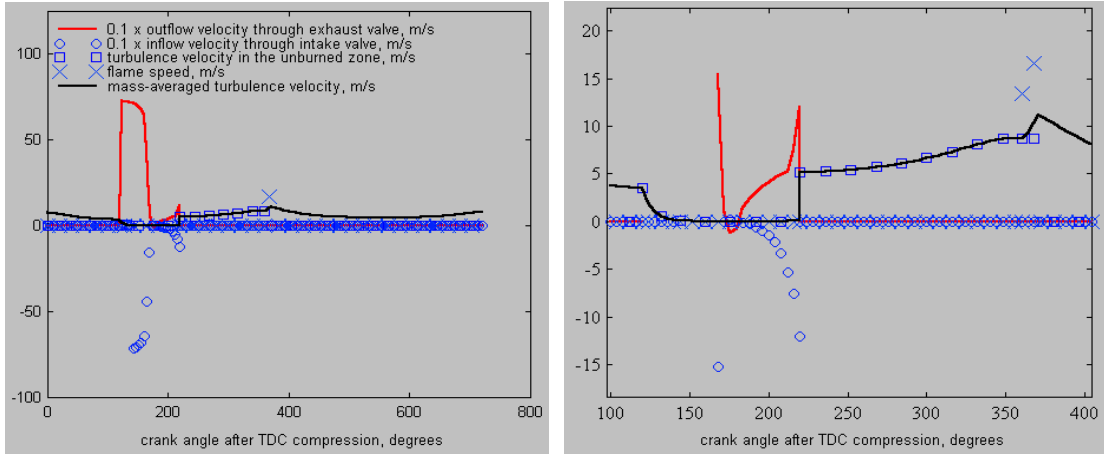


ESP Tee Dee 0.010 Burned Oil Cycle Energy Transfer Rates

Figure B.29

**Velocities:**

The component velocities of the burned oil case are shown in Figure B.30. While the flame speed curve is similar to the inert oil case, the mass-averaged turbulence, inflow, and outflow velocities are characteristically different. The outflow and inflow velocities near the opening of the exhaust (at 120°) and transfer port (at 140°) are much larger than the inert oil case, but are both similar near BDC. The mass-averaged turbulence velocity is symmetric about TDC (very unlike the inert oil case) and also much lower in magnitude than the inert oil case.



ESP Tee Dee 0.010 Burned Oil Cycle Flow Velocities  
Figure B.30

**Performance:**

Table B.3 shows the list of values output by ESP that summarize the performance data computed during the burned oil case.

Performance Output	Value	Units
net indicated work output/displacement	1.573E+06	Pa
mass of fuel/indicated work output	-3.792E-08	kg/J
flow mass/displacement mass at mixed charge density	-6.726E-01	--
heat transfer/net indicated work output	3.423	--
average polytropic exponent for compression	1.372	--
average polytropic exponent for expansion	1.208	--
cycle peak pressure	115.6	atm
crank angle at maximum pressure	370	degrees
crank angle at end of burn	371	degrees
mixed exhaust temperature at valve exit	822	K

ESP Tee Dee 0.010 Burned Oil Performance Summary  
Table B.3

Once again additional performance values for this case were calculated as shown in Table B.4. The fuel mass flow was determined by multiplying the fuel/mixture ratio with oil (given in Section 2.4.2 as 0.105) by the maximum intake flow in the mass flows diagram (0.0008 kg/s).

Calculated Performance (Burned Oil)	Value	Units
Power	64.493	W
Power Density	4961.0	W/kg
Efficiency	0.0344	--
BSFC	0.0047	kg/W-hr

ESP Derived Burned Oil Performance Values  
Table B.4

From Table B.4, it is evident that the power values for the ESP simulation are again well above the expected peak capability of the Tee Dee 0.010. Just as in the inert oil

case, these elevated values are most likely a result of the inability of ESP to model the specific loss mechanisms associated with two-stroke engines and small-scale combustion. The lower efficiency value in this case relative to the inert oil case is a result of the very high theoretical heating value of the fuel when oil is included in the calculation.

### **Error Analysis**

#### *Sources of Error*

To the extent at which engine geometry is used in the ESP model, some error can be attributed to the fact that the geometry measurements were taken by approximate hand measurements with an uncertainty of at least 0.5 mm for lengths and at least 0.5 degrees for angles.

Another major source of error is the values of the parameters entered into ESP that were approximated using the default values. The default engine is a large four-stroke engine, so it is reasonable to assume sizable errors from the inaccuracy of parameters such as combustion efficiency.

The most significant source of error, however, is the inherent limitations of the simulation code to model two-stroke operation. ESP was intended for use with larger four-stroke engines, so inaccuracies in the cycle computation can be expected and, in fact, witnessed in the output plots. ESP can only be run at four strokes at a time, but the output suggests it may be incapable of executing combustion more than once for every four strokes. Additionally, ESP does not model losses specific to the mechanisms of small two-stroke engines such as scavenging or crankcase compression.

The lack of proper loss modeling is evident in the high power values and the linear power curve created by running ESP over a wide RPM range as shown in Figure B.31. In addition to the inflated power values, power attenuation is not noticed as would be expected in the upper RPM range (as shown in Figure 2.20) from such factors as the drop in volumetric efficiency. This suggests ESP may be incapable of modeling engines running at very high speeds.

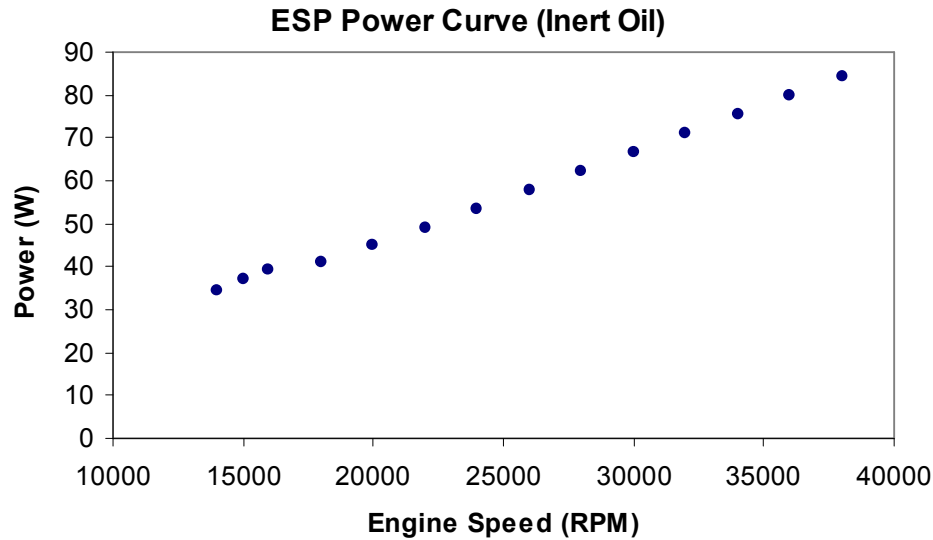


Figure B.31

*Comparative Analysis*

Because both the inert oil and burned oil configuration results were similarly far from the measured performance of the engine, only one case was used for a comparative error analysis. The differences between the inert oil results of ESP run at the 10 full-throttle RPM settings tested in Section 3 and their corresponding measured values are shown below. Percentages listed indicate the percentage off from the measured value. Tables B.5, B.6, B.7, and B.8 show fuel flow, power, BSFC, and efficiency respectively.

RPM	ESP: Fuel Flow (kg/s)	Meas: Fuel Flow (kg/s)	Diff (kg/s)	%Diff
15470	1.199E-04	1.220E-05	-1.08E-04	883
15839	1.221E-04	7.143E-06	-1.15E-04	1609
15935	1.221E-04	1.124E-05	-1.11E-04	987
16417	1.221E-04	1.124E-05	-1.11E-04	987
16567	1.243E-04	1.316E-05	-1.11E-04	844
17034	1.025E-05	1.395E-05	3.71E-06	27
17163	1.040E-05	1.111E-05	7.13E-07	6
17588	1.090E-05	1.316E-05	2.26E-06	17
18648	1.243E-05	1.695E-05	4.52E-06	27
19711	1.395E-05	1.346E-05	-4.90E-07	4

ESP and Measured Fuel Flow Comparison

Table B.5

RPM	ESP: P (W)	Meas: P (W)	Diff (W)	%Diff
15470	37.97	9.26	-28.71	310
15839	38.88	7.70	-31.18	405
15935	39.11	10.24	-28.87	282
16417	40.30	10.00	-30.29	303
16567	40.66	9.89	-30.78	311
17034	38.99	7.54	-31.45	417
17163	39.24	8.43	-30.81	365
17588	40.05	9.85	-30.20	307
18648	42.13	6.40	-35.73	558
19711	44.34	6.88	-37.46	545

ESP and Measured Power Comparison

Table B.6

RPM	ESP: BSFC (kg/W-hr)	Meas: BSFC (kg/W-hr)	Diff (kg/W-hr)	%Diff
15470	1.137E-02	4.742E-03	-6.63E-03	140
15839	1.130E-02	3.340E-03	-7.96E-03	238
15935	1.124E-02	3.950E-03	-7.29E-03	184
16417	1.091E-02	4.044E-03	-6.86E-03	170
16567	1.100E-02	4.792E-03	-6.21E-03	130
17034	9.459E-04	6.659E-03	5.71E-03	86
17163	9.540E-04	4.743E-03	3.79E-03	80
17588	9.799E-04	4.810E-03	3.83E-03	80
18648	1.062E-03	9.533E-03	8.47E-03	89
19711	1.133E-03	7.047E-03	5.91E-03	84

ESP and Measured BSFC Comparison

Table B.7

RPM	ESP: Efficiency	Meas: Efficiency	Diff	%Diff
15470	0.0188	0.0450	0.026	58
15839	0.0189	0.0639	0.045	70
15935	0.0190	0.0541	0.035	65
16417	0.0196	0.0528	0.033	63
16567	0.0194	0.0446	0.025	56
17034	0.2257	0.0321	-0.194	604
17163	0.2238	0.0450	-0.179	397
17588	0.2179	0.0444	-0.174	391
18648	0.2011	0.0224	-0.179	798
19711	0.1885	0.0303	-0.158	522

ESP and Measured Efficiency Comparison

Table B.8

Figure B.32 shows the average of percentage difference from measured of the fuel flow, power, and efficiency values. BSFC was not included in the average because it is proportional to efficiency.

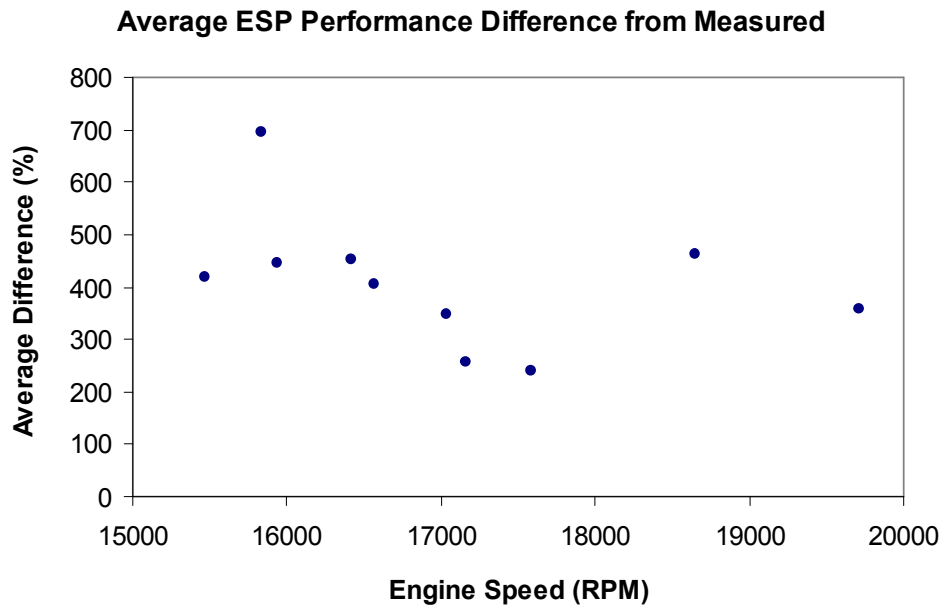


Figure B.32

From Figure B.32, it can be seen that ESP results are closest to the measured results near 17,588 RPM, where it is off by an average of 238%. These large differences, however, clearly indicate that ESP, as configured, is incapable of accurately modeling the performance of the Cox Tee Dee 0.010.

Even with specific Tee Dee 0.010 parameter input and custom adjustments to the configuration, ESP's inability to properly model two-stroke engine mechanisms and small-scale loss factors is evident.

## References

- [1] Aichlmayr, H., Kittelson, D., Zachariah, M., "Micro-HCCI combustion: experimental characterization and development of a detailed chemical kinetic model with coupled piston motion", The Combustion Institute, 2003.
- [2] Aichlmayr, H., Kittelson, D., Zachariah, M., "Miniature free-piston homogeneous charge compression ignition engine-compressor concept-Part I: performance estimation and design considerations unique to small dimensions", *Chemical Engineering Science* 57, 2002.
- [3] Aichlmayr, H., Personal Communication, 2006.
- [4] Alder PC Repair & Web Design, "WELCOME TO MICRO-FLITE", 2005, Internet Site, <http://www.micro-flite.com/>, Retrieved June 7, 2006.
- [5] Anderson, J., *FUNDAMENTALS OF AERODYNAMICS, Second Edition*, pg. 34, McGraw-Hill, Inc., 1991.
- [6] Annen, K., Stickler, D., Woodroffe, J., "LINEARLY-OSCILLATING MINIATURE INTERNAL COMBUSTION ENGINE (MICE) FOR PORTABLE ELECTRIC POWER", 41st Aerospace Sciences Meeting and Exhibit, AIAA 2003-1113, 2003.
- [7] Cadou, C., Menon, S., "SCALING OF LOSSES IN SMALL IC AERO ENGINES WITH ENGINE SIZE", 42nd AIAA Aerospace Sciences Meeting and Exhibit, AIAA 2004-690, Reno, Nevada, 5-8 January 2004.
- [8] Cadou, C., Moulton, N., Menon, S., "Performance Measurement and Scaling in Small Internal Combustion Engines", 41st AIAA Aerospace Sciences Meeting and Exhibit, AIAA 2003-0671, Reno NV, 6-9 January 2003.
- [9] Cadou, C., Sookdeo, T., Moulton, N., Leach, T., "PERFORMANCE SCALING AND MEASUREMENT FOR HYDROCARBON-FUELED ENGINES WITH MASS LESS THAN 1 KG", 1st AIAA Unmanned Aerospace Vehicles, Systems, Technologies, and Operations Conference and Workshop, AIAA 2002-3448, Portsmouth, VA, May 20-22, 2002.
- [10] Chen, N., "Deep Reactive Ion Etch Process Development for MEMS Rotary Engine Power System", Plasma Etch Users Group, 2004.
- [11] Chinn, P., "ENGINE REVIEW Cox Tee-Dee .010", MODEL AIRPLANE NEWS, August 1961.
- [12] Chinn, P., "Engine Test Review", *Aeromodeller*, October 1979.

- [13] Cox, "TEE DEE ENGINE SPARE PARTS ORDER FORM", Centuri Corp., 2000.
- [14] Cox, Internet Image, <http://www.coxmodels.com/images/C00130.JPG>, retrieved June 6, 2006.
- [15] Cugat, O, Delamare, J., Rey, P., "Thermo-mechanical micro-sources", MINATEC 2003 Genoble, 2003.
- [16] Dahm, W., Ni, J., Mijit, K., Mayor, J., Qiao, G., Dyer, S., Benjamin, A., Gu, Y., Lei, Y., Papke, M., "Micro Internal Combustion Swing Engine (MICSE) for Portable Power Generation Systems", 40th AIAA Aerospace Sciences Meeting, AIAA 2002-0722, 2002.
- [17] DARPA, "Palm Power Research Goals", <http://www.darpa.mil/DSO/thrust/matdev/palmpower/research.html>, Retrieved April 18, 2006.
- [18] Das, S., Arnold, D., Zana, I., Park, J.-W., Lang, J., Allen, M., "MULTI-WATT ELECTRIC POWER FROM A MICROFABRICATED PERMANENT-MAGNET GENERATOR", 2005.
- [19] Dev, S., "Logistics-Fueled, Man-Portable Generator Sets for Soldier Power, Battery Charging and APU Needs", NDIA Tri-Service Power Expo May 02, 2005.
- [20] Dev, S., "Logistics-Fueled, Man-Portable Generator Sets for Soldier Power, Battery Charging and APU Needs", International Soldier Systems Conference December 14 - 16, 2004.
- [21] Dev, S., "Heavy Fuel Engines for Small Unmanned Systems, Current Challenges and Future Prospects", AUVSI's Unmanned Systems North America 2004 Symposium & Exhibition, 2004.
- [22] Disseau, M., Scarborough, D., Jagoda, J., "THE DEVELOPMENT AND INVESTIGATION OF A SMALL HIGH ASPECT RATIO, TWO-STROKE ENGINE", 41st Aerospace Sciences Meeting and Exhibit, AIAA 2003-689, 2003.
- [23] D-STAR, "DSTAR-Brochure", D-STAR Engineering Corporation, Internet Document, <http://www.dawnbreaker.com/vas/docs/DSTAR-Brochure.pdf>, Retrieved April 18, 2006.
- [24] Epstein, A., "MILLIMETER-SCALE, MEMS GAS TURBINE ENGINES", Proceedings of ASME Turbo Expo, 2003.

- [25] Epstein, A., Jacobson, S., Protz, J., Frechette, L., "SHIRTBUTTON-SIZED GAS TURBINES: THE ENGINEERING CHALLENGES OF MICRO HIGH SPEED ROTATING MACHINERY", 8th International Symposium on Transport Phenomena and Dynamics of Rotating Machinery, 2000.
- [26] Freiheit, R., "*1/8A ENGINE MANUAL & HANDBOOK*", MICRO-FLITE, 2005.
- [27] Fu, K., "MEMS Rotary Internal MEMS Rotary Internal Combustion Engine", ME 219 Lecture (May 2), University of California, Berkeley, 2002.
- [28] Gierke, C., *2-Stroke Glow Engines For R/C Aircraft*, Volume 1, Air Age Media, 2005.
- [29] Gong, Y., Sirakov, B., Epstein, A., Tan, C., "Aerothermodynamics of Micro-Turbomachinery", Proceedings of ASME Turbo Expo, 2004.
- [30] Green, A., Vice President Sales & Marketing OPTIMUM Power Technology, Personal Communication, 2006.
- [31] Hepperle, M., "Aerodynamics for Model Aircraft", 2005, Internet Site, <http://www.mh-aerotools.de/airfoils/index.htm>, Retrieved June 6, 2006.
- [32] Hill, P., Peterson, C., *Mechanics and Thermodynamics of Propulsion*, Addison-Wesley Publishing Company, Inc., 1992.
- [33] Holmes, A., Hong, G., Pullen, K., Buffard, K., "AXIAL-FLOW MICROTURBINE WITH ELECTROMAGNETIC GENERATOR: DESIGN, CFD SIMULATION, AND PROTOTYPE DEMONSTRATION", IEEE, 2004.
- [34] Jacobson, S., Das, S., Savoulides, N., Steyn, J., Lang, J., Li, H., Livermore, C., Schmidt, M., Teo, C., Umans, S., Epstein, A., Arnold, D., Park, J.-W., Zana, I., Allen, M., "PROGRESS TOWARD A MICROFABRICATED GAS TURBINE GENERATOR FOR SOLDIER PORTABLE POWER APPLICATIONS", IEEE International Workshop on Agent and Services Computing, 2004.
- [35] Jacobson, S., Personal Communication, 2006.
- [36] Johnson, P., "Propellers For Model Aircraft", 2003, Internet Site, [http://www.airfieldmodels.com/information\\_source/model\\_aircraft\\_engines/propellers.htm](http://www.airfieldmodels.com/information_source/model_aircraft_engines/propellers.htm), Retrieved June 26, 2006.
- [37] Jumper, C., "Micro Planes", 2003, Internet Site, <http://users3.ev1.net/%7Ecdjump/main/teedee/index.html>, Retrieved June 11, 2006.

- [38] Lee, M., "Dr Kyle Jiang: Microengine Project", <http://www.eng.bham.ac.uk/mechanical/people/jiang/micro.htm>, University of Birmingham, Retrieved April 18, 2006.
- [39] Li, H., Savoulides, N., Ho, L., Jacobson, S., Khanna, R., Teo, C.-J., Wang, L., Ward, D., Epstein, A., Schmidt, M., "FABRICATION OF A HIGH SPEED MICROSCALE TURBOCHARGER", Hilton Head, 2004.
- [40] Liu, L., Teo, C., Epstein, A., Spakovszky, Z., "Hydrostatic Gas Journal Bearings for Micro-Turbomachinery", Journal of Vibration and Acoustics, Vol. 127, ASME, APRIL 2005.
- [41] Lumley, J. Personal Communication, 2006.
- [42] Lumley, J., *ENGINES AN INTRODUCTION*, Cambridge University Press, 1999.
- [43] Mackey, C., "Biography of WILLIAM E. ATWOOD", National Model Aviation Museum, 2001, Internet Document, <http://www.modelaircraft.org/museum/bio/Atwood.pdf>, Retrieved June 06, 2006.
- [44] Mathworks, Inc., "MATLAB Function Reference: ode23, ode45, ode113, ode15s, ode23s, ode23t, ode23tb", 2006, Internet Site, <http://www.mathworks.com/access/helpdesk/help/techdoc/ref/ode23tb.html>, Retrieved November 1, 2006.
- [45] Menon, S., Moulton, N., Cadou, C., "Performance Measurement in Small Internal-Combustion Engines", Journal of Propulsion and Power, In Press (2006).
- [46] National Research Council, Committee of Soldier Power/Energy Systems, *Meeting the Energy Needs of Future Warriors*, THE NATIONAL ACADEMIES PRESS. pg. 23, 63, 2004.
- [47] NIST, "NIST Chemistry WebBook", U.S. Secretary of Commerce, 2005, Internet Site, <http://webbook.nist.gov/chemistry/>, Retrieved October 14, 2006.
- [48] OPTIMUM Power Technology, "Products", 2006, Internet Site, <http://www.optimum-power.com/main-sim2.htm>, Retrieved July 4, 2006.
- [49] Papac, J., Figueroa, I., Dunn-Rankin, D., "Performance Assessment of a Centimeter-Scale Four-Stroke Engine", 2003.
- [50] Pello, A., "Micro-Power Generation Using Combustion: Issues and Approaches", Twenty-Ninth International Symposium on Combustion, July 21-26, 2002.
- [51] Pisano, A., Personal Communication, 2006.

- [52] Revering, A., "Andrew Revering's List of Meteorological Formulas", Internet Site, <http://www.aprweather.com/pages/calc.htm>, Retrieved August 21, 2006.
- [53] Ricardo, H., *THE HIGH-SPEED INTERNAL-COMBUSTION ENGINE*, pg. 186-202, Blackie & Son Limited, 1953.
- [54] Ronney, P., "Microscale reacting flows and power generation", Applications of Combustion AME 514 Lecture, University of Southern California, 2004.
- [55] SAE Standard, Engine power test code-Spark ignition and compression ignition-net power rating, SAE J1349, June 1995.
- [56] Spadaccini, C., Peck, J., Waitz, I., "Catalytic Combustion Systems for Micro-Scale Gas Turbine Engines", Proceedings of ASME Turbo Expo, 2005.
- [57] Spakovszky, Z., Liu, L., "Scaling Laws for Ultra-Short Hydrostatic Gas Journal Bearings", Transactions of the ASME, Vol. 127, June 2005.
- [58] Stanford University, "Homepage of ESP Software", 2001, Internet Site, <http://esp.stanford.edu/>, Retrieved July 9, 2006.
- [59] Steyn, J., Kendig, S., Khanna, R., Lyszczarz, T., Umans, S., Yoon, J., Livermore, C., Lang, J., "GENERATING ELECTRIC POWER WITH A MEMS ELECTROQUASISTATIC INDUCTION TURBINE-GENERATOR", 2005.
- [60] Stuart, R., "GLOW FUEL MIXING AND USE", 2006, Internet Site, <http://www.lcrc.org/stu11.htm>, Retrieved June 26, 2006.
- [61] Tanner, S., "Weather Station History", The Weather Underground, Inc., 2006, Internet Site, <http://www.wunderground.com/weatherstation/WXDailyHistory.asp?ID=KMDBERWY1>, Retrieved August 21, 2006.
- [62] Taylor, C., *The Internal-Combustion Engine in Theory and Practice*, The Technology Press of the Massachusetts Institute of Technology and John Wiley & Sons, Inc., New York & London, 1960.
- [63] Towne, E., "Biography of LEROY M. COX", National Model Aviation Museum, 1999, Internet Document, <http://www.modelaircraft.org/museum/bio/Cox.pdf>, Retrieved June 06, 2006.
- [64] Turns, S., *An Introduction to Combustion: Concepts and Applications*, McGraw-Hill Higher Education, 2000.

- [65] UC Regents, [http://www-bsac.eecs.berkeley.edu/groups/bmad/mems\\_reps/home.htm](http://www-bsac.eecs.berkeley.edu/groups/bmad/mems_reps/home.htm), 2003, Retrieved April 14, 2006.
- [66] Warring, R., "ENGINE ANALYSIS COX TEE-DEE .010", *Aeromodeller*, October 1961.
- [67] White, A., "A Review of Some Current Research in Microelectromechanical Systems (MEMS) with Defence Applications", DSTO Aeronautical and Maritime Research Laboratory, Australia, 2002.
- [68] Wong, C., Zhang, X., Jacobson, S., Epstein, A., "A Self-Acting Gas Thrust Bearing for High-Speed Microrotors", *JOURNAL OF MICROELECTROMECHANICAL SYSTEMS*, VOL. 13, NO. 2, APRIL 2004.
- [69] Young, B., "The new MOTA V6.10 for Windows®", 2006, Internet Site, <http://bevenyoung.com.au/mota.htm>, Retrieved July 4, 2006.
- [70] Young, B., Personal Communication, 2006.